IGNITION AND COMBUSTION CHARACTERISTICS

OF COAL/GRAPHITE PARTICLES

UNDER VARIABLE PRESSURES

A THESIS

Presented to

The Faculty of the Division of Graduate Studies

By

Kalyanasundaram Annamalai

In Partial Fulfillment

of the Requirements for the Degree

Doctor of Philosophy

in the School of Mechanical Engineering

Georgia Institute of Technology

May, 1975

IGNITION AND COMBUSTION CHARACTERISTICS

OF COAL/GRAPHITE PARTICLES

UNDER VARIABLE PRESSURES

Approved:

_____
P. Durbetaki, Chairman

_____
W. C. Strahle

_____
C. W. Gorton

_____
H. C. Ward

_____
W. Z. Black

Date approved by Chairman: 5/19/1975

ACKNOWLEDGMENTS

I would like to thank Dr. Durbetaki, my thesis advisor, for his continued interest, suggestions and advice as a professor and as a friend throughout the course of this thesis. I extend my thanks to Dr. W. C. Strahle for his critical discussions on Dirac-delta functions and for serving as an active member of the reading committee. The author thanks Dr. Gorton, Dr. Ward and Dr. Black for serving on the reading committee and for their comments and suggestions which were subsequently incorporated in the thesis.

I wish to express my appreciation to the School of Mechanical Engineering, Georgia Institute of Technology, for financially supporting my graduate studies through teaching and research assistantships.

In addition, I extend my affection and warmest appreciation to my wife, Vasanthal, for her patience, understanding and help during the course of the thesis.

Also, I wish to thank numerous friends who helped in the course of executing the computer programs relevant to the thesis.

Finally, I wish to dedicate this thesis to my parents, Kalyanasundaram and Pattu, and to my late brother-in-law, Masilamani, without whose help I would not have even known about engineering studies.

TABLE OF CONTENTS

          and Exact Solutions
5.3.3. A TIP Diagram for the Estimation
          of TIP Parameters

VI.   COMBUSTION ANALYSIS OF A HARD PRESSED GRAPHITE
      OR CHAR PARTICLES.   118

      6.1. A Hypothesis for the Occurrence of the
            Peak Erosion Rate
      6.2. Assumptions
      6.3. Governing Equations and Boundary
            Conditions
      6.4. Numerical Methods of Solution
            6.4.1. Sandwich Method
            6.4.2. Initial Value Method

VII. RESULTS AND DISCUSSION FOR THE COMBUSTION
      CHARACTERISTICS.   138

      7.1. Selection of Chemical Kinetics Constants
      7.2. Variation of Burning Rates
            7.2.1. Effect of Particle Temperature
            7.2.2. Effect of Particle Size
            7.2.3. Effect of Pressure
      7.3. General Correlation for Peak Burning
            Particle Temperatures

VIII. CONCLUSIONS.   158

APPENDIX A.   162

      A.1. Derivation for the Deflagration Rate
            of Coal Under Pyrolysis
      A.2. Pyrolysis in Absence of Gas Phase
            Oxidation
      A.3. Ignition Conditions for a Coal Under
            Pyrolysis
      A.4. Critical Parameters for Gas Phase
            Ignition

APPENDIX B.   171

      B.1. Heterogeneous Ignition-Exact Solution
      B.2. Critical Parameters for the Heterogeneous
            Ignition
      B.3. Heterogeneous Ignition-Approximate
            Solution

LIST OF TABLES

LIST OF ILLUSTRATIONS

NOMENCLATURE

$\vec{A}$ area vector

A_i pre-exponential factor in Arrhenius equation referring to reaction i

a   equation (E.31)

a   equation (63d)

a_{ji} equation (81)

b   equation (E.31)

b   equation (63d)

C   molal concentration

C_p specific heat at constant pressure

D   mean diffusion coefficient

$D_{c,g}$ correlating group for GIT, equation (56c)

$D_{c,h}$ correlating group for HIT, equation (63f)

D_{ij} binary diffusion coefficient

$D_{T,j}$ thermal diffusion coefficient

D_{III} third Damkohler number--a ratio of chemical reaction rate to molecular diffusion rate

D_{III}^o third Damkohler number based on a reference particle size

D_{IV} fourth Damkohler number, a ratio of heat liberation rate due to chemical reaction to the molecular conduction rate

d   particle diameter

d_o initial diameter of the particle

E   activation energy

F	a matrix defined by equation (80)
$\underset{\rightarrow}{f}$	body force per unit mass
$\overline{f}$	property per unit volume
$f(r_w)$	a general function of r_w, equation (36)
GIT	gas ignition temperature
g_1, g_2	equations (36d, 36e), also see equations (B.7) and (B.8)
HIT	heterogeneous ignition temperature
h	enthalpy per unit mass
h_i	heat of formation at standard conditions
K	conductance
k	reaction rate constant
Le	Lewis number, $\lambda / \rho D\ C_p$
l	order of reaction with respect to volatile content in the solid coal
M	a matrix defined by equation (80c); see Table 3 for a different definition
$M_1, M_2, M_3,$ M_4, M_5	equations (54d, 54f, 55d, 65b, 66b)
m	order of pyrolysis with respect to particle size
m_1	order of heterogeneous oxidation of carbon to CO with respect to particle size, = 1 for surface oxidation
m_i	symbol for chemical species i
m	mass burning rate
n	overall order of reaction
n_i	order of reaction with respect to species i
$\underset{\rightarrow}{n}$	outer normal to the surface

$\underset{\rightarrow}{\vec{P}}$	stress tensor
p	pressure
Q_g	heating value of the gaseous fuel
Q_w	heat of pyrolysis
$Q_{w,h}$	heat of reaction for heterogeneous oxidation of coal
$\bar{Q}_w^+$	Q_w/Q_g
$\overset{\circ}{Q}$	heat rate
$\underset{\rightarrow}{q}$	heat flux vector with respect to mass average velocity
q^o	heat of reaction
R	equation (62c)
R^o	universal gas constant
R_s	specific reaction rate
r	radial coordinate
s	equation (81)
T	temperature
TIP	transition of ignition phase
t	time
$\underset{\rightarrow}{\vec{U}}$	unit tensor
u	internal energy per unit mass
$\underset{\rightarrow}{V}_i$	diffusion velocity of species i
V	volatile content in the solid coal at any time
V*	initial volatile content
$\underset{\rightarrow}{v}$	bulk velocity vector
$\underset{\rightarrow}{v}_i$	absolute velocity vector of species i
v	velocity in the radial direction

W	molal mass
$\dot{w}$	chemical reaction rate per unit volume
$\dot{w}'$	chemical reaction rate per unit surface area
X	mole fraction
x	see Table 3
Y	mass fraction
$Y(1), Y(2)$ $Y(3), Y(4)$ $Y(5), Y(6)$	equations (73a, 73b, 73c, 75)
Z	equation (62e)
z	potential energy
α	see Table 3
$\alpha_1, \alpha_2, \alpha_3$ α_4, α_5	see equations (54c, 54g, 55c, 65c, 66c)
α_g, α_h	equations (65d, 65e)
α_g', α_h'	equations (C.9, C.10)
β	coupling function, equation (23)
γ_g, γ_h	equations (66d, 66e)
Γ_a, Γ_b	equations (69a, 69b)
δ	remainder terms in Taylor series, equation (81), also used as Dirac-Delta function, equation (37)
ε	flux fraction
η	ratio of nondimensional bulk velocity at $\xi = \xi$ to the value at the surface $\xi = \xi_w$, ξ/ξ_w
θ	nondimensional temperature, $T\, R°/E_g$
$\hat{\theta}$	$T\, R°/E_w$
$\bar{\theta}$	$T\, R°/E_{w,h}$
κ	bulk viscosity

λ	thermal conductivity
μ	absolute viscosity
ν_i	moles of species i participating in a reaction
ν'	moles of reactant in a reaction
ν''	moles of product in a reaction
$\nu_s, \bar{\nu}_s, \nu_a$	stoichiometric coefficient of pyrolysate, coal, and carbon
ν_b	stoichiometric consumption of CO_2 per unit mass of carbon for reduction reaction
ξ	nondimensional bulk velocity, a ratio of mass average velocity to the diffusion velocity
ρ	density
σ	Stefan-Boltzmann constant
τ	nondimensional time, equation (36c)
ϕ	nondimensional coupling function, equation (24)

Subscripts

a	atmospheric condition when associated with pressure, refers to reaction $C + 1/2\ O_2 \rightarrow CO$
ad	adsorption
b	refers to reaction $C + CO_2 \rightarrow 2\ CO$
C	carbon
Chem	chemical
CO	carbon monoxide
CO_2	carbon dioxide
crit	critical
d	deformation
di	diffusion
de	desorption

eq	equilibrium
F	fuel
g	gas phase
h	heterogeneous
I	ignition
i,j	species i,j
L	loss
min	minimum
N	nitrogen
0	oxygen
p	peak when associated with temperature, principal species
pr	product
R	radiation
s	solid
T	thermal
V	volatiles
w	wall condition
∞	condition at infinity
+	gas side condition
-	solid side condition

Superscripts

T	transpose
+	nondimensional quantity
*	condition at the stoichiometric surface
.	rate
~	modified condition unless otherwise specified

SUMMARY

This dissertation is mainly concerned with the
ignition problem of a coal particle. Only a minor part of
the dissertation deals with the combustion of a single
particle. A century-long held notion was that the ignition
of coal particles always occurs in the gas phase, as in a
totally pyrolyzing material. Recent experimental results
disproved such a sequence, at least for small bituminous
coal particles. Coals undergo only partial pyrolysis and
hence ignition could occur in one of the two possible modes:
(i) exothermic gasification due to heterogeneous oxidation
(regime I) and (ii) endothermic pyrolysis and subsequent
oxidation of the pyrolysate in the gas phase (regime II).

A steady state ignition theory is developed for
partially pyrolyzing solid particles. The theory is formu-
lated on an asymptotic basis; regime I is assumed to proceed
independent of regime II.

For regime I, Semanov's thermal theory is used to
obtain the heterogeneous ignition temperature (HIT) and the
solutions reveal that an increase in particle size, oxygen
concentration and pressure results in decrease of HIT.
Critical situations are encountered where the ignition no
longer occurs with a finite jump in temperature. Such
conditions are represented in the form of universal plots

for arbitrary system parameters. Approximate explicit solutions for HIT are developed and compared with results from steady state and non-steady state theories and as well as from experiments reported elsewhere.

For regime II, the gas phase reaction is treated as a simple discontinuity. Adiabatic ignition criterion is invoked to define the gas ignition temperature (GIT). The solutions reveal that a decrease in particle size and an increase in oxygen concentration increases the GIT. Critical conditions are found where the intensive reaction surface just touches the particle surface. Such conditions are estimated from the diagrams presented here for arbitrary system parameters. Approximate solutions for GIT are developed under limiting conditions of heat transfer or pyrolysis control of ignition process.

Superimposing the results for HIT and GIT, the conditions for transition of ignition phase (TIP) are found. Using the approximate results for HIT and GIT, a TIP diagram is constructed to determine the TIP conditions.

A phenomenon associated with char or graphite burning is the peculiar peak burning rate at a particular surface temperature. This is explained with variable activation energy for surface reactions at low pressures. Here it is shown that such a peak could occur with assumption of constant activation energy. Steady state combustion analysis of a surface heated particle in cold surroundings

is made. The resulting eigenvalue type problem is solved using the initial value method. The variation of burning rates with surface temperature, particle size and pressure are studied. A general correlation for the peak burning surface temperature in terms of particle size and pressure is given. According to the analysis presented here, the occurrence of a peak is an indication of existence of CO in the products.

CHAPTER I

INTRODUCTION

1.1. Relevance

When pulverised coal is injected into a hot furnace (about 50,000 lb/hour), the coal undergoes rapid heating (of the order of about 10^4 to 10^5 degrees C per second), partial pyrolysis (about 40 to 50 percent of a high volatile coal gets gasified), ignition, combustion of the volatiles and then rapid combustion of char (combustion intensity around 35,000 BTU per hour per cubic foot atm) [1]. Residence time to achieve sufficient efficiency and a specified composition of the products and carbon particles (if any) in the exhaust gases, to a large extent, depends upon the ignition and combustion characteristics of the coal. Coals undergo only partial pyrolysis [2] as opposed to fabrics, waxes and thermo-plastic polymers which undergo almost complete thermal degradation. For totally pyrolysing (endothermic) materials ignition is expected to occur in the gas phase. On the other extreme, a hard solid graphite should undergo heterogeneous ignition on the surface. For materials with partial pyrolysis, ignition could occur in one of the two possible modes: (i) exothermic gasification at the surface through heterogeneous oxidation and (ii)

endothermic pyrolysis at the surface or throughout the volume of the particle and subsequent oxidation in the gas phase. For example if the coal is highly carbonized, ignition starts on the surface and if it is highly volatile (volatile content ~35%), ignition probably starts in the gas phase. The latter process starves oxygen availability on the surface thus retarding the erosion rate of carbon for some duration of time. Once the pyrolysis is over, heterogeneous combustion starts. However the oxidation rate of this char with residual volatile matter must be very rapid since the volatiles, previously released, leave a good number of pore spaces inside the coal particle. For example particles of bituminous coal, heated in inert, swelled more and had a more open structure [3] than those heated in a gas containing oxygen. This indicates that the intensity of pyrolysis is slower in the latter case, because of simultaneous surface combustion. Moreover the flame propagation rate depends upon the mechanism of ignition [4]. If ignition occurs in the gas phase, then it is observed that the rate is controlled by the pyrolysis and vice versa. Thus the rate of oxidation and as well as the flame propagation rate, to a certain extent, depends upon what happened during the preignition period. Moreover it is of interest to know the transitional point (the transitional volatile content in the solid coal) where switching of ignition phase occurs. Then it is necessary to carry out an ignition analysis to

determine the phase of ignition.

A phenomenon in the combustion of char is the peculiar peak erosion rate of carbon at certain surface temperature, particularly at low system pressures. This occurrence was explained with a hypothesis of variable activation energy [5] particularly at low pressures. This peak rate occurs even under normal pressures although only at reduced level [6]. The hypothetical assumptions behind the reduction of the overall variable activation energy are questionable (see discussion section of reference [5]) since there appears to be no physical or direct experimental basis for the assumptions.

There has been a recent interest in MHD power generation and gas dynamic lasers which normally require combustion under high pressures [7-10]. The British Coal Utilization Research Association (BCURA) started developing a gas turbine operating on the combustion gases of coal. Fluidized beds operate at pressures of 7 atm [11]. The hydrogenation reaction of coal takes place in the range of 500-1000°C and at a pressure of about 70 atm [12]. Moreover operating under high pressures reduces the plant size (at least for a fluidized bed steam generator) to about 1/20th of a conventional plant of similar output and the power generation efficiency is increased by about 2 to 5 percent [13]. Hence data on ignition and combustion characteristics of coal under higher pressures are needed. The only work in this

direction was done by Nettleton and Stirling who used a
shock tube to create pressures of about 25 atm and they
exposed the coal particles in this transient flow system
[14,15]. Their data is very limited and difficult to
interpret in our analytical form.

1.2. Objectives

This dissertation is divided into two main parts:
(i) steady state ignition analysis of a highly volatile coal
particle and (ii) steady state combustion analysis of a
graphite particle. However, the major portion of this
thesis is concerned with the ignition analysis.

1.2.1. Ignition Analysis of a Coal Particle

The objective here is to carry out an analysis on
the ignition process of a highly volatile coal particle and
obtain a general relation between the ignition temperature
and other physical and chemical parameters. It is intended,
if possible, to present an explicit relation for the ignition
temperature under limiting conditions. A further objective
of this part of the work is to obtain a criterion for the
phase of ignition at least in a qualitative sense and explain
the possibility of the transition of ignition phase (TIP)
with varying system parameters. Finally it is aimed to
establish the characteristics of the ignition behavior under
variable pressures.

1.2.2. Combustion Analysis of a Graphite Particle

The objective of this part of the research is to obtain the combustion characteristics of a surface heated graphite/char particle, with the hypothesis of constant activation energy at the surface. It is intended to show that the peak erosion rate can occur even under these assumptions due to interaction of mass transfer with chemical reactions. The effects of pressure are considered in the analysis.

CHAPTER II

STATE OF THE ART

2.1. Ignition

A thermal theory for the ignition of solids has been presented by Frank-Kamenetskii [16] assuming negligible oxidation in the gas phase and constant activation energy for the surface reactions. The ignition temperature, according to Semenov's steady state non-stationary thermal theory, is defined as that temperature at which the rate of heat loss is equal to the rate of heat generation by chemical reaction and rate of change of heat loss rate with respect to temperature is equal to the rate of change of heat liberation rate with respect to temperature. Bandyopadhyay et al. applied this thermal theory to the problem of ignition of a coal particle using unsteady conservation equation and assuming that the ignition is due to heterogeneous surface reactions [17]. One feature of this non-stationary thermal theory is that the rate of temperature rise with time is a maximum just at the point of ignition. However, Thomas et al. conclude from unsteady state thermal theory that there could be a finite jump in temperature or a maxima in the rate of temperature rise for the ignition of large particles and this however is not a necessary feature for the ignition

of small char particles [18]. This is a result of the fact
that particle size is too small to contribute significant
release of the heat compared to heat loss. The ignition
temperature of char at normal pressure is about 1000 K while
for a highly volatile coal, experiments indicate an ignition
temperature around 700 to 800 K [14].

Coal undergoing a rapid heating process evolves
gaseous reactants, most notably H_2 and CH_4, and small
fractions of CO, CO_2, C_2H_2, C_2H_6, C_3H_8, etc. [14,19,20]. An
approximate chemical formula for a low rank (usually high
moisture content) coal is represented typically as $C_{100}H_{73}O_{10}N$
[21] using ultimate analysis. This formula indicates the
type and total quantity of volatile species that could be
evolved during pyrolysis. Rate of production of volatiles
is governed by the kinetics of pyrolysis. The kinetics of
pyrolysis are dependent upon the rate of heating [22]. For
example if one produces acetylene (C_2H_2), and then if all
the hydrogen is utilized one finds that about 27 percent of
original carbon content is left as char. This rapid
utilization was found to be dependent upon heating rate.
At high heating rates, more volatiles are released. For
example, coal having 35 percent ASTM volatile matter may
release 48 percent volatiles if the heating rate is 8000°C/
sec. One reason for this is that rapid heating avoids
polymerization reactions (i.e. carbon atoms getting together).
Frequently in the degasification process of these volatile

coals, there exists a critical temperature at which the rate of release of volatiles is maximum. Nettleton and Stirling found that there is a qualitative relation between the critical temperature of volatility and the ignition temperature [14]. A higher critical temperature normally means a higher ignition temperature and vice versa. The existence of a critical temperature for pyrolysis has the undertones of Arrhenius law in chemical reactions.

The rate of pyrolysis may be governed by the following factors and rate controlling processes:

(i)   If the heating rate is high and the particle size is large, the pyrolysis rate is dependent upon the propagation of thermal waves in the particle [23], and the rate approaches the surface reaction.

(ii) If the heating rate is very high and the particle size is too small, there is insufficient time for the particle to pyrolyse and hence ignition may start on the surface if this reaction is relatively faster or the particle may simply ablate [1].[†]

(iii) For other heating rates and medium sized particles, the kinetics of pyrolysis is governed by the following processes:

[†]For example, many times chemical time to form a new structure is more than the collision time. If the heating time to ablation temperature is too small compared to chemical time, then ablation occurs.

(a) thermal decomposition control

(b) pore diffusion control, and

(c) desorption rate from the surface of the
particle.

For a volumetric thermal decomposition reaction
occurring throughout the volume, the rate of change of the
volatiles content is proportional to the amount of volatiles
left in the solid for a first order volumetric reaction.
The reaction occurs throughout the volume. Thus,

$$dV/dt = -k \, V$$

where k is the decomposition constant and V is the volatile
content left (see Reference [11]). For this case the
evolution time of volatiles will be independent of the
particle size.

For diffusion control through macropores Essenhigh
[24] applied a shrinking droplet model to the pyrolysis of
coal particle. Essenhigh treated the carbon matrix as an
inert porous body through which the volatiles escape and
vaporize like a liquid. He was able to predict that

$$t_v = k_o d_o^2$$

where t_v is the evolution time, k_o is evolution constant
and d_o is the initial particle diameter. Note that evolution

time depends upon the particle size similar to a droplet
burning model.

Experiments appear to confirm thermal decomposition
control for small particles and pore diffusion control for
large particles. The activation energy for the decomposition
control mechanism is around 30 kcal/mole (chemical inter-
action)[†] while for the diffusion control the value is about
15 kcal/mole (physical interaction) [23]. For an experiment
conducted on pure thermal pyrolysis of coal without combus-
tion, Nelson reports about 90 kcal/mole just at the start
of intensive volatisation (critical region) [19]. For some
polymers and coals the value may fall in the range of 50-60
kcal/mole [2].

In an actual system where the coal is injected in
pulverized form into the furnace, the process of pyrolysis
and subsequent combustion are quite complicated. However
there are five distinct stages of burning [20]:

    (i)   rapid volatile loss prior to ignition,

    (ii) ignition and a small degree of oxidation of
carbon along with volatiles in the solid,

    (iii) intensive volatization and combustion of
volatiles with practically no oxidation of
carbon,

    (iv) burning of both volatiles and carbon, and

[†]A chemical interaction requires a change of
structure.

(v)   burning of solid carbon along with volatiles in the solid.

It was Howard and Essenhigh who first proposed that the ignition of a volatile coal can occur on the surface thus disproving a century long held notion that ignition of coal always occurs in the gas phase [20]. This contention is justified by the fact that there is some oxidation of carbon along with solid volatiles prior to ignition. Could it be probable that the ignition on the surface is due to the volatiles ignition on contact with the surface? Thomas et al. subjected brown coal particles to a stagnation flow system and showed from photographs of flame that surface ignition is possible [25]. Nettleton et al. indicate that there is a honeycomb structure, typical of volatile evolution, just after ignition thus indicating the probability of gas phase ignition. Moreover these authors found that there is a good correlation between ignition temperature and critical temperature of volatility. However, in order to verify this contention, they added some inhibitors which suppress gas phase reaction [26] and found that these inhibitors had no effect on the ignition temperature. Then they reversed their previous conclusion and interpreted this result to mean surface ignition; these inhibitors, according to Wicke [27], have a tendency to cover the surface of the coal. Hence it is surprising that Nettleton and Stirling did not notice any change in ignition temperature even if ignition initiates on

the surface. On the other hand, one could argue that there exists already complete surface coverage of the coal with oxygen; but this complete coverage could not happen since one finds most often a first order dependence of heterogeneous oxidation on oxygen concentration, indicative of adsorption control. It is apparent from the above discussion that there exists a problem regarding determination of the phase of ignition.

2.2. Combustion

Unlike the combustion of liquid droplets, in the case of small particles of coal, the rate controlling process to a significant level, is the chemical kinetics. This conclusion is drawn from the experimental results of Baum et al. [28], Bryant [29], and Essenhigh et al. [30]. One can summarize the present status of combustion of heterogeneous solid particles by raising the following questions:

(i) Is the burning rate diffusion controlled or controlled by chemical kinetics?

(ii) If the rate is controlled by chemical kinetics what is the controlling mechanism?

   (a) Is the reaction a surface reaction or a volume reaction?

   (b) If it is a volume reaction, is the reaction controlled by pore diffusion of oxidant or product? Is the reaction controlled by surface

reaction at the interfaces inside the particle? If the oxidant can well diffuse into the interior and the products cannot, can the particle explode? Can the exploded particle form soot?

(c)   Is the interface reaction controlled by adsorption or by formation* of activated complexes or by desorption?

(d)   Do active and inactive sites exist on the solid interface as assumed by Strickland-Constable and Nagle [5,31] and Blyholder et al. [32]? Do these sites undergo reversible and irreversible reactions amongst themselves?

(e)   Could one compare these sites and solid activated complexes to the unstable intermediate radicals in the gas phase reaction kinetics?

(f)   Do secondary reactions exist? Is it possible one could obtain both CO and CO_2 for large particles which could not be otherwise obtained for small particles under the same conditions due to thermal wave under large heating rates? (For large particles the interior may produce CO_2 which may undergo secondary reaction as it

---

*Adsorption is normally a surface phenomenon while absorption occurs throughout the volume. Chemisorption is a process where adsorption occurs with a change of structure.

escapes to the surface.)

(g) Are the secondary reactions also governed by
site theory?

Though all the questions are not answered with the
present knowledge, the following are some of the conclusions
drawn from the experimental results:

(i) If the driving potential is the partial pressure
of oxidant in the free stream, then the specific reaction
rate is primarily controlled by the sum of three major
resistances due to (a) diffusion, (b) adsorption, and (c)
desorption. Figure 1 shows the electrical analogy of these
chemical and transfer processes.
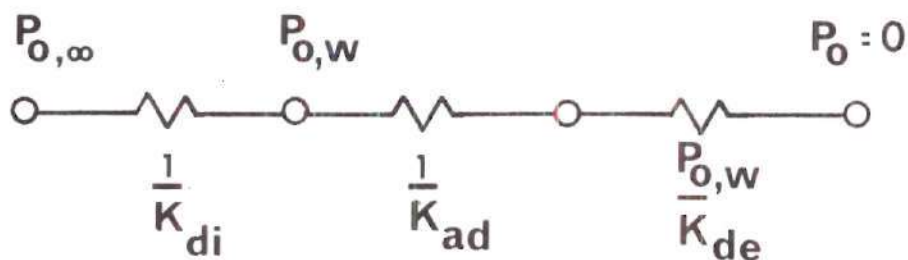
Figure 1. Electrical Analogy of Transfer
and Chemical Processes

Thus

$$R_s = p_{o,\infty} / (1/K_{di} + 1/K_{ad} + p_{o,w}/K_{de})$$

where R_s is the specific reaction rate, $p_{o,\infty}$ is the partial

pressure of oxidant in the gas stream, $p_{o,w}$ is the partial pressure of oxidant at the surface and K_{di}, K_{ad} and K_{de} are respectively conductances due to diffusion, adsorption and desorption. These conductances can be calculated from the knowledge of mass transfer and chemical kinetics. Adsorption resistance is very large when the O_2 concentration is low and the temperature of the particle is high, and activation energy lies in the range of 4000 to 23,000 cal/mole. Desorption resistance is dominant when the O_2 concentration is high and the particle temperature is low. The activation energy ranges from 20,000 to 80,000 cal/mole for desorption process [30].

(ii) The active and inactive sites theory seems to explain the behavior of maximum erosion rate particularly at low pressures; but it lacks direct experimental proof.

(iii) The volumetric reaction is revealed by the fact that there is decrease of density with decrease in size, more particularly for coals [33,34].

(iv) Diffusion control of the rate seems to be true only for large particles (more than about 200 microns).

(v) At low temperatures the reaction being slow, gas diffuses into the char and reaction takes place throughout the volume while at high temperatures since the reaction is fast, most of the oxygen is consumed at the surface; then there is almost only surface reaction [3]. The reaction order also varies from zero to one depending upon the

fractional surface coverage of oxide complex being one or zero [35]; however, this alone does not explain the order of reaction since as pressure increases, the order appears to be increasing thus contradicting the above hypothesis [35].

In addition to the above complicated chemical kinetics, there is swelling with intensive pyrolysis, and rupturing of the carbon matrix with intense production of steam for a low rank coal. Hence theoretical analysis of coal is complex. Hard pressed graphite or char particles with overall global reaction behavior are amenable to some form of theoretical treatment.

Intensive experiments were carried out on graphites by Strickland-Constable [5], Nagle et al. [31] and Rosner et al. [36,37]. Strickland-Constable gave a site theory as mentioned previously. According to this theory, oxidant can attack only active sites and form active solid complexes. In addition, as the particle temperature is increased, some of the active sites 'anneal' to inactive sites. Each of these surface chemical species occupies a certain fraction of the surface. The solid complexes evaporate and condense. It is a competition between the differing rates of all these processes which eventually leads to the occurrence of maxima of erosion rate with the variation of surface temperature. There appeared to be no physical basis for the existence of these sites as acknowledged by the authors themselves. In order to evaluate the rate, they evaluated

the necessary chemical parameters using the experimental data. In short this hypothesis assumed overall variable activation energy at the surface to explain the peak rate. Instead of obtaining a single maxima as revealed by experiments for some graphites this theory appeared to give two maxima or more for these graphites.

The objective here is not to question the validity of variable activation energy for the heterogeneous chemical reactions at the surface. This fact has been confirmed experimentally at very low pressures [36,37] where gas phase kinetics are almost suppressed. However, it is intended to show analytically that such a maxima could occur with the assumption of constant activation energy at the surface, under normal pressures, due to interference of mass transfer and kinetics of reaction. Since the maxima occurs due to the competition of finite chemical reaction rates between the surface and the gas phase, it is necessary to solve the governing equations with finite chemical kinetics for all reactions. For limiting diffusion controlled burning rates with reduction and oxidation of carbon, the reader is referred to the works of Fendell [38].

CHAPTER III

FORMULATION OF THE PROBLEM

The present analysis deals with spherical, highly volatile, furnace heated coal particle for the ignition problem and with spherical, hard pressed, uniformly heated graphite or char particles for the combustion problem. First, the general formulation of the conservation equations for mass, momentum, species, and energy are presented including the integral formulation for the reduction of interface conditions following Williams [39]. Then these equations are reduced for a spherical solid particle with suitable assumptions so that solutions could be obtained without mathematical complexity.

3.1. General Conservation Equations

Overall continuity:

$$\frac{\partial \rho}{\partial t} + \nabla \cdot (\rho \underset{\rightarrow}{v}) = 0 \tag{1}$$

where

ρ = density of the mixture of gases,

$\underset{\rightarrow}{v}$ = mass average velocity of the mixture,

t = time.

Momentum:

$$\frac{\partial \vec{v}}{\partial t} + \vec{v}\cdot\nabla\vec{v} = -\nabla\cdot\vec{P}/\rho + \sum_{i=1}^{N} Y_i \vec{f}_i \tag{2}$$

where

$\vec{f}_i$ = external force per unit mass on species i,

$\vec{P}$ = pressure tensor,

Y_i = mass fraction of species i.

Energy:

$$\rho\frac{\partial u}{\partial t} + \rho\vec{v}\cdot\nabla u = -\nabla\cdot\vec{q} - \vec{P}:(\nabla\vec{v}) + \rho\sum_{i=1}^{N} Y_i \vec{f}_i\cdot\vec{V}_i \tag{3}$$

where

u = specific internal energy of the gas mixture,

$\vec{q}$ = heat flux,

$\vec{V}_i$ = diffusion velocity of species i,

N = total number of chemical species.

Species:

$$\frac{\partial Y_i}{\partial t} + \vec{v}\cdot\nabla Y_i = \dot{w}_i/\rho - [\nabla\cdot(\rho Y_i\vec{V}_i)]/\rho \tag{4}$$

where

$\dot{w}_i$ = rate of production of species i by chemical reaction per unit volume.

The integral formulation of the conservation equations is necessary to obtain the interface conditions. Thus,

$$\frac{D}{Dt} \int \overline{f} dv = \frac{d}{dt} \int \overline{f} dv + \int \overline{f} (\underset{\rightarrow}{v} - v_d) \cdot d\underset{\rightarrow}{A} \qquad (5)$$

where for mass, $\overline{f} = \rho$,

momentum, $\overline{f} = \rho \underset{\rightarrow}{v}$,

energy, $\overline{f} = \rho [u + \frac{v^2}{2} + z]$,

species, $\overline{f} = \rho_i$, $\underset{\rightarrow}{v} = \underset{\rightarrow}{v}_i$,

and v_i = absolute velocity of species i,

z = potential energy per unit mass.

3.2. Constitutive Equations

Stress field:

$$\underset{\rightarrow}{\underset{\rightarrow}{P}} = [p + (\tfrac{2}{3} \mu - \kappa) \nabla \cdot \underset{\rightarrow}{v}] \underset{\rightarrow}{\underset{\rightarrow}{U}} - \mu [\nabla \underset{\rightarrow}{v} + (\nabla \underset{\rightarrow}{v})^T] \qquad (7a)$$

where

p = hydrostatic pressure,

μ = absolute viscosity,

κ = bulk viscosity,

$\underset{\rightarrow}{\underset{\rightarrow}{U}}$ = unit tensor,

$(\nabla \underset{\rightarrow}{v})^T$ = transpose of the matrix.

Heat transfer field:

$$q = -\lambda \nabla T + \rho \sum_{i=1}^{N} h_i Y_i \vec{V}_i + R°T \sum_{i=1}^{N} \sum_{j=1}^{N} \frac{X_j D_{T,j}}{W_i D_{ij}} (\vec{V}_i - \vec{V}_j)$$

where

λ = thermal conductivity of the mixture,

h_i = specific enthalpy of species i,

$R°$ = universal gas constant,

X_j = mole fraction of species j,

$D_{T,i}$ = thermal diffusion coefficient of species i,

W_i = molal mass of species i,

D_{ij} = binary diffusion coefficient of species i in j.

Mass transfer field:

$$\nabla X_i = \sum_{j=1}^{N} \frac{X_i X_j}{D_{ij}} (\vec{V}_i - \vec{V}_j) + (Y_i - X_j) \frac{\nabla p}{\rho} + \frac{p}{\rho} \sum_{i=1}^{N} Y_i Y_j (\vec{f}_i - \vec{f}_j) +$$

$$\frac{\nabla T}{T} \sum_{i=1}^{N} \frac{X_i X_j}{\rho D_{ij}} (\frac{D_{T,j}}{Y_j} - \frac{D_{T,i}}{Y_i})$$

Thermal Equation of State:

$$p = \rho R°T \sum_{j=1}^{N} (\frac{Y_j}{W_j})$$

Caloric Equation of State:

$$h_i = h_i^o + \int_{T^o}^{T} C_{p,i} \, dT \tag{9a}$$

where

h_i^o = heat of formation for species i,

$C_{p,i}$ = specific heat at constant pressure for species i.

Thermodynamic identity:

$$u = \sum_{i=1}^{N} h_i Y_i - p/\rho \tag{9b}$$

3.3. Assumptions for the Interface
Conservation Equations

The interface conservation equations can be obtained from the integral formulation of conservation equations (5) and (6) with the following assumptions:

    (i)   No surface stresses are involved.

    (ii) Kinetic and potential energies are negligible compared to enthalpy.

  (iii) No diffusion occurs inside the solid phase.

   (iv) Uniform chemical reactions take place on the surface. Even if reactions occur inside the solid phase as in the case of volumetric reactions, they are suitably represented by chemical reactions at the surface.

    (v) No time rate of change of any quantity occurs

on the surface (e.g., the fraction of area of
solid oxides does not vary with time).

(vi) The interface is not moving. This means that
either the interface is kept stationary by
feeding the solid mass at the same rate of
erosion or a quasi-steady state is assumed for
the problem. The latter is justified when
the density of the gas is small compared to
the density of the solid. However at higher
pressures this assumption must be relaxed [40].

Mass:

$$\rho \vec{V}_+ \cdot \vec{n}_+ = \rho \vec{V}_- \cdot \vec{n}_+ \tag{10}$$

Momentum:

$$p_+ = p_- \tag{11}$$

Energy:

$$\{\rho[h\vec{V} + \Sigma h_i Y_i \vec{V}_i] - \lambda \nabla T + \dot{\vec{q}}_R\}_+ \cdot \vec{n}_+ = \{\rho[h\vec{V}] - \lambda \nabla T + \dot{\vec{q}}_{R-}\} \cdot \vec{n}_+ \tag{12}$$

where

$\dot{\vec{q}}_R$ = heat flux vector due to radiation,

$\vec{n}_+$ = outward normal to the surface,

p_+ = pressure on the gas side of the surface,

p_- = pressure on the solid side of the surface,

λ = thermal conductivity coefficient,

h = enthalpy of mixture.

Species:

$$\{\rho Y_i (\vec{v}+\vec{V}_i)\}\cdot\vec{n}_+ = \{\rho Y_i \vec{v}\}_-\cdot\vec{n}_+ + \dot{w}_i' \qquad (13)$$

where

$\dot{w}_i'$ = mass rate of production of species i per unit surface area.

3.4 General Assumptions for the Conservation Equations

(i) Spherical symmetry exists.

(ii) No body forces, no Soret and Dufour effects, no diffusion due to pressure gradient (only Fick's law), no bulk viscosity, no pressure loss due to frictional effects and no pressure change due to Mach number of diffusion since the diffusion velocities involved are very low. Hence there is a constant pressure in the gas phase.

(iii) Binary diffusion coefficients of all pairs are equal. Rigorous analysis of multi-component diffusion validate this assumption at least for open gravity diffusion flames [41].

(iv) Lewis number is equal to unity.

(v) Chemical reactions both in the gas phase and
the interface occur in a single step and they
are represented by the global Arrhenius law.

$$\Sigma \; \nu_i' \; m_i \; \xrightarrow{k_j} \; \Sigma \; \nu_i'' \; m_i \qquad\qquad (14a)$$
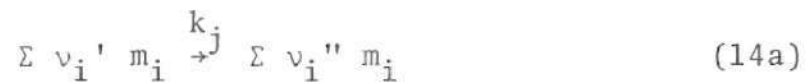
where

$k_j = A_j \; \exp \; (-E_j/R^\circ T),$

$\nu_i' =$ molal stoichiometric coefficient for species i
appearing as reactant,

$\nu_i'' =$ molal stoichiometric coefficient for species i
appearing as product,

$m_i =$ symbol for chemical species i,

$k_j =$ specific reaction rate constant for reaction j,

$A_j =$ frequency factor for the reaction j,

$E_j =$ global activation energy for the reaction j.

(vi) Initial unsteady state is not considered. This
is justified if the particle size is not too
small to consume its whole mass within this
transient period. The unsteady state introduced
in the gas phase due to regression at the
surface is negligible for solid particles (see
assumption (vi), section 3.3.). Only the
quasi-steady state problem will be considered.

(vii) Specific heats of all species are equal;

constant, mean specific heat is assumed.

3.5. Simplified Conservation Equations
in the Gas Phase

Applying the assumptions presented in Section 3.4., the conservation equations for the gas phase simplify as shown below.

Mass:

$$\frac{1}{r^2} \frac{d}{dr} (r^2 \rho v) = 0 \tag{15}$$

Momentum:

$$p = constant \tag{16}$$

Energy:

$$\rho v \frac{dh_T}{dr} = \frac{1}{r^2} \frac{d}{dr} (r^2 \rho D \frac{dh_T}{dr}) + \dot{w}_p \, q^\circ / \nu_p w_p \tag{17}$$

where

h_T = thermal enthalpy of the mixture, $= \int C_p dT$,

q° = heat released in the reaction (14a),

ν_p = stoichiometric coefficient of the principal species p (reference species).

Species:

$$\rho v \frac{dY_i}{dr} = \frac{1}{r^2} \frac{d}{dr} (r^2 \rho D \frac{dY_i}{dr}) + \dot{w}_i \qquad (18)$$

where

D = mean binary diffusion coefficient.

3.6. Simplified Interface Conservation Equations

Applying the assumptions presented in Section 3.3. the integral form of the conservation equations simplify as shown below.

Mass:

$$(\rho v)_+ = (\rho v)_- \qquad (19)$$

Momentum:

$$p_+ = p_- \qquad (11)$$

Energy:

$$\rho (vh + \sum_{i=1}^{N} h_i Y_i V_i) - (\lambda \frac{dT}{dr})_+ = (\rho vh)_- - (\lambda \frac{dT}{dr})_- + (\dot{q}_{R-} - \dot{q}_{R+}) \qquad (20)$$

where

λ_+ = thermal conductivity of gas mixture at the surface

λ_- = thermal conductivity of the solid

Species:

$$[\rho Y_i(v+V_i)]_+ = [\rho Y_i(v+V_i)]_- + \dot{w}_i', \quad i = 1, \ldots N \quad (21)$$

3.7. Transformations of Gas Phase
Conservation Equations

The following transformations are introduced to reduce the conservation equations to nondimensional form.

Dimensionless Bulk Velocity:

$$\xi = \dot{m} \int_r^\infty (4\pi\rho D r^2)^{-1} dr \quad (22)$$

where

$\dot{m} = 4\pi r^2 \rho v$, rate of mass removed from the surface, (22a)

$\xi = v/(D/r)$, non-dimensional bulk velocity. (22b)

Coupling Function:

$$\beta_{ip} = (Y_i/\nu_i W_i) - (Y_p/\nu_p W_p) \quad (23a)$$

$$\beta_{Tp} = (h_T/q^\circ) - (Y_p/\nu_p W_p) \quad (23b)$$

where

β_{ip} = species coupling function and

β_{Tp} = thermal coupling function.

Normalized Coupling Function:

$$\phi = \frac{\beta_{jp} - \beta_{jp,\infty}}{\beta_{jp,w} - \beta_{jp,\infty}}, \quad j=T, \quad j=1,\ldots,N-1 \qquad (24)$$

where

ϕ = normalized coupling function,

$\beta_{jp,w}$ = coupling function at the surface and

$\beta_{jp,\infty}$ = coupling function as $r\to\infty$

Non-dimensional Temperature:

$$\theta = T/(E_g/R^\circ) \qquad (25)$$

where

T = thermodynamic temperature,

E_g = gas phase activation energy and

θ = nondimensional thermodynamic temperature.

Flux Fraction:

$$\varepsilon_i = Y_i \left(1 + \frac{V_i}{V}\right) \qquad (26)$$

where

ε_i = flux fraction of species i.

With these transformations the coupled equations (17) and (18) reduce to,

$$\frac{d^2\phi}{d\xi^2} + \frac{d\phi}{d\xi} = 0 \qquad (27)$$

with the boundary conditions,

$$\phi = 1, \text{ at } \xi = \xi_w$$

$$\phi = 0, \text{ at } \xi = 0 \qquad (28)$$

where

$\xi_w = \dot{m}/4\pi\rho D r_w$, the nondimensional bulk velocity at the surface and

r_w = radius of the particle.

The solution for equations (27) with (28) is given as:

$$\phi = \frac{1-e^{-\xi}}{1-e^{-\xi_w}} \qquad (29)$$

There are 'N' equations involved in ϕ. However there are 'N+1' unknowns (N species and the thermal enthalpy) which are functions of the independent variable ξ. An additional equation for the principal species p is,

$$\frac{d^2Y_p}{d\xi^2} + \frac{dY_p}{d\xi} = -\,(\underline{+})\, \frac{D_{III,g}\xi_w^2 e^{-\frac{1}{\theta}}}{\xi^4 \theta^{\Sigma\nu_i'}} \left(\prod_{i=1}^{M} Y_i^{\nu_i'} \right) \qquad (30)$$

where the sign on the right hand side is positive if the species p is produced and negative if it is consumed. Also

$$D_{III,g} = \frac{\nu_p W_p A_g r_w^2}{\rho D} \left(\frac{p}{E_g}\right)^{\Sigma \nu_i'} \frac{W^{\Sigma \nu_i'}}{\Pi W_i^{\nu_i'}} \tag{31}$$

where

A_g = preexponential factor for the gas phase oxidation,

$D_{III,g}$ = Third Damkohler number for the gas phase oxidation of volatiles based on the rate of principal species.

Here one must make two comments about this Damkohler number.

(i) This is the third Damkohler number, a ratio of chemical reaction rate to the diffusion rate.

(ii) The molal mass of the mixture of the gases W does not remain constant and varies by an order of magnitude depending on the molal masses of the involved species. If the molal masses are almost same, then the ratio $(W^{\Sigma \nu_i'} / \Pi W_i^{\nu_i'})$ is unity. Here, for the estimation of the Damkohler number it is assumed that the molal masses are the same in the gas phase; this assumption seems to be justified in view of the fact that the magnitude of error is larger in the selection of frequency factors.

3.8. Transformations of Interface
Conservation Equations

Using the same transformations defined by equations (22) to (26) on equations (19) to (21), the interface conservation equations are,

Mass:

$$\dot{m}_+ = \dot{m}_- = \text{constant} \qquad (32)$$

Momentum:

$$p_+ = p_- = \text{constant} \qquad (33)$$

Energy:

$$\left(\frac{d\theta}{d\xi}\right)_+ - \left(\frac{d\theta}{d\xi}\right)\frac{\lambda_-}{\lambda_+} = - \sum_{i=1}^{N} \left\{ \varepsilon_{i,+} \frac{h_{i,+}}{C_p \, E_g/R^\circ} - \frac{h_{i,-}}{C_p \, E_g/R^\circ} \right\}$$

$$- \{\dot{q}_{R-} - \dot{q}_{R+}\} \frac{r_w R^\circ}{\xi_w \lambda_+ E_g} \qquad (34)$$

where C_p is the specific heat of the mixture of gases at constant pressure. If r_w is very small or λ_+ is very large, the radiation term could be neglected. This assumption facilitates a simple solution for the ignition temperature.

Species:

$$\epsilon_{i,+} = \epsilon_{i,-} \pm \sum_{\ell=1}^{k} \left\{ D_{III,w} \prod_{j=1}^{M} Y_{j,w}^{\nu_j{}'} \frac{e^{-E_w{}^+/\theta_w}}{\theta_w} \Sigma \nu_j{}' \right\}_\ell, \quad \ell=1\ldots k \quad (35)$$

where there are k reactions producing the species i, the + sign indicates production of species i, and

A_w = preexponential factor for pyrolysis,

$$D_{III,w} = \frac{A_w}{\rho D} \frac{f(r_w)\nu_i w_i}{4\pi r_w} \left(\frac{p}{E_w}\right)^{\Sigma \nu_j{}'} \frac{W^{\Sigma \nu_j{}'}}{\Pi W_j{}^{\nu_j{}'}}, \quad (36)$$

$D_{III,w}$ = surface Damkohler number based on species i,

E_w = activation energy for surface reaction,

θ_w = nondimensional surface temperature.

The function $f(r_w)$ in the surface Damkohler number depends upon the type of reaction occuring at the solid phase. For example, if the pyrolysis follows the first order volumetric reaction, then $f(r_w)$ must be equal to $(4\pi r_w{}^3/3)$. The surface Damkohler number is then proportional to $r_w{}^2$ and the mass flux at the surface is proportional to the particle radius. On the other hand if the pyrolysis occurs only at the surface, then $f(r_w)$ must be equal to $(4\pi r_w{}^2)$. However, if the pyrolysis is controlled by diffusion through the macropores, the function $f(r_w)$ is not explicit in r_w. Extending the analysis of Essenhigh, one can obtain such a function as follows [24] (see Figure 2).

$$\dot{m}_v = - \rho_v D_s \frac{dY_v}{dr} 4\pi r^2 \quad (36a)$$

Integrating between $r = r_w$ and $r = r_{eq}$,

$$\dot{m}_V = 4\pi\rho_V D_S r_w (Y_{V,eq} - Y_{V,w}) r_{eq}^+ / (1 - r_{eq}^+] \qquad (36b)$$

where

D_S = diffusion coefficient in the solid,

ρ_V = density of volatiles,

$Y_{V,w}$ = volatile concentration at the surface,

$Y_{V,eq}$ = equilibrium concentration under infinite kinetics rate,

r_{eq}^+ = equilibrium radius of the shrinking reservoir of volatiles, and

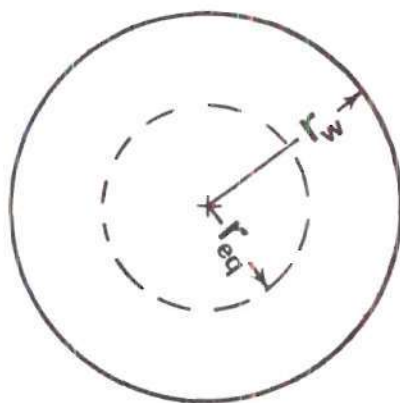r_{eq} = r_{eq}/r_w nondimensional equilibrium radius

Figure 2. Shrinking Volatile Drop Model

CHAPTER IV

IGNITION ANALYSIS OF A HIGHLY VOLATILE COAL PARTICLE

In this section, an ignition analysis of a pyrolyzing
highly volatile coal is carried out. General conservation
equations were presented in Section 3. Further assumptions
are made in Section 4.1, to simplify the general conserva-
tion equations of both the gas phase and interface. With
the objective for the determination of an ignition parameter
in mind, an ignition criterion is presented in Section 4.2.
The conservation equations are then integrated in Section
4.3 in order to obtain the general solutions for coal
deflagration rate and the nondimensional temperature
gradient. Explicit solutions are obtained in Section 4.4.1,
for the gas phase Damkohler number necessary to ignite the
volatiles in the gas phase, at a given furnace temperature
and deflagration rate of the coal. The solutions for the
ignition problem are further analyzed in Section 4.4.2 under
limiting cases of pyrolysis reaction at the surface and
explicit solutions for the nondimensional ignition tempera-
ture are presented in terms of known physical and chemical
parameters. Similarly a heterogeneous ignition analysis is
carried out in Section 4.5. Based upon the solutions of
Sections 4.4 and 4.5, a theory for Transition of Ignition

Phase (TIP) is presented in Section 4.6, which explains the probability of change of ignition phase when chemical and physical parameters of the system or surroundings are varied.

4.1. Assumptions

(i) At temperatures below the critical temperature (where the rate of volatile release is a maximum) the rate of oxidation of coal is too low to cause ignition on the surface. Pyrolysis is the only surface reaction and consequently a higher bound on the ignition temperature could be found.

(ii) The pyrolysis rate is independent of pressure. This is confirmed experimentally at least for lignite coals [42]. Normally volatile yield is increased if pressure is decreased; however the increase is very small since the char forming reaction is found to be slow [42]. However, the results to be deduced can still be used with minor modifications for different pressures if necessary. The order of reaction for the pyrolysis may vary from zero order to the first order volumetric content of the volatiles in the coal [14,43,2]. The pyrolysis occurs generally with heat absorption [2,28,11,4].

(iii) The rate of volatile release at the coal surface

is represented by a global Arrhenius law. This is consistent with the procedure used for the pyrolysis of some solid materials [44,45].

(iv) Radiative heat transfer is negligible. Contrary to expectations, radiative contribution is only about 20-25 percent of the total heat transfer <u>at the time</u> of ignition;[†] however, induction time is strongly dependent upon radiative heat transfer.

(v) The temperature throughout the solid particle is uniform. This is found to be true for small particles [4].

(vi) The specific heat of the gas mixture remains constant.

(vii) The heating rate of the coal particle is not high enough to cause "explosion flame" of the particle without pyrolysis [23]; i.e. the ratio of induction time of pyrolysis to the heating time is very small. An example of this condition is the shock tube experiments on ignition of coal particles.

(viii) No secondary reactions of volatiles with carbon

[†]This is true if $\dfrac{4\sigma T_w^3 r_w}{\lambda} < 1$, for small difference of temperature between the radiative sources. The group $4\sigma T_w^3 r_w/\lambda$ represents a ratio of radiative heat transfer to conductive heat transfer.

are considered. Even if secondary reactions with solid carbon do occur only the overall reaction scheme will be considered. For example, hydrogen is sometimes produced as a result of decomposition of methane with solid carbon in the pores [19]. In this case the overall reaction produces only H_2.

(ix) Surface temperatures involved are not high enough to cause ablation.

(x) There is a reaction between the volatiles and the oxidant in the gas phase. The volatiles, as mentioned earlier, are dominated by CH_4 and/or H_2. For the reaction scheme considered here, only one of the volatile species is reacting with the oxidant and the reaction is of general order. Normally the volatile species are dominated by methane on a mass basis*[45]. Moreover, stoichiometric requirement of oxygen for the pyrolysate lies around 4.0 [20]. The results to be presented are still true if a global reaction is available for the total pyrolysate.

Subject to the assumptions presented above, the system of equations which describe the ignition process of

_____

*In the range of pyrolysis temperature 1100°K to 1500°K.

a highly volatile coal particle, can now be solved to
establish the behavior of the particle, the conditions of
ignition, as well as a criterion for ignition. Since this
is a non-linear boundary value type problem, the solutions
must be carried out using an iterative procedure and for a
specific set of numerical data. The iterative procedure
which normally tends to obscure the trend of results can be
avoided and at the same time retain all the relevant
parameters if one makes the following additional assumptions
for the reaction in the gas phase.

    (xi) For a gas mixture with high activation energy,
most of the reaction occurs in a small interval
of temperature; this temperature is maximum
for a stoichiometric mixture; i.e., the flame
speed of a gas mixture of oxidant and fuel is
maximum when the mixture is at stoichiometric
proportion. Hence, one can justify for a
high activation reaction system that all the
reaction is concentrated at a stoichiometric
surface and the gas phase reaction can be
represented by a Dirac-delta function, similar
to a heterogeneous catalytic surface reaction.
It is not uncommon to treat a laminar deflagra-
tion wave as a simple discontinuity [39].

The approximation of concentrating all the reaction
at a surface was first used by Spalding [47] to obtain an

extinction criterion for an opposed jet diffusion flame. Later the theory was developed in a more general form by Peskin and Wise [48] for the ignition and deflagration of fuel drops evaporating under infinite evaporation kinetics. The same approximation was used by Annamalai and Durbetaki [49] to obtain the minimum injection rate and critical sizes of hydrocarbon droplets and coal particles necessary for maintaining a flame. This approximate approach is shown to be useful in providing an explicit solution for the gas phase Damkohler number in terms of the dimensionless burning rate and at the same time an explicit approximate solution for gas ignition temperature (GIT) in terms of known physical and chemical parameters of the system. Thus a qualitative picture and physical insight into the problem of ignition of a coal particle could be established.

4.2. A Criterion for Ignition

Strictly speaking the thermal ignition temperature[†] is defined as that temperature at which there is a "jump" transition process for a selected variable (e.g. burning rate, or heat transfer rate, etc.) from a chemically controlled regime to a diffusion controlled regime for a quasi-steady state problem (see Figure 3). This is called as absolute ignition criterion. Physically speaking if the temperature

---

[†]Ignition caused by pure thermal acceleration of exothermic reaction as opposed to ignition caused by radicals build up.
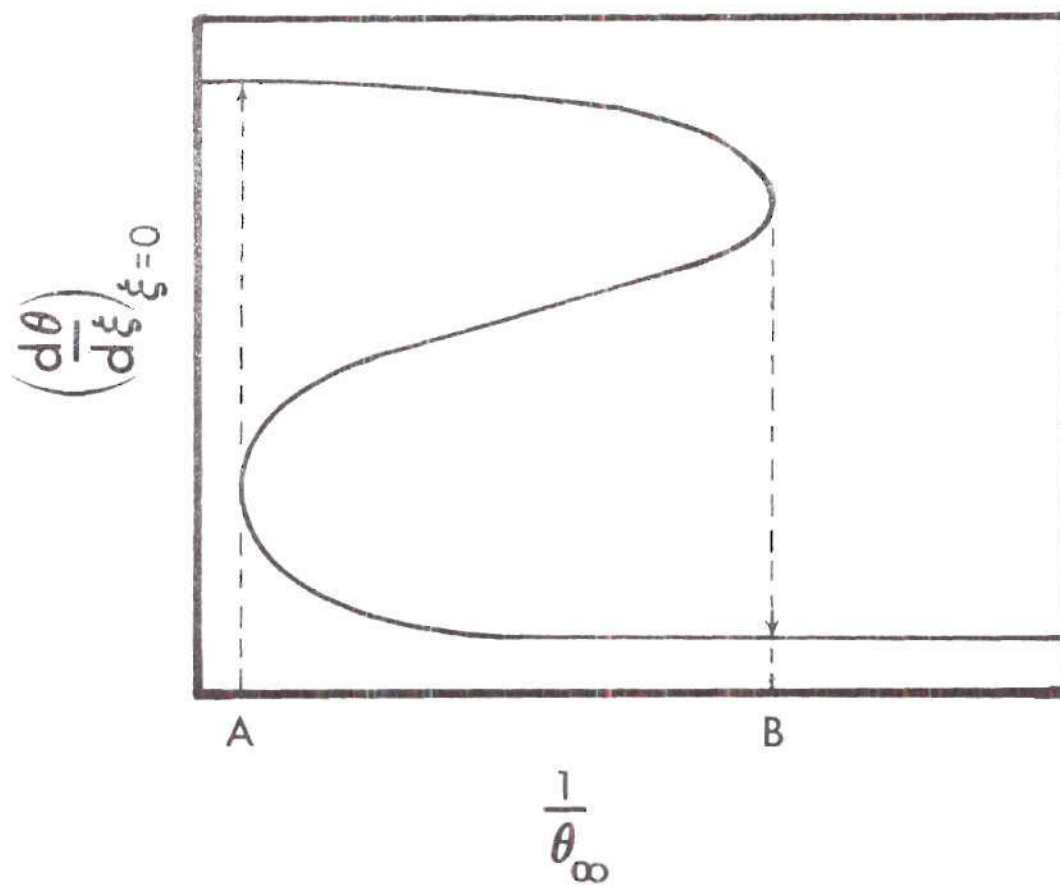
Figure 3. Illustration of Ignition Point Using
the Absolute Method
A: Ignition
B: Extinction

of the furnace into which a coal particle is introduced, is below the level which will cause an appreciable rate of gas phase reaction, then there is a steady rate of heat transfer from the furnace atmosphere to the particle. On the other hand, if the furnace temperature is high enough to cause a significant rate of reaction in the gas phase, then this reaction supplies heat to the furnace gases. If one compares the temperature gradients around the particle for the above two cases, one expects to find a furnace temperature at which the transfer rate will be zero. Summerfield et al. applied this adiabatic condition for the ignition of gases from a solid propellant in a hot stagnant atmosphere [50]. Such an adiabatic condition was used to perceive the ignition phenomenon for a hydrocarbon droplet [48,51]. Later Alkidas and Durbetaki applied this adiabatic condition, known as Van't Hoff criterion, to the problem of ignition of a combustible mixture by a heated surface, in the stagnation flow of an axisymmetric jet [52,53,54]. This criterion will be used to define the ignition temperature of volatiles evolved from the pyrolysis of coal. One must note that the Van't Hoff criterion is only a necessary condition of a self heating process occurring in the mixture and is not a sufficient condition for the ignition. The difference between these two temperatures or the corresponding difference in Damkohler numbers for given furnace temperature is not significant [54].

4.3.   General Solution of Coal Deflagration

Under Pyrolysis

4.3.1.   Equations and Boundary Conditions

The general conservation equations (27) through (36) with principal species as oxygen are simplified with the assumptions listed in Section 4.1. These equations are then solved with appropriate boundary conditions, in order to obtain the thermal gradient around the particle in terms of known physical and chemical parameters. The solutions are presented in this section while the details of the derivations are shown in Appendix A.1.

Governing Equations:

$$\frac{d^2 Y_0}{d\xi^2} + \frac{dY_0}{d\xi} = D_{III,g} \frac{\xi_w^2 \, e^{-\frac{1}{\theta}}}{\xi^4 \, \theta^n} Y_0^{n_0} Y_V^{n_V} \delta(\xi - \xi^*) \qquad \dagger \qquad (37)$$

where

Y_V = mass fraction of the volatiles,

Y_0 = mass fraction of oxygen,

ξ^* = nondimensional bulk velocity at the
        stoichiometric surface,

$\delta(\ )$ = Dirac-delta function,

$n = n_0 + n_V$, overall order of reaction,   (37a)

$\dagger$It is very important to see Appendix F for a discussion of this approximation.

$$D_{III,g} = \frac{\nu_0 W_0}{\rho D} A_g \, r_w^{\,2} \, (\frac{p}{E_g})^n \tag{37b}$$

n_0 = order of reaction with respect to oxygen

n_V = order of reaction with respect to volatile.

The variables θ and Y_V are obtained in terms of ϕ from the equation:

$$\phi = \frac{1 - e^{-\xi}}{1 - e^{-\xi_w}} \tag{29a,b}$$

where ϕ's are defined from equations (24) with $j = T$, $p = 0$ and $j = V$, $p = 0$.

Chemical Kinetics:

At the surface, Coal $\rightarrow$ V+C(s) $\tag{38a}$

In the gas phase, V+O_2 $\rightarrow$ V.O_2 $\tag{38b}$

Boundary Conditions:

As $\xi \rightarrow \xi_w$, $(\frac{d\theta}{d\xi}) = -Q_w^+$ $\tag{39}$

$$\varepsilon_V = 1 = D_{III,w} \frac{e^{-E_w/\theta_w}}{\xi_w} \tag{40}$$

$\varepsilon_i = 0$, for all $i \neq V$ $\tag{41}$

As $\xi \rightarrow 0$, $Y_0 = Y_{0,\infty}$ $\tag{42a}$

$$Y_V = Y_{V,\infty} \tag{42b}$$

where

$$D_{III,w} = \nu_V W_V A_w f(r_w) Y_{V,s}^{\ell} / r_w \rho D \tag{43}$$

$Y_{V,s}$ = mass fraction of volatiles in the solid at the time of ignition, $\simeq Y_{V,s}^{*}$

$Y_{V,s}^{*}$ = initial volatile content,

ℓ = order of reaction for the pyrolysis,

$Q_W^{+} = \dfrac{Q_W}{(C_p E_g / R^{\circ})}$, nondimnesional heat of absorption, (43a)

$Q_W = h_{V,+} - h_{V,-}$, heat of absorption (43b)

$h_{V,+}$ = enthalpy of the volatiles on the gas side,

$h_{V,-}$ = enthalpy of the volatiles in the solid phase,

ε_V = flux fraction of the volatiles,

$Y_{V,\infty}$ = ambient mass fraction of volatiles in the gas phase,

$Y_{0,\infty}$ = ambient mass fraction of oxygen in the gas phase.

Equation (37) subject to the boundary conditions (39) through (42) is integrated and the details of the solutions are shown in Appendix A.1. The results are shown below.

4.3.2. Results for Deflagration

Dimensionless bulk velocity at the surface:

$$\xi_w = \ln\left\{ 1 + \frac{\dfrac{\theta_\infty - \theta_w}{Q_w^+} + \dfrac{Y_{0,\infty}}{\nu_s}}{\dfrac{Q_w^+}{Q_g^+} + \dfrac{Y_{0,w}}{\nu_s}} \right\} \tag{44}$$

where

$\nu_s = \nu_0 W_0/\nu_V W_V$, stoichiometric mass of oxygen per unit amount of volatiles.

Dimensionless bulk velocity at the stoichiometric surface:

$$\xi^* = \ln\left\{ 1 + \frac{Y_{0,\infty}}{\nu_s} \right\} \tag{45}$$

Stoichiometric parameter:

$$\phi_{V0}^* = \frac{1}{1 - e^{-\xi_w}}\left\{ \frac{Y_{0,\infty}/\nu_s}{(1 + Y_{0,\infty}/\nu_s)} \right\} \tag{46}$$

Mass fraction of oxygen at the stoichiometric surface:

$$Y_0^* = Y_{0,w}\, e^{\xi_w - \xi^*} \tag{47}$$

Nondimensional temperature at the stoichiometric surface:

$$\theta^* = \theta_\infty + Q_g^+ \left\{ \frac{Y_{0,\infty}/\nu_s}{1 + \frac{Y_{0,\infty}}{\nu_s}} - \frac{Y_0^*}{\nu_s} \right\} - \frac{Y_{0,\infty}}{\nu_s} \left\{ \frac{Q_W^+}{(1 + \frac{Y_{0,\infty}}{\nu_s})} \right\}$$

$$- \frac{Y_{0,\infty}}{\nu_s} \left\{ \frac{(\theta_\infty - \theta_W)}{(1 + \frac{Y_{0,\infty}}{\nu_s})} \right\} \tag{48}$$

Gas phase Damkohler number:

$$D_{III,g} = \nu_s^{1-n_0} \frac{\xi^{*4}}{\xi_W^2} \frac{\theta^{*n}}{Y_0^{*n}} e^{\frac{1}{\theta^*}} \left\{ \frac{(Y_{0,\infty} - Y_0^*)/\nu_s}{(1 - e^{-\xi^*})} - \frac{Y_0^*}{\nu_s} \right\} \tag{49}$$

Nondimensional thermal gradient at large distance from the particle:

$$\left(\frac{d\theta}{d\xi} \right)_{\xi=0} = \theta_o' = \frac{\theta^* - \theta_\infty}{(1 - e^{-\xi^*})} \tag{50}$$

4.3.3. Comments

(1) One observes from equation (44) that the inert gas nitrogen does not appear in the equation. Hence for pyrolysis without any chemical reaction (i.e. oxygen acts as inert gas), the oxygen mass fractions are set equal to zero and

$$\tilde{\xi}_W = \ln \left\{ 1 + \frac{\tilde{\theta}_\infty - \tilde{\theta}_W}{\tilde{Q}_W^+} \right\} \tag{50a}$$

where

$\tilde{\xi}_W$ = the dimensionless pyrolysis rate in absence of gas phase chemical reaction,

$$\tilde{\theta}_W = T_W / (E_W/R^\circ),$$

$$\tilde{\theta}_\infty = T_\infty / (E_W/R^\circ),$$

(50b)

and from equation (40),

$$\tilde{\theta}_W = 1/\{ \ln (\frac{D_{III,W}}{\tilde{\xi}_W}) \}$$

(50c)

This is indeed the result for the dimensionless pyrolysis rate without gas phase chemical reaction (see Appendix A.2).

(2) From equation (45) one notes that as $Y_{0,\infty} \to 0$ $\xi^* \to 0$; i.e. the stoichiometric surface tends to infinity.

(3) Equation (48) is physically interpreted as follows: Reaction surface temperature = ambient temperature + temperature rise due to chemical heat release - temperature drop due to heat supply for pyrolysis - temperature drop due to heating of volatile mass from wall temperature to ambient temperature.

(4) Given the following physical and chemical parameters,

nondimensional ambient temperature (θ_∞)

ambient oxygen mass fraction $(Y_{0,\infty})$

nondimensional activation energy at the surface (E_w^+)

third Damkohler number at the surface $(D_{III,w})$

dimensionless endothermic heat of reaction at the
surface (Q_w^+)

dimensionless exothermic heat of reaction in the gas
phase (Q_g^+)

the required third Damkohler number in the gas phase $(D_{III,g})$ to generate a nondimensional bulk velocity at the surface (ξ_w) can be obtained using equations (44) through (49). The thermal gradient at large distance from the surface, required to determine the ignition temperature using the criterion presented in Section 4.2., is found from equation (50).

4.4. Solution for the Gas Ignition Temperature (GIT)

4.4.1. General Solution

In order to estimate the required furnace temperature for ignition in the gas phase, the Van't Hoff criterion is invoked, where $\theta_o' = 0$. The derivation is presented in Appendix A.3. The following results are obtained.

At the time of ignition,

$$\theta_o' = 0 \tag{51}$$

$$\theta_{\infty,I} = Q_W^+ (e^{\xi_W - \xi^*} - 1) + \frac{E_W^+}{\ell n(D_{III,w}/\xi_w)} \tag{52}$$

$$\left\{\begin{array}{l}\text{heat transfer}\\\text{at the surface}\end{array}\right\} \quad \left\{\begin{array}{l}\text{chemical kinetics}\\\text{at the surface}\end{array}\right\}$$

$$D_{III,g} = \frac{\nu_s^{1-n_0} \dfrac{Q_W^+}{Q_g^+} e^{\xi_W - \xi^*} \xi^{*4} \theta_{\infty,I}^n e^{\frac{1}{\theta_{\infty,I}}}}{\xi_w^2 [\{1 - \dfrac{Q_W^+}{Q_g^+} e^{\xi_W - \xi^*}\}\{1 - e^{-\xi^*}\}]^n} \tag{53}$$

4.4.2. Comments

(1) The reaction surface temperature is equal to the gas ignition temperature at the time of ignition; this is due to the adiabatic ignition criterion. When one uses the absolute ignition criterion (multi-transition), $\theta^* > \theta_{\infty,I}$ since one takes into account the heat loss to the furnace from the reaction zone.

(2) The nondimensional GIT consists of contributions from two mechanisms at the surface: (i) the transport of heat to the surface for the evolution of volatiles and (ii) the release of volatiles by finite chemical kinetics. On a close observation it is seen that the second term of equation (52) is nothing but the surface temperature (θ_w). As $D_{III,w} \to \infty$ $\theta_w \to 0$, which is not physically realistic. This is due to the neglect of the reverse char forming reaction. Under equilibrium conditions θ_w attains a finite value

(e.g. droplet burning with condensation and evaporation).

(3) The results obtained are true for any general order of gas phase and pyrolysis reactions. The results are valid when θ_w approaches an equilibrium value.

(4) Equation (53) is a very useful result for a variable pressure system. When H_2 reacts with O_2 in air, the reaction rate decreases with increase in pressure up to about 2 atm and then increases with further increase in pressure [55]. Since the pressure dependence mainly arises from the overall reaction order, then the overall reaction order must have been different at different pressures. At about 1 atm, the reaction rate of H_2 with O_2 is proportional to the hydrogen concentration while for methane with oxygen, the reaction rate is proportional to oxygen concentration [56]. This indicates that the reaction order is generally around unity at normal pressures for the oxidation of pyrolysate which mainly consists of H_2 and CH_4.

(5) With the surface Damkohler number as a parameter the gas phase Damkohler number is solved as a function of nondimensional bulk velocity at the surface from equation (53), for a given set of physical and chemical parameters. From equation (52), the coal particle ignition temperature $\theta_{\infty,I}$ is obtained.

4.4.3. Critical Parameters for Gas Ignition

There arises a situation where the stoichiometric or the reaction surface just hinges on to the particle surface.

Since the coal particle is not assumed to be very porous
to allow the flame to enter the particle (this violates the
boundary condition in a physical sense) we presume that for
specified physical and chemical parameters there is likely
to occur a critical condition where the reaction surface
just touches the particle surface. Such parameters are
called critical parameters and hence, no solution exists
beyond these values. This is readily obtained from equation
(52) by letting $\xi_w \to \xi^*$. Hence,

$$\theta_{\infty,I} = E_w^+ / \ln \left(\frac{D_{III,w}}{\xi^*} \right) \tag{53a}$$

Note that as $(D_{III,w}/\xi^*) \to 1$, $\theta_{\infty,I} \to \infty$. Using (53a) in (53)

$$D_{III,g} = \frac{\nu_s^{1-n_0} \bar{Q}_w^+ \xi^{*2} \left(\dfrac{E_w^+}{\ln \dfrac{D_{III,w}}{\xi^*}} \right)^n \left(\dfrac{D_{III,w}}{\xi^*} \right)^{\frac{1}{E_w^+}}}{\left\{ (1-\bar{Q}_w^+)(1-e^{-\xi^*}) \right\}^n} \tag{53b}$$

where

$$\bar{Q}_w^+ = Q_w / Q_g . \tag{53c}$$

There are four main parameters of interest in the
problem: (i) particle size, (ii) volatile content, (iii)
ambient mass fraction of oxygen and (iv) pressure. Given
any three parameters, the fourth one can be estimated from

the results shown below. The details of solution are shown
in Appendix A.4.

(a) Critical Size: It is of interest to estimate the
critical size for given volatile content, below which gas
ignition can not occur; i.e., all the volatiles can burn or
ignite only when surface ignition occurs; or for given
particle size if the volatile content falls below a certain
value, then these volatiles can burn or ignite once surface
ignition occurs. Such critical conditions are,

$$\left(\frac{d_w^+}{\sqrt{\xi^*}} \right)^{\frac{m}{2}} 2M_1 = \alpha_1 \; \ell n \; (\frac{d_w^{+m/2}}{\sqrt{\xi^*}})^2 \qquad (54a)$$

where

$$d_w^+ = d_w^\circ / \{d_w^\circ / (D_{III,w}^\circ)^{\frac{1}{m}}\} \qquad (54b)$$

d_w° = arbitrarily selected particle diameter,

$D_{III,w}^\circ$ = surface Damkohler number based on d_w°,

  = $2A_w (d_w^\circ)^m / \rho D$

m = order of pyrolysis with respect to particle
  size,

$$\alpha_1 = \left[\frac{D_{III,g}^\circ}{(D_{III,w}^\circ)^{\frac{2}{m}}} \frac{(1-\bar{Q}_w^+)(1-e^{-\xi^*})}{E_w^+} \right]^{\frac{1}{n}} \frac{1}{\bar{Q}_w^+ \nu_s^{1-n_0} \xi^{*2-\frac{2}{m}}} \qquad (54c)$$

$D^{\circ}_{III,g}$ = gas phase Damkohler number based on d°_{w}

$$M_1 = \frac{1}{n}\left(\frac{1}{E^+_w} - \frac{2}{m}\right) \tag{54d}$$

One can plot $(d^+_w{}^{m/2}/\sqrt{\xi^*})$ versus α_2 with M_1 as a parameter.

(b) <u>Critical Volatile Content</u>: From equations (53b), separating out the group containing $(D_{III,w}/\xi^*)$,

$$\left(\frac{D_{III,w}}{\xi^*}\right)^{M_2} = \alpha_2 \ \ell n \ \left(\frac{D_{III,w}}{\xi^*}\right) \tag{54e}$$

where,

$$M_2 = \frac{1}{n\,E^+_w} \tag{54f}$$

$$\alpha_2 = \left[\frac{D_{III,g}}{\nu_s{}^{1-n}\,\bar{Q}^+_w{}^0\,\xi^{*2}}\right]^{\frac{1}{n}} \frac{\{1-Q^+_w\}\{1-e^{-\xi^*}\}}{E^+_w} \tag{54g}$$

Since $D_{III,w}$ is proportional to $Y^{\ell}_{V,s}$ (see equation (43)), the solution of equation (54e) gives the minimum volatile content for gas phase ignition. Such a volatile content below the critical level has to ignite along with the oxidation of solid carbon.

(c) _Critical Ambient Oxygen Mass Fraction:_ In this case the particle size is fixed. One is interested to know the critical $Y_{0,\infty}$ which would cause the reaction surface to anchor on the particle surface. In order to obtain a more general result the following approximation is used.

$$Y_{0,\infty} < 1$$

Also $\nu_s > 1$ for most of the pyrolysates. Hence $\xi^* \ll 1$. For small ξ^*,

$$1 - e^{-\xi^*} \simeq \xi^* \tag{55a}$$

Using such an approximation, the following results are obtained

$$\left(\frac{d_w^+}{\sqrt{\xi^*}} \right)^{\frac{m}{2}} = \alpha_3 \; \ell n \; \{ \frac{d_w^{+m/2}}{\sqrt{\xi^*}} \}^2 \tag{55b}$$

where

$$\alpha_3 = \frac{1}{E_w^+} (1-\bar{Q}_w^+) \left(\frac{D_{III,g}}{D_{III,w}} (2-n) \frac{1}{\bar{Q}_w^+ \, \nu_s}^{1-n_0} \right)^{\frac{1}{n}} \tag{55c}$$

$$M_3 = (nE_W^+ + 1 - 2E_W^+)/nE_W^+ \qquad (55d)$$

Note that equations (55b) and (54a) are mathematically similar. It is shown later that such a nonlinear algebraic equation also occurs in the prediction of TIP points.

4.4.4. Explicit Approximate Solutions for Ignition Under Limiting Cases

As seen from equation (53), the exponential functions are much stronger compared to the other functions. Hence the terms in square brackets of equation (53) will be treated as constant and this constant is evaluated by letting $\xi_W \to \xi^*$. Moreover the term (Q_W^+/Q_g^+) is much less than unity. Under these conditions the following explicit relations are obtained.

Case (i) Chemical Kinetics Control of Pyrolysis at the Surface. This is the most common case in a real system since normally Q_W^+ is very small. For every gram of volatiles released by pyrolysis, about 400 to 700 calories of heat has to be supplied to the solid. This could be supplied by surface oxidation of the solid carbon of about .10 grams for every gram of volatiles released (this estimation is based on the oxidation of carbon to carbon monoxide). Under these conditions the endothermic heat of absorption Q_W^+ approaches a low value (but nonzero). Comparatively speaking, $D_{III,W}$ approaches small value or the activation

energy at the surface is very large. For example, if H_2 is the volatile species, E_W^+ approaches to a value of about three for a pure pyrolysis without combustion. In other words, the heat transfer term in equation (52) is very small compared to the chemical kinetics term. Hence,

$$\xi_w = \left[\frac{D_{III,w}}{D_{IV,g}} \right]^{\frac{1}{E_W^+}} \frac{E_W^+}{(2E_W^+ + 1)} \tag{56a}$$

$$\frac{1}{\theta_{\infty,I}} = \frac{1}{2E_W^+ + 1} \, \ell n \, D_{c,g} \tag{56b}$$

where,

$$D_{c,g} = D_{IV,g} \, D_{III,w}^2 \tag{56c}$$

$$D_{IV,g} = \frac{1}{\underset{\nu_s}{1-n_0}} \frac{D_{III,g}}{\bar{Q}_W^+} \frac{1}{\xi^{*4}} \left[\frac{(1-e^{-\xi^*})(1-\bar{Q}_W^+) \, \ell n \, \frac{D_{III,w}}{\xi^*}}{E_W^+} \right]^n \tag{56d}$$

Note that $D_{IV,g} \propto p^{+n}$

where

$$p^+ = p/p_a$$

p_a = ambient pressure.

The slope of a plot of the inverse of the nondimensional temperature versus $\ln p^+$ can be at the most of the order of magnitude equal to n, the general overall reaction order. Also, the ignition temperature increases very strongly with decrease in the size of the particle for volumetric pyrolysis as seen from equations (56b) and (56c).

In order to plot the expression given in equation (55) one must have knowledge of the gas phase activation energy. In order to circumvent this, the following equation can be adopted for the experimental correlation. From equation (56b) one solves for $p^+ = 1$ and $p^+ = p^+$, and find the ratio,

$$\frac{(T_\infty, I)_{p^+=1}}{(T_\infty, I)_{p^+=p^+}} = 1 + \frac{\ln p^{+n}}{\ln (D_{IV,g} D_{III,w}^2)_{p^+=1}} \tag{58}$$

Note that

$$D_{IV,g} \ \alpha \ \frac{1}{E_w^{\ n}}$$

Case (ii) Heat Transfer Control at the Surface. For this case the chemical kinetics is very fast compared to the heat transfer rate and hence $D_{III,w} \to \infty$. Again the exponential functions are very strong compared to the other functions. Hence from equations (53) and (52),

If $\theta_w <<< \theta_{\infty,I}$,

$$\frac{1}{\theta_{\infty,I}} = \ln \{D_{IV,g}\} \tag{59a}$$

$$D_{IV,g} = \frac{D_{III,g}}{\nu_s^{1-n_0}} \frac{\xi_w^2}{\bar{Q}_w^+} \xi^{*4} \left(\frac{(1-\bar{Q}_w e^{\xi_w-\xi^*})(1-e^{-\xi^*})}{\{\bar{Q}_w^+ (e^{\xi_w-\xi^*}-1)\}} \right)^n \tag{59b}$$

If $n = 2$, $\bar{Q}_w^+ << 1$ and $\xi_w >> \xi^*$, then $D_{IV,g}$ is almost independent of ξ_w. This case does not appear to apply to most of the coal particles considered here and any further discussion is not relevant.

4.5. Solutions for the Heterogeneous Ignition Temperature (HIT)

4.5.1. Results for HIT

It was mentioned in Section 2.1 that a theory on heterogeneous ignition is available in the literature [17]. However there appears to be no steady state solution for heterogeneous ignition of coal particles which has included the effects of mass transfer on heat transfer; also explicit solution for HIT is not available. This section presents the governing equations and solutions.

Assumptions: (i) Gas phase reactions are absent, (ii) The surface reactions produce CO or react along with

volatiles in the solid phase, (iii) Radiative heat transfer is negligible, (iv) Oxygen in the solid coal is absent, (v) There is no pyrolysis and (vi) Semanov's thermal theory of ignition is applicable (see Section 2.1).

Mass:

$$\dot{m} = \text{constant} \tag{60a}$$

Species and Energy:

$$\frac{Y_0 - Y_{0,\infty}}{Y_{0,w} - Y_{0,\infty}} = \frac{\overline{\theta} - \overline{\theta}_\infty}{\overline{\theta}_w - \overline{\theta}_\infty} = \frac{1 - e^{-\xi}}{1 - e^{-\xi_w}} \tag{60b}$$

where

$$\overline{\theta} = T/(E_{w,h}/R^\circ), \quad \text{nondimensional temperature} \tag{60c}$$

$E_{w,h}$ = activation energy for heterogeneous reaction.

Chemical Reactions:

$$\text{Coal} + 0 \rightarrow \text{Coal.0} \tag{60d}$$

Boundary Conditions:

$$A \quad \xi = \xi_w, \quad \frac{d\overline{\theta}}{d\xi} = Q^+_{w,h} \tag{60e}$$

$$\varepsilon_0 = \overline{v}_s (D_{III,w})_h \, Y_{0,w} \, e^{-\frac{1}{\overline{\theta}_w}} / \xi_w \overline{\theta}_w, \quad = -\overline{v}_s \tag{60f,g}$$

$$\varepsilon_i = 0, \text{ for chemically inert species} \tag{60h}$$

where

$$Q_{w,h}^{+} = Q_{w,h}/(C_p E_{w,h}/R^{\circ}),$$

$Q_{w,h}$ = heating value per unit mass of coal for heterogeneous reaction,

$$\bar{\nu}_s = \nu_0 W_0/(\nu W)_{coal}, \tag{60j}$$

$$(D_{III,w})_h = A_{w,h} \; r_w \; P/E_{w,h} \quad \rho D, \tag{60k}$$

Damkohler number for heterogeneous reaction

$A_{w,h}$ = preexponential factor for heterogeneous reaction.

See Appendix B.1 for the details of results. At the time of ignition,

$$\xi_w = (D_{III,w})_h \; \frac{e^{-\frac{1}{\bar{\theta}_w}}}{\bar{\theta}_w} \; Y_{0,\infty} \{e^{-\xi_w} - \frac{1 - e^{-\xi_w}}{Y_{0,\infty}/\bar{\nu}_s}\} \tag{61a}$$

$$\bar{\theta}_w - \bar{\theta}_\infty = (e^{\xi_w} - 1) \; Q_{w,h}^{+} \tag{61b}$$

$$1 = e^{\xi_w} \; \frac{d\xi_w}{d\bar{\theta}_w} \; Q_{w,h}^{+} \tag{61c}$$

Equations (61) can be solved by using the Newton-Raphson technique.

4.5.2. Comments

(1) If

$$(\tilde{D}_{IV,w})_h = (D_{III,w})_h \, Q^+_{w,h} \, \bar{\nu}_s, \text{ modified}$$

$$\text{fourth Damkohler number, and} \quad (61d)$$

$$e^{\xi_w} \simeq 1 + \xi_w,$$

then one can attempt to universally correlate HIT with $(D_{IV,w})_h$ with $(Y_{0,\infty}/\nu_s)$ as a parameter.

(2) As mentioned earlier (section 2.1) there arises a situation when there is no longer a finite jump in temperature at the time of ignition for small particles and low oxygen concentration. Such critical parameters are given.

4.5.3. Critical Parameters for Heterogeneous Ignition

Here rather than following an iterative procedure for a set of numerical data, only approximate solutions are presented. Critical conditions for heterogeneous ignition arise when the maximum slope of the heat release rate with the wall temperature falls below the heat loss rate with wall temperature; i.e. at the critical point,

$$\left(\frac{dQ^+_{chem}}{d\bar{\theta}_w}\right)_{max} = \frac{dQ^+_L}{d\bar{\theta}_w} \quad (62a)$$

where

$$\dot{Q}^+_{chem} = \text{heat liberation rate,} \quad \frac{\dot{Q}_{chem}\, R^\circ}{4\pi\lambda_w r_w E_{w,\hbar}}, \quad = \xi_w Q^+_{w,\hbar}$$

$$\dot{Q}^+_L = \text{heat loss rate,} \quad \frac{\dot{Q}_L\, R^\circ}{4\pi\lambda_w r_w E_{w,\hbar}},$$

Let $\quad e^{\xi_w} \simeq 1 + \xi_w$.

With these approximations in equations (61) and (62a) the maximum $(d\dot{Q}_{chem}/d\overline{\theta}_w)$ is found (see Appendix B.2). Then at the time of ignition for a critical condition,

$$\overline{\theta}_w^{\,6} - 4\overline{\theta}_w^{\,5} + 6\overline{\theta}_w^{\,4} + \overline{\theta}_w^{\,2}\left(\frac{R}{2}-4\right) + \overline{\theta}_w^{\,2}\left(1-\frac{3}{2}R\right) + \frac{5}{4}R\overline{\theta}_w - \frac{R}{4} = 0 \quad (62b)$$

where

$$R = Q^+_{w,h}\left(\frac{Y_{0,\infty}}{\overline{\nu}_s}\right) / \left(1 + \frac{Y_{0,\infty}}{\overline{\nu}_s}\right) \quad (62c)$$

Also,

$$\frac{Z_{crit}\, R\, \dfrac{e^{-\frac{1}{\overline{\theta}_w}}}{\overline{\theta}_w}\left(\dfrac{1}{\overline{\theta}_w^{\,2}} - \dfrac{1}{\overline{\theta}_w}\right)}{1 + Z_{crit}\,\dfrac{e^{-1/\overline{\theta}_w}}{\overline{\theta}_w}} = 1 \quad (62d)$$

where

$$Z_{crit} = (\tilde{D}_{III,w})_h \ (1 + \frac{Y_{0,\infty}}{\bar{\nu}_s}) \tag{62e}$$

$$(\tilde{D}_{III,w})_h = (D_{III,w})_h \ \bar{\nu}_s \tag{62f}$$

It is readily seen that with $\bar{Q}^{+}_{w,h}$ as a parameter, Z_{crit} as an independent variable and $(Y_{0,\infty}/\bar{\nu}_s)$ as a dependent variable one can obtain universal plots to determine the critical conditions.

4.5.4. Approximate Explicit Solution for HIT

An approximate solution is obtained in order that an explicit ignition criterion for determining the phase of ignition can be presented later. The approximate procedure for finding HIT is based on the assumption that mass transfer effects are small. However, this assumption is used only to find a correlating group. Derivations are shown in Appendix B.3. The results are presented below:

$$1 = Y_{0,\infty} \ (D_{IV,w})_h \ e^1 \ \frac{e^{-1/\bar{\theta}_{\infty,I}}}{\bar{\theta}^3_{\infty,I}} \tag{63a}$$

where

$\bar{\theta}_{\infty,I}$ = ambient nondimensional temperature at the time of ignition.

And one can solve for $\bar{\theta}_{\infty,I}$. A fit is made for $\bar{\theta}^3_{\infty,I}$ in terms of an exponential

$$\frac{1}{\bar{\theta}^3_{\infty,I}} = \bar{b} \; e^{\bar{a}/\bar{\theta}_{\infty}} \qquad (63b)$$

where $\bar{b}$ and $\bar{a}$ are evaluated by a least square fit. Thus, from equations (63a) and (63b)

$$\frac{1}{\bar{\theta}_{\infty,I}} = \{\frac{1}{1-\bar{a}}\} \; \ell n \; \{D_{c,h}\} \qquad (63c)$$

where

$$D_{c,h} = \bar{b} \; (D_{IV,w})_h \; Y_{0,\infty} \; . \qquad (63d)$$

When

$$10 < \frac{1}{\bar{\theta}_{\infty,I}} < 20,$$

$$\bar{a} = 0.160, \; (1-\bar{a})^{-1} = 1.19$$

$$\qquad (63e)$$

$$\bar{b} = e^{5.617}$$

4.6. A Criterion for the Phase of Ignition

The criterion for the phase of ignition to be deduced could give qualitative accuracy though there is a doubt regarding quantitative accuracy because of the assumptions involved. On an overall basis there are three distinct reaction regimes:

(i) the heterogeneous oxidation,

(ii) the endothermic pyrolysis at the surface, and

(iii) the exothermic gas phase oxidation of the pyrolysate.

Note that heterogeneous oxidation includes not only oxidation of carbon but also the oxidation of some volatiles in the solid phase. The problem is formulated on an asymptotic basis; i.e., regime (i) is assumed to proceed independently of regimes (ii) and (iii). In the presence of volatile evolution, the oxidation rate of solid carbon will be less since some oxygen will be consumed by oxidation of volatiles in addition to the decrease due to the radial mass injection. Also the oxidation rate of the pyrolysate will be lower since there is less oxygen concentration in the reaction zone, for this non-asymptotic case. Thus there is a decrease in the oxidation rates of carbon and as well as of the pyrolysate. This occurrence validates the following ignition criterion for determining the phase of ignition which is based on the results for GIT and HIT obtained on an asymptotic basis. If both pyrolysis and subsequent oxidation of the

volatiles in the gas phase, and heterogeneous surface
oxidation proceed at the same rate which would have occurred
if only one of the above two oxidation processes were taking
place, then ignition is said to occur in that particular
phase whose required ignition temperature is lower. Accord-
ingly, if ignition is to occur in the gas phase

$$T_{I,g} < T_{I,h} \tag{64a}$$

where

$$T_{I,g} = GIT,$$

$$T_{I,h} = HIT.$$

Then using equations (67e), (56b), and (64a), one obtains
the following equation for determining the phase of ignition.

$$\left\{ \frac{(D_{c,h})^{1.4332(2\overline{E}_w^+ + \overline{E}_g^+)}}{D_{c,g}} \right\} \begin{array}{c} < \\ = \\ > \end{array} \left\} 1, \begin{array}{c} \text{gas phase} \\ \text{TIP point} \\ \text{heterogeneous} \end{array} \right. \tag{64b}$$

where,

$$\overline{E}_w^+ = E_w/E_{w,h}, \quad \overline{E}_g^+ = E_g/E_{w,h}^+$$

For a given set of kinetic parameters, one is interested to know TIP particle size and TIP mass fraction of oxygen, where transition of ignition occurs from one phase to the other phase. *See Appendix C for derivations.*

4.6.1. TIP Particle Size

The result for the TIP particle size derivation is

$$\left(\frac{d_w^+}{\sqrt{\xi^*}}\right)^{\frac{m}{2}} \; 2M_4 = \alpha_4 \; \ell n \left(\frac{d_w^+}{\sqrt{\xi^*}}\right)^{\frac{m}{2}} \; 2 \tag{65a}$$

where

$$M_4 = \frac{1.4332 \; (2\overline{E}_w^+ + \overline{E}_g^+)}{mn} - \frac{2m+2}{mn} \tag{65b}$$

$$\alpha_4 = \left[\frac{\alpha_g}{\alpha_h \; 1.4332 \; (2\overline{E}_w^+ + \overline{E}_g^+)}\right]^{\frac{1}{n}} \tag{65c}$$

$$\alpha_g = \frac{(1-e^{-\xi^*})^n}{\xi^{*(2m-2)/m}} \; \frac{\overset{\circ}{D}_{III,g}}{\overset{\circ}{D}_{III,w}^{2/m}} \; \frac{1}{E_w^{+n}} \; \frac{1}{\nu_s^{1-n_0}} \; \frac{(1-\overline{Q}_w^+)^n}{\overline{Q}_w^+} \tag{65d}$$

$$\alpha_h = \xi^{*\frac{1}{m}} \; \frac{(\overset{\circ}{D}_{III,w})}{(\overset{\circ}{D}_{III,w})^{\frac{1}{m}}} \; \overline{Q}_{w,h}^+ \; e^{4.57} \; Y_{0,\infty} \tag{65e}$$

One observes that the equation is mathematically similar to equations (54a) and (55b).

4.6.2. TIP Oxygen Mass Fraction

As before $(e^{\xi^*}-1)$ is approximated as ξ^* for small ξ^*.

$$\left(\frac{D_{III,w}}{\xi^*}\right)^{2M_5} = \alpha_5 \ \ell n \ \left(\frac{D_{III,w}}{\xi^*}\right)^2 \tag{66a}$$

where

$$M_5 = \frac{-4-1.433 \ (2\bar{E}_w^+ + \bar{E}_g^+)+n}{n} \tag{66b}$$

$$\alpha_5 = \left[\frac{\gamma_g}{1.433(2\bar{E}_w^+ + \bar{E}_g^+)} \right]^{\frac{1}{n}} \tag{66c}$$

$$\gamma_g = \frac{(1-\bar{Q}_w^+)^n}{\bar{Q}_w^+} \ \frac{D_{III,g}}{\nu_s}^{1-n_0} \ (D_{III,w})^{(n-2)} \ \frac{(\ell n \ \frac{D_{III,w}}{\xi^*})^n}{E_w^{+^n}} \tag{66d}$$

$$\gamma_h = D_{III,w} \ \nu_s \ (D_{III,w})_h \ \bar{Q}_{w,h}^+ \ e^{4.57} \tag{66e}$$

Needless to say, the equation is the same as in section 4.6.1. For a given particle diameter d_w, the required concentration can be evaluated.

CHAPTER V

RESULTS AND DISCUSSION FOR THE

IGNITION CHARACTERISTICS

In this section selective quantitative results which
are obtained through the use of equations presented in
Section 4 are discussed. Section 5.1 lists the kinetic
values for the three reactions: (i) heterogeneous oxidation,
(ii) pyrolysis at the surface and (iii) gas phase oxidation
of the pyrolysate. The results for the gas ignition tempera-
ture (GIT) including the variation of HIT with (a) oxygen
concentration, (b) particle size, and (c) pressure, and as
well as the critical parameters for gas ignition are discussed
in Section 5.2.1. Section 5.2.2 compares the iterative
results with the approximate explicit results. The results
for the heterogeneous ignition temperature (HIT) are
presented in Section 5.3. Section 5.3.1 discusses the
variation of HIT with the fourth Damkohler number, oxygen
concentration, and particle size. The critical parameters
for heterogeneous ignition are discussed in the same section.
Comparison of the iterative results with the approximate
results for HIT is made in Section 5.3.2 and results are
discussed. Finally Section 5.4 presents a "transition of
ignition phase" (TIP) diagram for the indication of probable

ignition phase and the corresponding physical and chemical parameters are found from the same diagram. Also, an example is given for a bituminous coal particle to illustrate the order of error involved between the graphical procedure (somewhat more exact result) with the results obtained from the TIP diagram (an approximate procedure).

5.1. Chemical Kinetics and Physical Constants

A quantitative evaluation of ignition temperature due to gas phase or surface reactions requires the chemical kinetics of all three reactions (see Section 4.6). Also, the overall chemical kinetics for surface oxidation which includes oxidation of some volatiles in the solid phase is needed. For surface oxidation, the chemical kinetic constants were presented by Bhaduri, et al. [17] which are tabulated for three different coals in Table 1. The chemical kinetic constants, tabulated here, are such that a theoretical prediction for HIT gives a good correlation with experimental results. Table 2 presents the kinetics of pyrolysis at heating rates comparable to furnace conditions for a variety of coals [42,57]. Note that though Tables 1 and 2 tabulate kinetic constants for the same type of coals (i.e. bituminous, lignite and anthracite), they are not chemically similar coals, i.e. bituminous coals extracted at different places will have somewhat different chemical kinetics. But one could not trace such a tabulation in the literature. Hence

Table 1. Chemical Kinetics Data for Heterogeneous Oxidation of Coals

Coal No.	Coal Type	Q_w cal/gm	$E_{w,h}$ cal/mole	$Q_{w,h}^+$	$(D_{III,w})_h$ for $100\mu m$ Particle	$\bar{\nu}_s$	Reference
1	Bituminous	4978	29600	1.29	380.0	1.72	[17]
2	Lignite	2500	20000	.955	85.0	.885	[17]
3	Anthracite	6010	33490	1.370	418.0	1.885	[17]
4	Brown	2267.0	13550	1.285	43.0	1.333	[18]

Table 2. Chemical Kinetics Data for Pyrolysis of Some Coals

Coal No.	Coal Type	E_w cal/mole	Dry Basis Volatile Content	$*D_{III,w}$	References	Remarks
11	Bituminous	17700	.31	260.0	[57]	Heating rate 2.5 to $4.0 \times 10^4 °C/sec$
12	Bituminous	17700	.35	400.0	[57]	Same
13	Bituminous	17700	.367	1025.0	[57]	Same
14	Bituminous	17700	.351	470.0	[57]	Same
15	Bituminous	11800	.398	2.80	[42]	Based on single reaction model $10^4 °C/sec$
21	Lignite	11100	.374	1.05	[42]	Same
31	Anthracite	28100	.114	1015.0	[57]	Heating rate 2.5 to $4 \times 10^4 °C/sec$

$Q_w \simeq 420$ cal/gm of pyrolysate [24,59], $Q_w^+ \simeq .085$

$*$Based on dry basis volatile content for particle of 100μm diameter. Normally moisture is removed at about 100°C.

one assumes a priori for calculation purposes that they are chemically similar coals. Finally, the overall kinetics of the pyrolysate are not available; on the other hand (i) the stoichiometric requirement of oxygen for complete combustion of the pyrolysate and (ii) an analysis of the pyrolysate, strongly indicate that the pyrolysate is dominated by methane gas. Hence for the purpose of quantitative estimation of GIT, one assumes that the kinetics of oxidation of pyrolysate is the same as those of methane. For methane oxidation VanTigglen et al. reported the overall kinetics based on flame velocity measurements [58].

$$E_g = 38000 \ \text{cal/mole}$$

$$A_g \nu_0 W_0 = 2.48 \times 10^{10} \ \text{gm/mole-sec}$$

$$n_0 = 1.4$$

$$n_V = -.4$$

$$Q_g = 11979 \ \text{cal/gm}, \quad Q_g^+ = .242$$

For properties assume,

$$(\rho D)_{1300°K} = .67 \times 10^{-3} \ \text{gm/cm-sec},$$

$$C_p = .26 \text{ cal/gm } °K.$$

Though the solutions presented in Section 4 are generally true for any variation in physical and chemical constants with respect to pressure, particle size heating rate etc., it is assumed that all kinetic and physical constants do not vary with pressure, for the quantitative calculations.

Tables 1 and 2 give the kinetic constants only in terms of Damkohler numbers, while the references give them in terms of frequency factors. The method of conversion is explained in Appendix D.

5.2. Gas Ignition Temperature (GIT)

5.2.1. Exact Solutions

(i) Variation with Oxygen Concentration. The non-linear algebraic equations (52) and (53) were solved using the Newton-Raphson method for the two unknowns ξ_w and $\theta_{\infty,I}$. Figure 4 shows variation of GIT with $Y_{0,\infty}$ for coal number 15. For a given $D_{III,g}$ and $D_{III,w}$, as $Y_{0,\infty}$ is increased the nondimensional GIT increases. This is explained as follows.

As the oxygen concentration is increased, first the stoichiometric surface moves toward the particle surface. For the same reaction temperature, then the surface temperature increases which then liberates more volatiles through pyrolysis. But this increased amount of volatiles
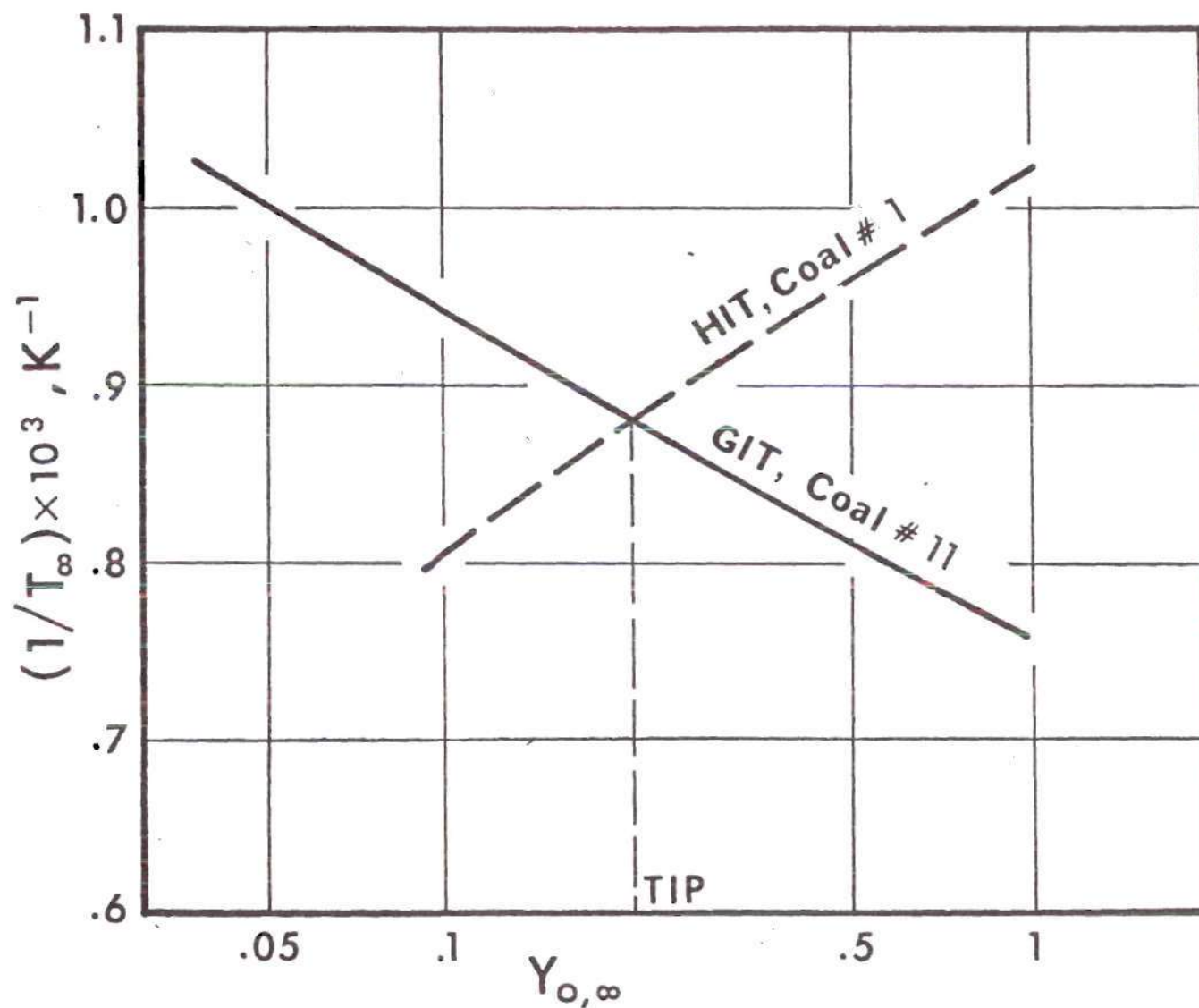
Figure 4.   Variation of GIT (Gas Ignition Temperature) with Ambient Oxygen Mass Fraction at Fixed Particle Size; Bituminous Coal

necessitates more heat supply from the reaction zone which now has a reduced reaction surface area. With an adiabatic ignition criterion, this means that an increase in heat loss to the particle surface, the reaction rate has to be increased which will consume more oxygen and volatiles. The increase of reaction rate is achieved by the rise in reaction temperature which is nothing but the ignition temperature. The increased pyrolysis rate tries to push away the reaction surface; but the rate is controlled by finite kinetics at the surface. Hence, this effect is not significant in this model compared to "push in" by the increased oxygen concentration. This is contrary to the familiar droplet burning problem where the flame moves away from the particle surface with increase in oxygen concentration. This occurs because with an infinite kinetics model, both at the droplet surface and in the gas phase, the flux fraction of oxidant is proportional to the flux fraction of fuel, while in the present problem of ignition, such fast kinetics do not exist.

As the oxygen concentration is lowered, the reaction surface moves away from the particle surface. Since an adiabatic ignition criterion considers heat loss only to the particle surface, then there is negligible heat loss from the reaction surface and consequently, a very low ignition temperature is obtained. Low ignition temperature means low reaction temperature. Hence, it appears although

no gas phase reaction exists. Then one obtains the pyrolysis rates for the two cases: (i) gas phase reaction is present and (ii) gas phase reaction is absent. If the ratio of the former rate to the latter rate falls below about 1.1, at a certain oxygen concentration, then it is assumed that the model fails at this low oxygen concentration. This lower limit oxygen mass fraction lies around 0.05.

With increasing oxygen concentration, it is established that the reaction surface moves toward the particle surface. Then there must be an upper limit of oxygen concentration at which the reaction surface just touches the particle surface. Moreover, a higher flux of pyrolysate must be able to keep away the reaction surface from the particle surface and hence the upper limit oxygen mass fraction must increase. This trend is exhibited in Figure 5 for an arbitrary set of physical and chemical constants. The straight line AB corresponds to the critical condition $\xi_w = \xi^*$, while the other curves give the exact solution for ξ_w at different surface Damkohler numbers. The intersections of the curves with the line AB gives the corresponding upper limit oxygen concentrations for the given stoichiometry. For coal number 11, 21 and 31, at a particle size of 100 μm solutions could not be obtained.

(ii) Variation with Particle Size. The results for variation of GIT with particle size are plotted in Figure 6a and 6b. The approximate result indicates (see equation
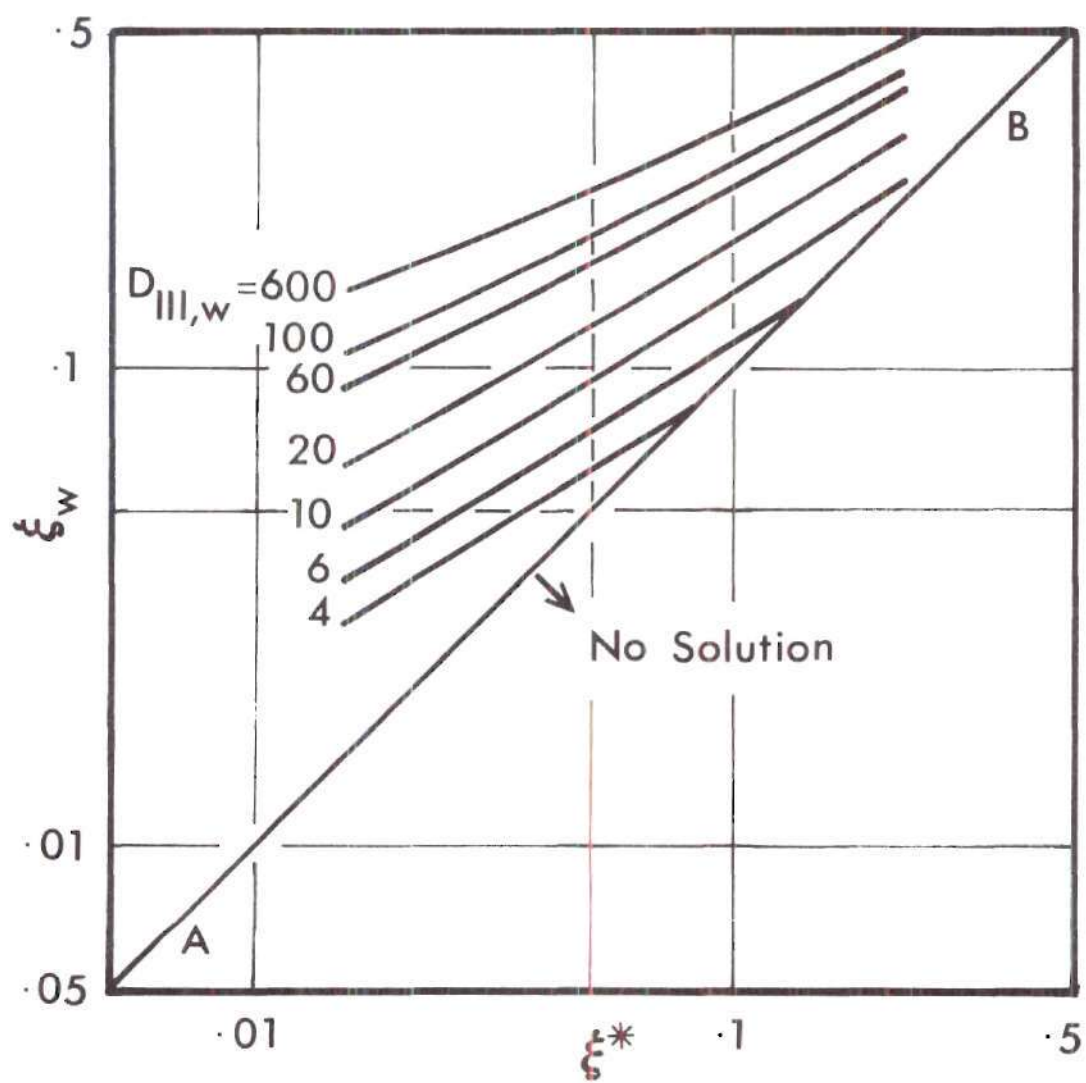
Figure 5. Variation of ξ_w with ξ^*

$(D_{III,g} = 200, \, Q_w^+ = .1, \, Q_g^+ = 2.5,$

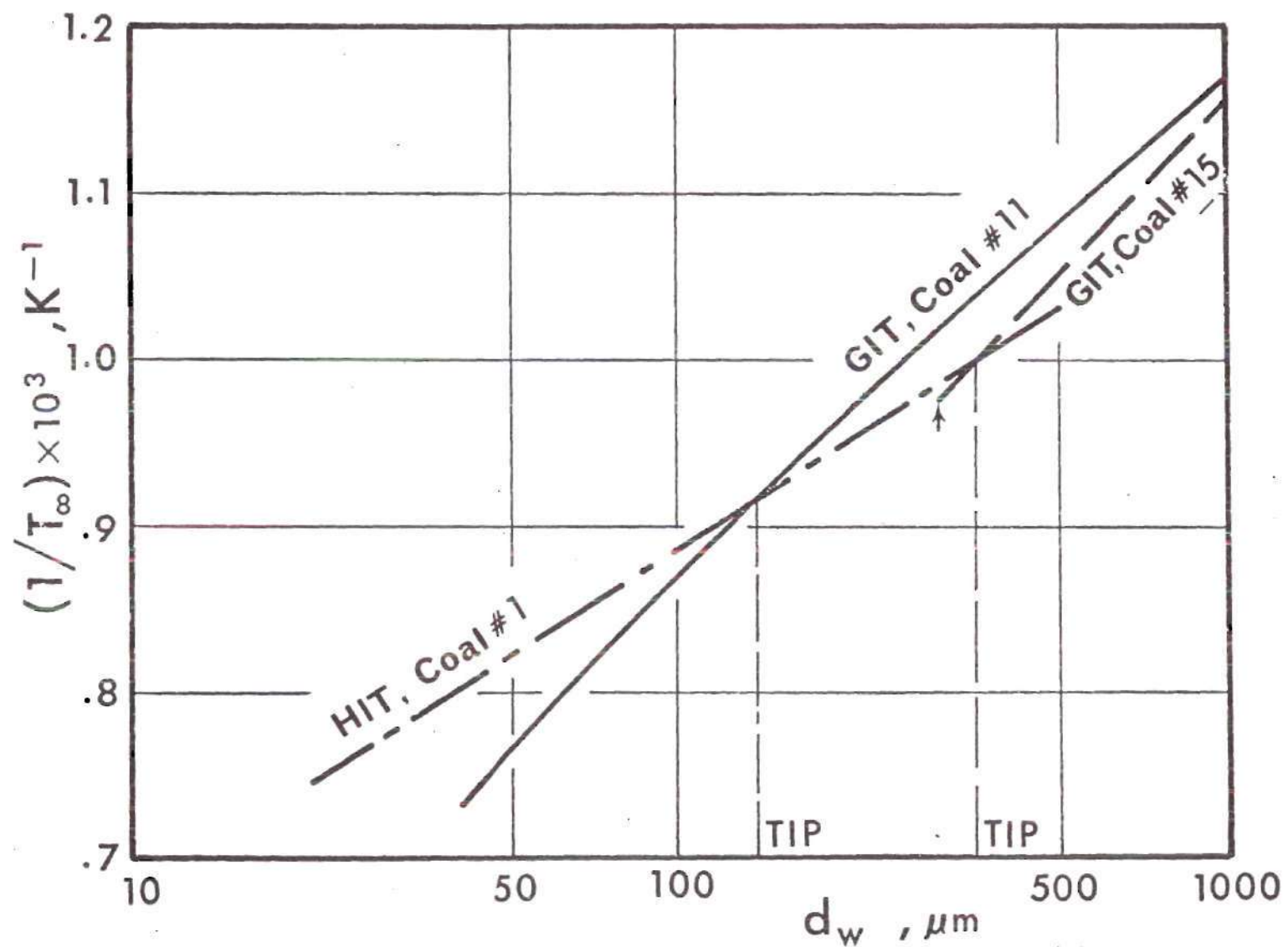$E_w^+ = .3, \, n_0 = .5, \, n_V = .5, \, \nu_s = 4)$

Figure 6a.   Variation of GIT and HIT with Particle Size at Fixed Oxygen
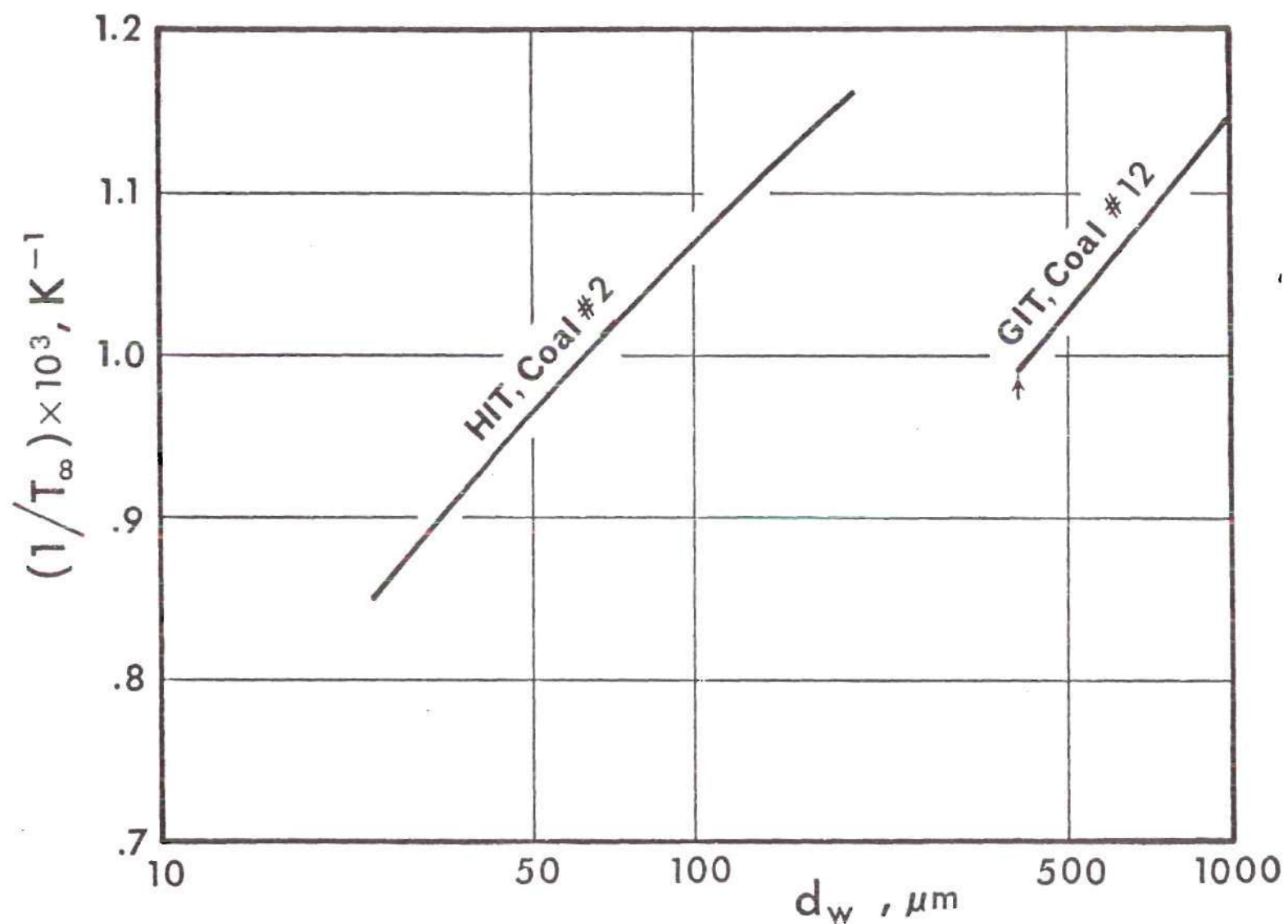Concentration; Bituminous Coal

Figure 6b.   Variation of GIT and HIT with Particle Size at Fixed Oxygen
Concentration; Lignite Coal

(56b)) that the GIT is a strong function of the particle size. With increase in the particle size, there is an increased liberation rate of pyrolysate from the particle as well as an increased gas phase reaction rate at lower temperatures; hence there is a decrease in the GIT. For the anthracite particles, since the activation energy is so high and the surface Damkohler number is low, one could not obtain the solution for the GIT even for a particle of diameter 1000 μm beyond the practical range of interest.

(iii) Variation with Pressure. Figure 7a illustrates the behavior of the GIT when the pressure of the ambient atmosphere is varied with oxygen concentration as a parameter for a given particle size. It is seen that an increase of pressure normally reduces the ignition temperature. However, the decrease is only about 50 percent when the pressure is increased from .01 atm to 10 atm. Figure 7b illustrates the behavior for coals number 21, 15 and 31. Results are doubtful at subatmospheric pressures since the kinetics of oxidation of methane are found to be entirely different [56].

(iv) Critical Parameters for Gas Ignition. The general equation for determination of the critical parameters for this problem is given as follows:

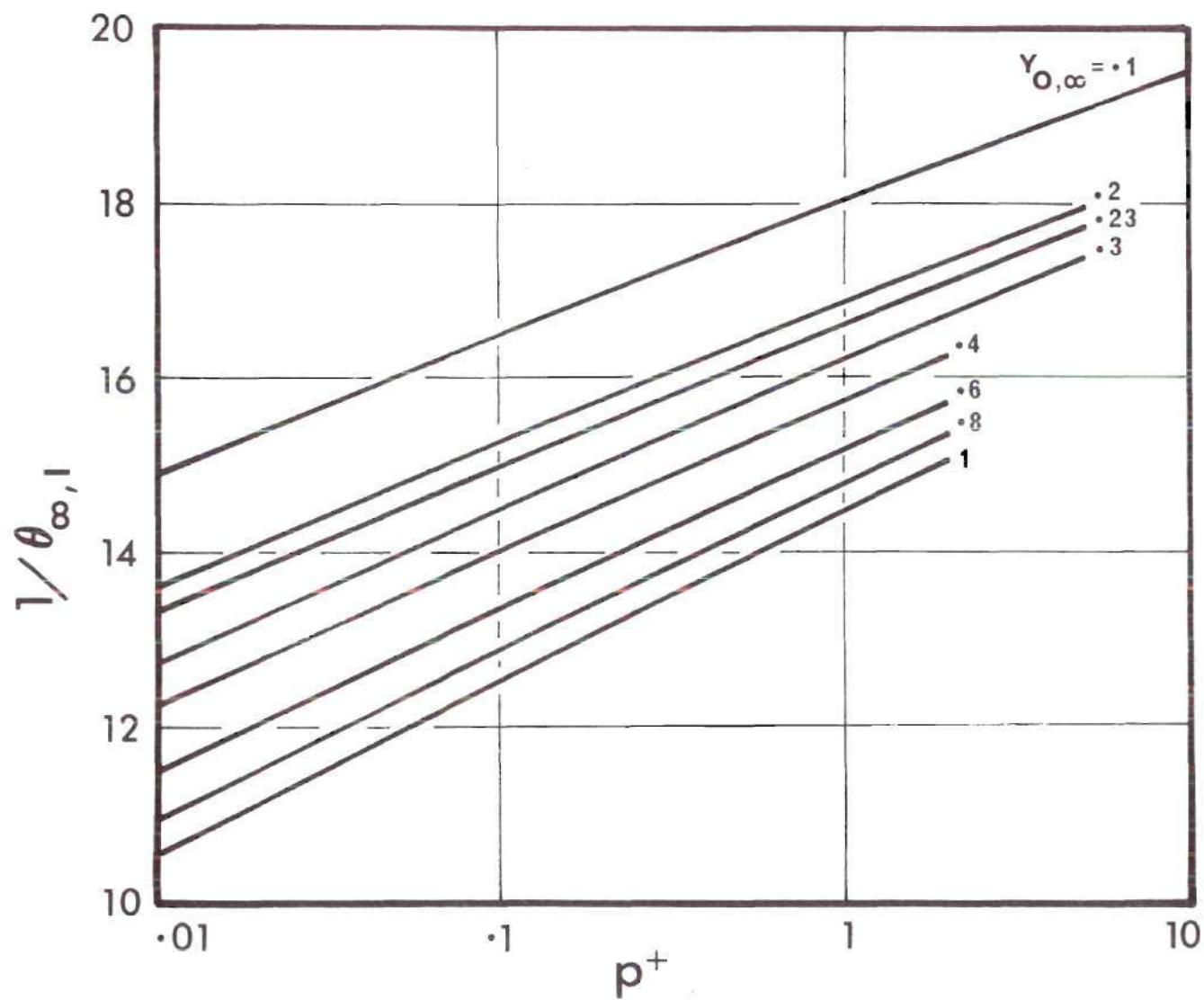$$x^{2M} = \alpha \, \ln x^2 \tag{67}$$

Figure 7a. Variation of $1/\theta_{\infty, I}$ with Pressure p^+; Coal No. 11, $d_w = 100$ μm
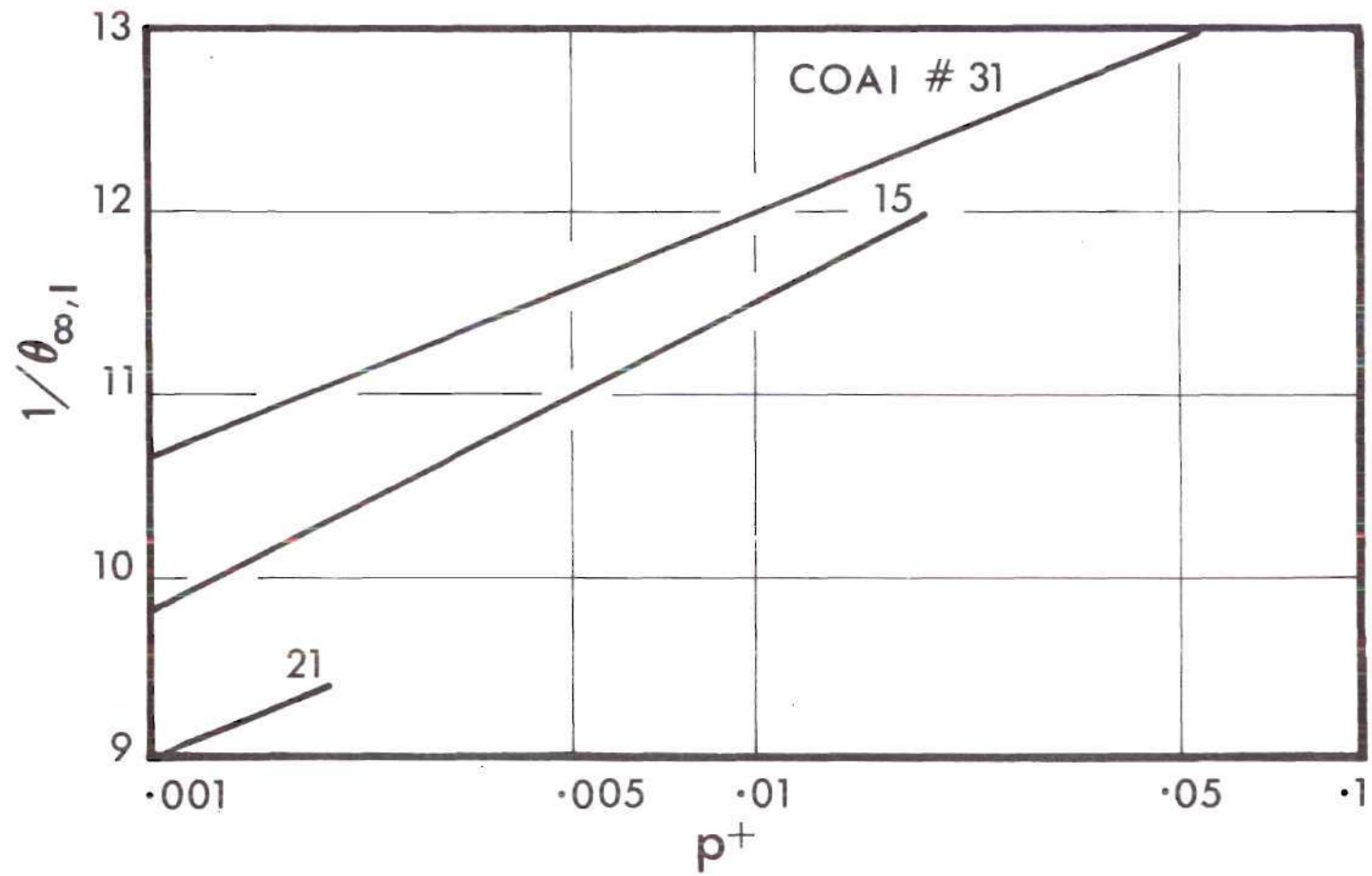
Figure 7b. Variation of $1/\theta_{\infty,I}$ with Pressure p^+; Coal Nos. 15, 21 and 31, $d_w = 100 \ \mu m$, $Y_{0,\infty} = 0.23$

where one solves for x for given α. The equations (54a), (54e), (55b), (65a) and (66a) are all of the above form when the order of reaction is not equal to zero and when pyrolysis is dependent on the size of the particle. Table 3 presents the definitions of x, M and α for the estimation of the critical parameters and as well as for the TIP points. Figure 8a gives the critical parameters for gas ignition when $M \geq 0$ and 8b when $M < 0$. There are four main parameters of practical interest: (i) critical size, (ii) volatile content, (iii) ambient oxygen concentration, and (iv) pressure. Given any three parameters, the fourth one can be readily determined from the critical diagrams. Also it is found that for $M < 0$, there is only one solution for x at given α; but for $M > 0$, there are two solutions.

On studying the mathematical behavior of equation (67) one finds that for all $M < 0$, the function $(\ln x^2/x^{2M})$ is a monotonically increasing function. Hence the constant $(1/\alpha)$ intersects the above curve only at one point. On the other hand for $M > 0$ as $x \rightarrow 1$ and $x \rightarrow \infty$, $(\ln x^2/x^{2M}) \rightarrow 0$ which then indicates that there is a maximum for $(\ln x^2/x^{2M})$. This maximum is found to occur at $x = e^{1/2M}$. Then one expects a minimum α (thus a maximum $(1/\alpha)$ at this x (see Figure 8a, point B) below which there is no solution for critical parameter. Thus,

$$\alpha_{min} = e \, M \qquad \qquad (67a)$$

Table 3. Definitions of α, x, and M for Critical Parameters and TIP Points

The Problem	x	M	α	Equation
Critical Parameters				
(1a) Size: $n \neq 0, m \neq 0$	$(\dfrac{D_{III,w}}{\xi^*})^{\frac{1}{2}}$	$(\dfrac{m-2E_w^+}{nmE_w^+})$	$\left\{ (D_{III,w}^o)^{\dfrac{D_{III,g}^o}{2/m}} Q_w^+ \nu_s^{1-n_o} \xi^{*(2-2/m)} \right\}^{1/n}$ $x \, (1-\bar{Q}_w^+)(1-e^{-\xi^*})/E_w^+$	$x^{2M} = \alpha \ln x^2$
(1b) Size: $n=0, m \neq 0$	same	$(\dfrac{m-2E_w^+}{mE_w^+})$	Raise the above to the power n and let $n \to 0$	$x^{2M} = \alpha$
(1c) Size: $m=0$	$(\dfrac{D_{III,g}}{\xi^*})^{\frac{1}{2}}$	1.0	$\left\{ (E_w^+/\ln(D_{III,w}/\xi^*)(1-\bar{Q}_w^+)x \right.$ $(1-e^{-\xi^*})\left\{ \bar{Q}_w^+ \xi^* \nu_s^{1-n_o}(D_{III,w}/\xi^*) \right\}^n \right\}^{1/E_w^+}$	same
(2a) Volatile Content: $n \neq 0$	See (1a)	$1/nE_w^+$	$(D_{III,g}/\nu_s^{1-n_o} Q_w^+ \xi^{*2})^{\frac{1}{n}} x$ $(1-\bar{Q}_w^+)(1-e^{-\xi^*})/E_w^+$	See (1a)

Table 3 (continued)

The Problem	x	M	α	Equation
(2b) Volatile Content: n=0	same	$1/E_w^+$	Raise the above to the power n and let n→0	See (1b)
(3a) Mass Fraction of Oxygen: n≠0	See (1a)	$(nE_w^+ - 2E_w^+ + 1)/$ nE_w^+	$(D_{III,g}/(D_{III,w})^{2-n} \, \nu_s^{1-n_0} \, \bar{Q}_w^+)^{1/n}$ $x(1-\bar{Q}_w^+)/E_w^+$	See (1a)
(3b) Mass Fraction of Oxygen: n=0	See (1a)	$(1-2E_w^+)/E_w^+$	Raise the above to the power n and let n→0	See (1b)

TIP Points

(4a) Size: m≠0,n≠0	See (1a)	$(1.433(2\bar{E}_w^+ +$ $\bar{E}_g^+) - (2m+2))/mn$	$(\alpha_g/\alpha_h^{1.433(2E_w^+ + E_g^+)})^{1/n}$	See (1a)
(4b) Size: m≠0,n=0	See (1a)	$(1.433(2\bar{E}_w^+ + \bar{E}_g^+)$ $- (2m+2))/m$	Raise the above to the power n and let n→0	See (1b)

Table 3 (concluded)

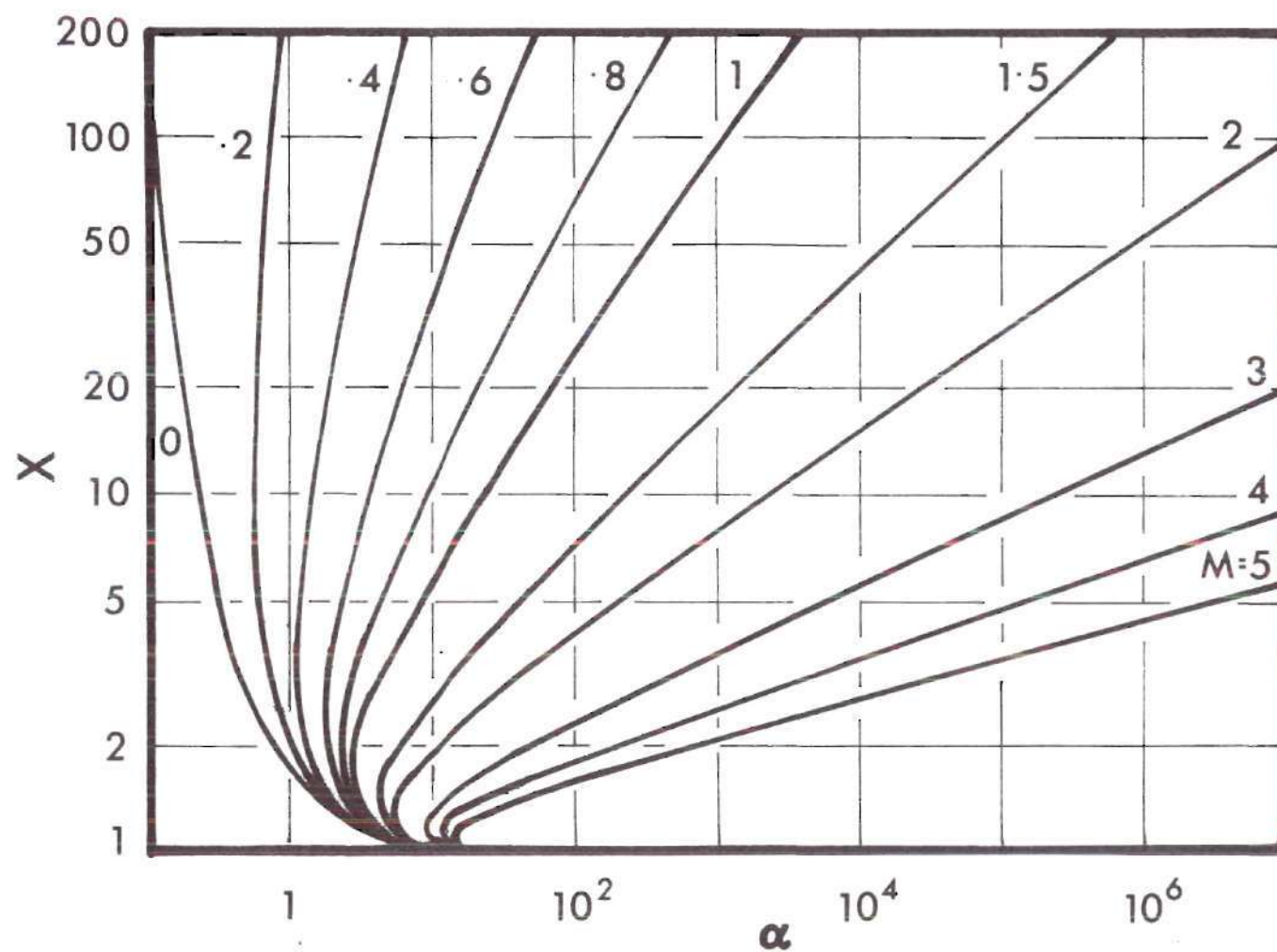| The Problem	x	M	α	Equation
(4c) Size: m=0	See (1c)	$(1.433(2\bar{E}_w^+ + \bar{E}_g^+) -2)/2$	$(\alpha_g'/(\alpha_h'))^{1.433(2\bar{E}_w^+ + \bar{E}_g^+) \, 1/n}$	See (1b)
(5a) Oxygen Mass Fraction: n≠0	See (1a)	$(-4-1.433(2\bar{E}_w^+ + \bar{E}_g^+)+n)/n$	$(\gamma_g/\gamma_h)^{(1.433(2\bar{E}_w^+ + \bar{E}_g^+) \, 1/n}$	see (1a)
(5b) Oxygen Mass Fraction: n=0	See (1a)	$-4-1.433(2\bar{E}_w^+ + \bar{E}_g^+)$	Raise the above to the power n and let $n \to 0$.	See (1b)

Figure 8a.   Solutions of Equation $x^{2M} = \alpha \ell n\ x^2$; $M > 0$
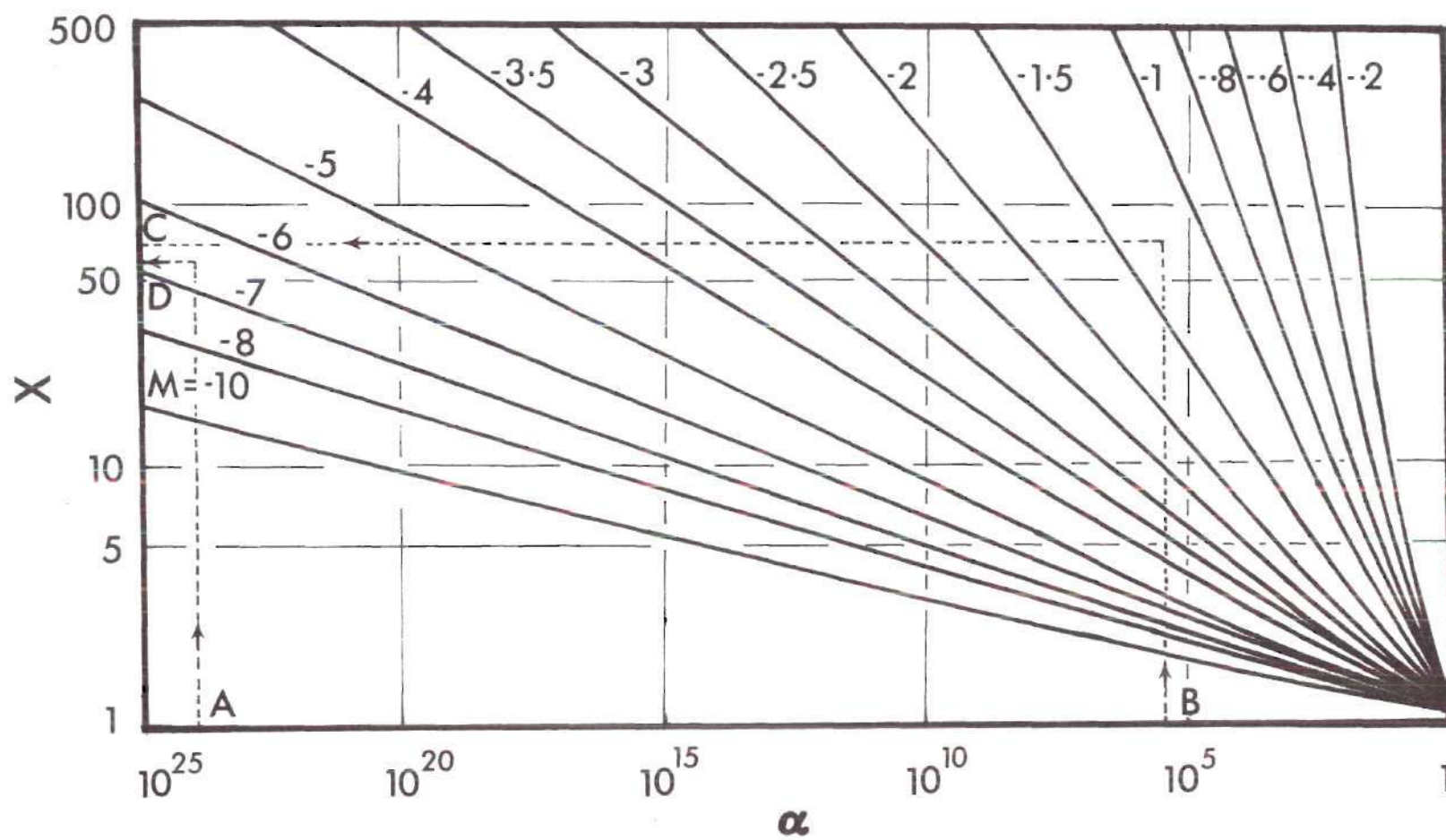
Figure 8b. Solutions of Equation $x^{2M} = \alpha \ln x^2$; $M < 0$

and correspondingly

$$x = e^{e/2\alpha_{min}}$$ (67b)

Figure 8c plots the characteristics of equation (67b) (line CD). Line AB in Figure 8c gives the variation of GIT when the system reaches a critical situation.

The physical meaning is as follows. Under the critical condition one is dealing with the ratio of two reactions: (i) the endothermic pyrolysis and (ii) the exothermic oxidation. This ratio is nothing but $(x^{2M}/\ln x^2)$, the ratio of pyrolysis reaction rate to the gas phase reaction rate. The term $(\ln x^2)$ arises due to the density effects in the gas phase reaction rate. The term (x^{2M}) is a ratio of exponential terms of pyrolysis reaction rate to the gas phase reaction rate and the corresponding Damkohler numbers. The density effect is dominant if (i) the GIT is very large and (ii) the activation energy for the pyrolysis is same as the activation energy for the gas phase reaction and the corresponding Damkohler numbers vary by the same order when the particle size is varied (M=0). The second solution always gives a smaller particle size compared to the first solution and hence involves a higher GIT. It is of present interest to find the ignition temperature which is the minimum required ambient temperature. Hence, the second
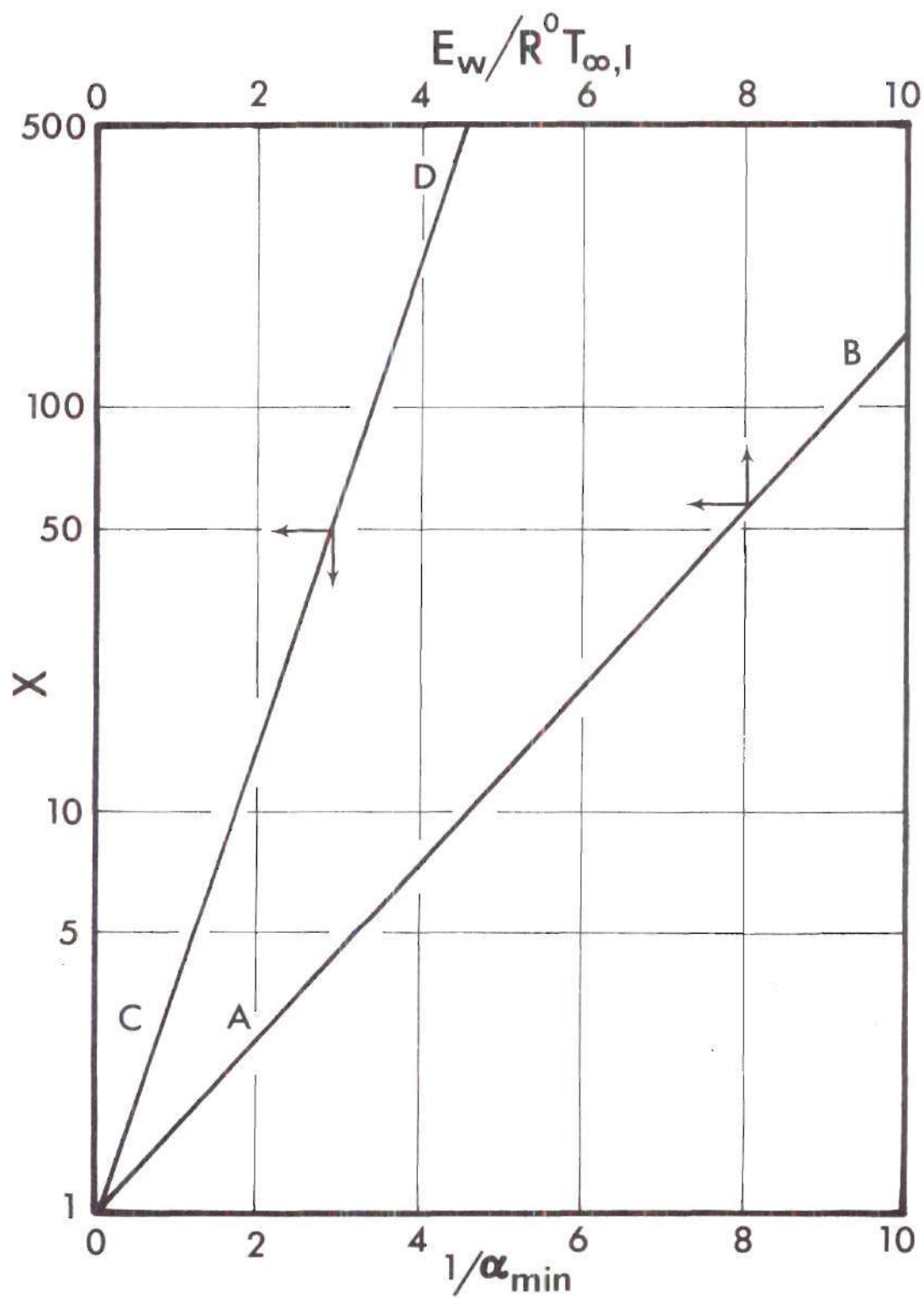
Figure 8c. Critical Ignition Temperatures
and Minimum Reaction Rate
Parameter α_{min}

solution is neglected.

As an illustration of Figures 8a and 8b, the same four coals are used for determination of the critical sizes. Figure 9a shows the critical sizes for coals number 11, 15, 21 and 31 for various pressures. The upper dark lines show the solutions for large x (smaller GIT) while the lower dotted lines show the solutions for small x (larger GIT). It appears that once a flame is established, the second solutions give particle sizes corresponding to gas phase extinction. This is sufficient condition, not a necessary condition. For coal number 15, such extinction size is about 14.3 µm. It is surprising that in spite of the approximations involved in the problem, there is good agreement with the experimentally estimated size which is about 15 µm. Howard [20] found that for bituminous particles of sizes below 15 µm, the coals can undergo only heterogeneous combustion along with volatiles in the solid. Similar sizes are shown for other types of coals. Figure 9b shows the effect of increasing the volatile content from the actual value to an arbitrary value of about 50% for lignite and bituminous coals. Note that increasing pressure increases the upper limit size for ignition. Similarly one can determine the critical volatile content and ambient oxygen mass fraction from the diagrams for any selected coal.
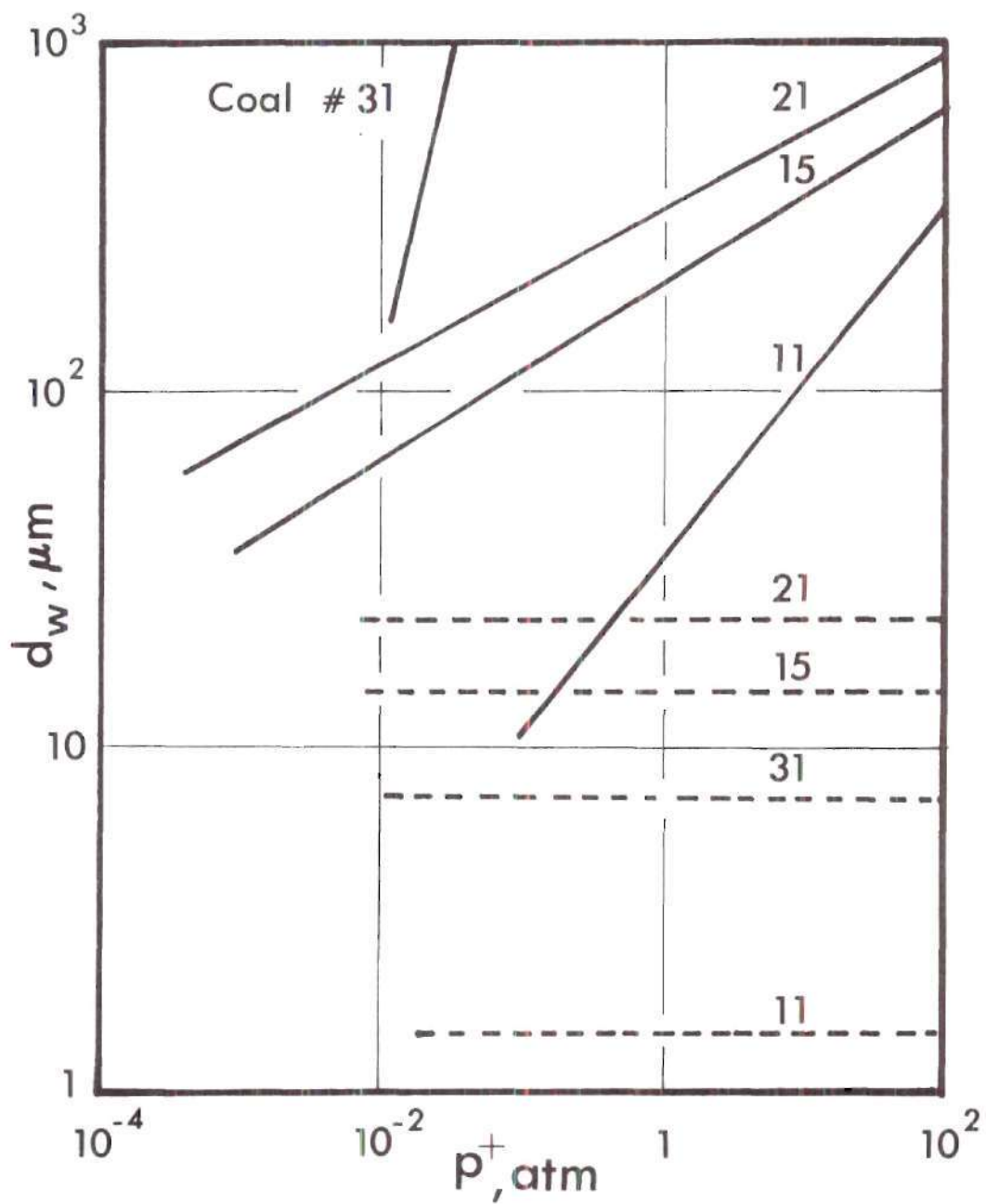
Figure 9a. Effect of Pressure on Critical Sizes
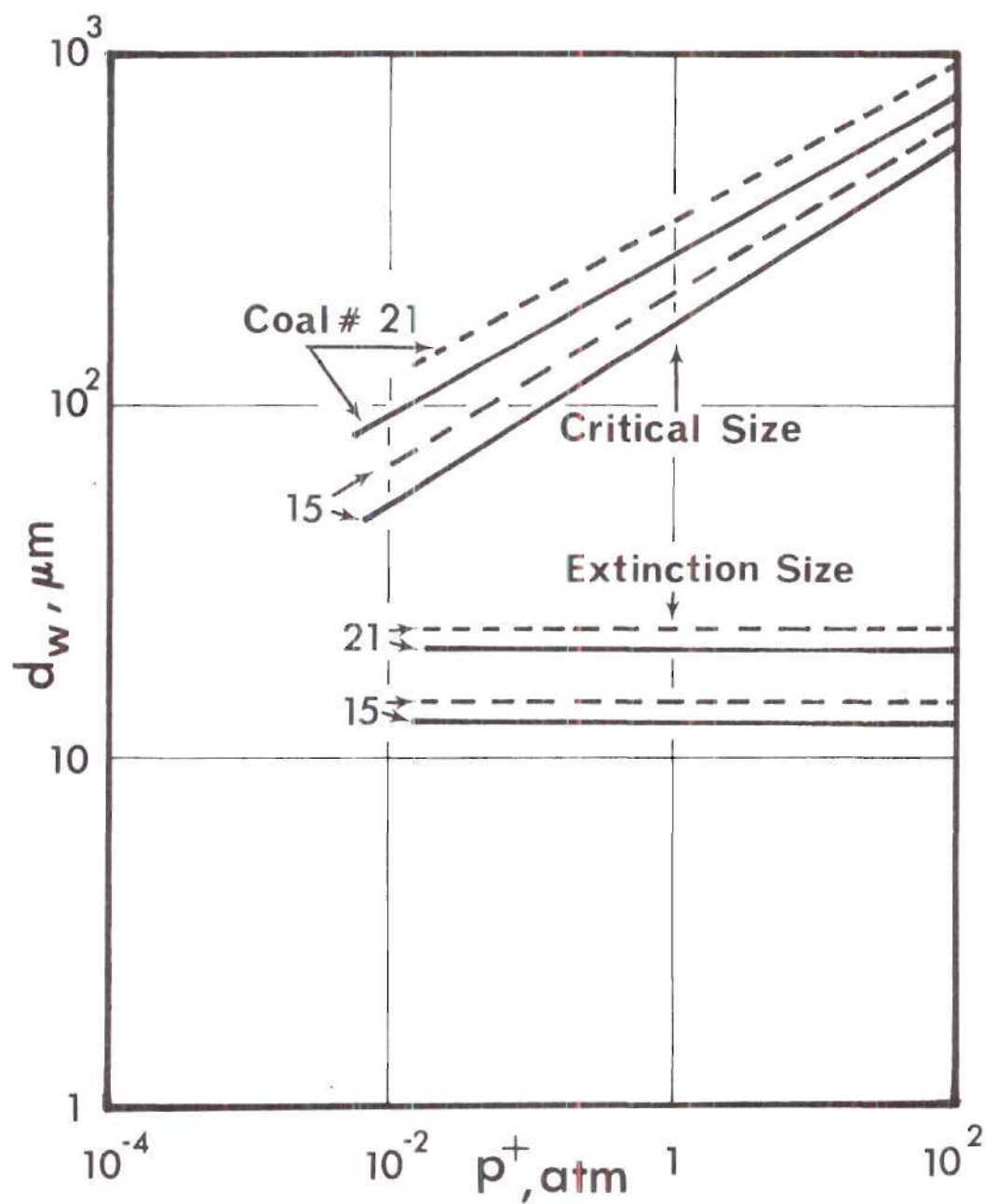of Various Coals; ——Critical Size,
----Extinction Size

Figure 9b. Effect of Increasing Volatile Content on Critical Sizes of Coal Particles; ——Volatile Content 50%; ----Volatile Content 40% (Coal No. 15), 37.5% (Coal No. 21).

5.2.2. Comparison Between Approximate and Exact Solutions for GIT

Approximate solutions are useful in the sense that for wide variety of coals with gas phase ignition, a general correlation with nondimensional group could be given. moreover, later it is seen that such an approximation leads to the prediction of the TIP points. For the three coals number 11, 15 and 2, comparison between exact results (equations (52) and (53)) and approximate results (equation (56b)) for GIT are made and are plotted in Figures (10a) and (10b) for a wide range of oxygen concentrations and particle sizes. The maximum deviation was found to be about 80°K for coal particle of about 400 μm in diameter. The discrepancy is higher for larger particle sizes since the surface Damkohler number increases to a large value thus reducing the chemical kinetics control term (see equation (52)). This term then approaches a value comparable to the heat transfer term which was not taken into account in obtaining the approximate solution. Similarly one should expect a discrepancy in the approximate solution when the heat of pyrolysis is large or when the activation energy for the pyrolysis is small.
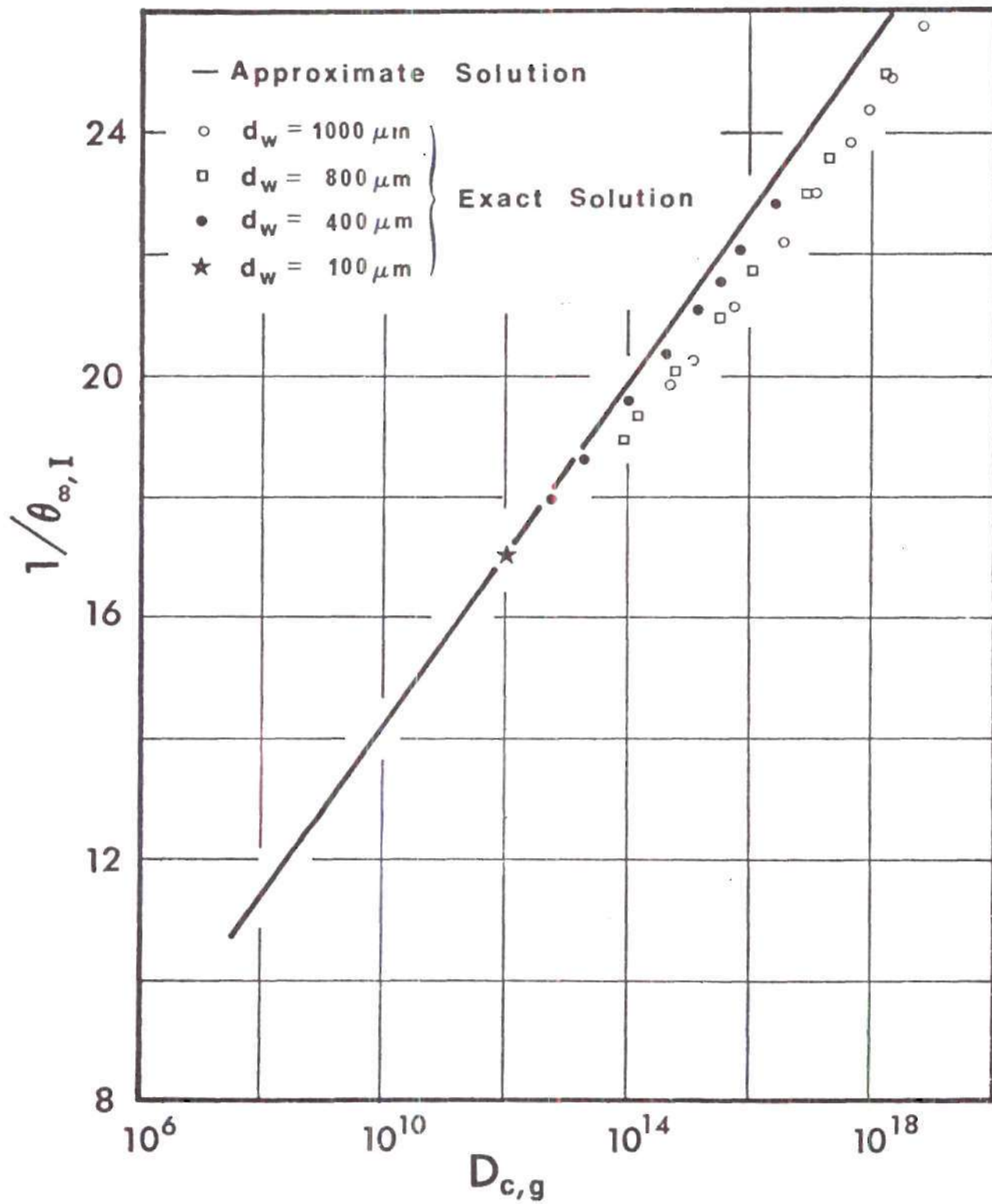
Figure 10a. Comparison of Approximate Solutions
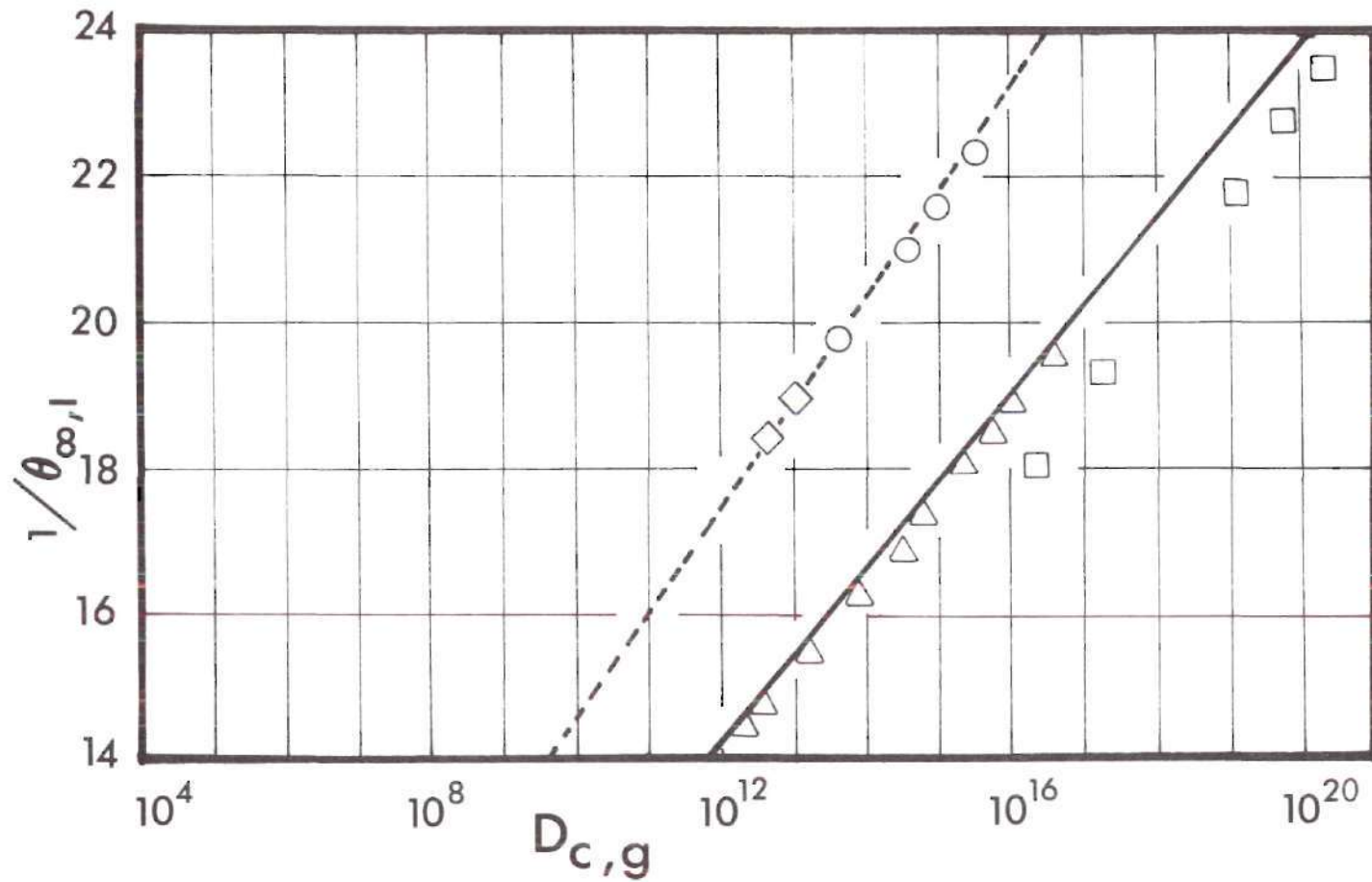with Iterative Solutions; Coal No. 15

Figure 10b. Comparison of Approximate Solutions with Iterative Solutions; Approximate Solutions: ——Coal No. 11, ---Coal No. 21; Iterative Solutions: For Coal No. 11, $\triangle$ d_w = 100μm, $\square$ d_w = 400μm; For Coal No. 21, $\diamondsuit$ d_w = 200μm, $\bigcirc$ d_w^w = 400μm.

5.3. Heterogeneous Ignition Temperature (HIT)

5.3.1. Exact Solutions

(i) Effect of Fourth Damkohler Number or Pressure.
Equations (61a), (61b) and (61c) were solved using the
Newton-Raphson technique for the two unknowns ξ_w and $\bar{\theta}_{\infty,I}$.
As mentioned earlier (see Section 4.5.2) the modified
fourth Damkohler number $((\tilde{D}_{IV,w})_h = (D_{IV,w})_h \bar{v}_s)$ is used to
correlate the heterogeneous ignition temperature. Figure
11 gives such a plot for $(1/\bar{\theta}_{\infty,I})$ versus $(D_{IV,w})_h$ with Y_0^*
as parameter. Widely varying $Q_{w,h}^+$ values have been selected.
Even then one finds that the curves are not shifted very
much except at low oxygen concentration, where one cannot
justify mass transfer to a first order approximation. This
is due to the reason that for low $Q_{w,h}^+$ and $Y_{0,\infty}$, a higher
mass flux is needed to ignite the particle which would not
then justify an expansion of e^{ξ_w} to $(1+\xi_w)$. Also since
$(D_{IV,w})_h$ is proportional to p^+ and r_w, any increase in
particle size, and pressure will result in decrease of the
HIT. Also, a higher oxygen concentration results in lower
ignition temperature since the reaction rate is increased.
This is contrary to what happened in the gas ignition
problem where any amount of increase in the reaction rate
requires a higher mass flux attendant with increase in
endothermic heat supply. The results were doubtful when
$Y_{0,\infty} \to 1.0$, since there is doubt regarding adsorption or
desorption control for the heterogeneous reaction. However

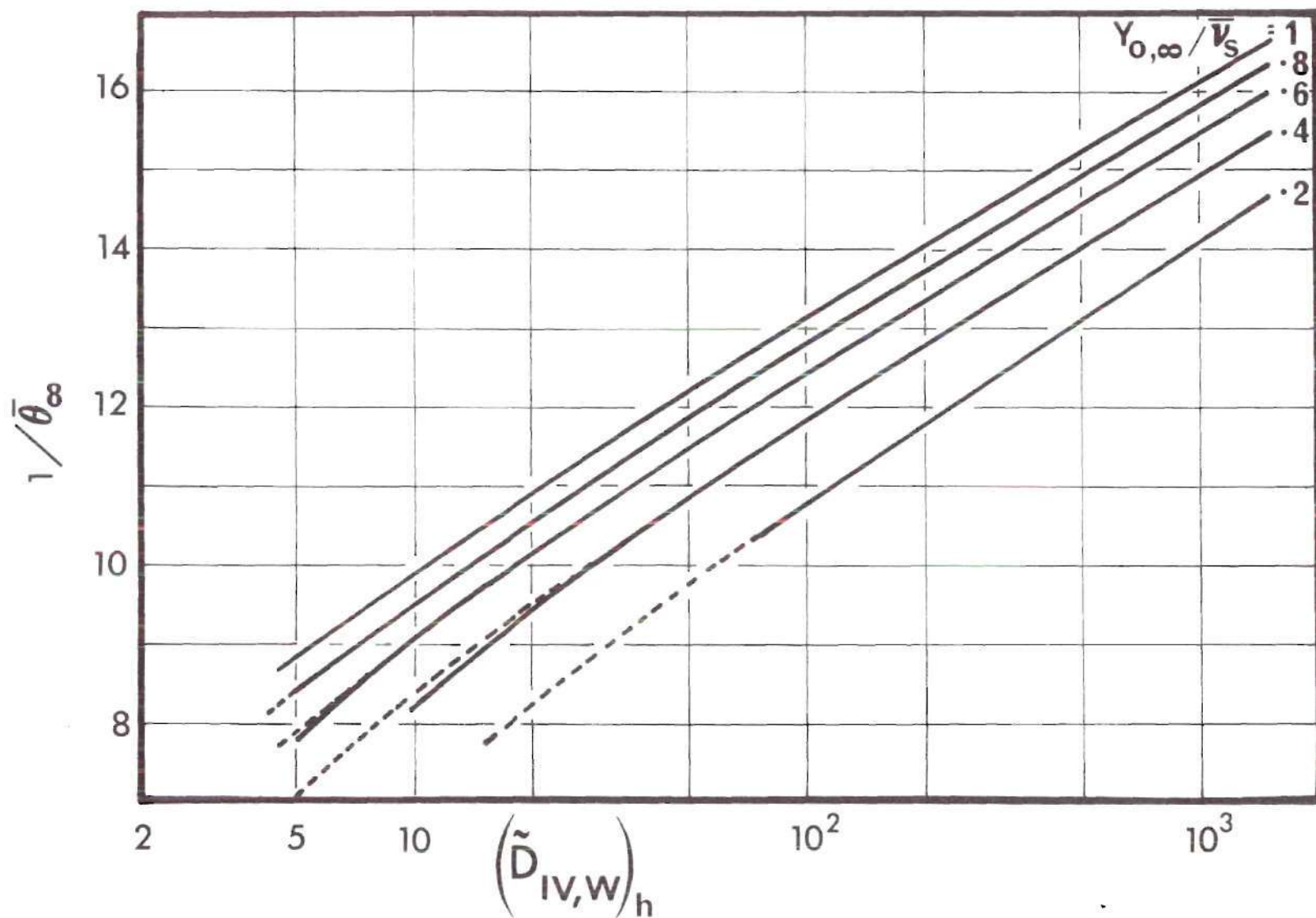Figure 11. $1/\overline{\theta}_\infty$ versus $(\tilde{D}_{IV,w})_h$ with $Y_{0,\infty}/\overline{\upsilon}_s$ as Parameter;
—— $Q_{w,h}^+ = .5$, --- $Q_{w,h}^+ = 1.5$.

assumption of adsorption control at $Y_{0,\infty} = 1$ is not uncommon.

(ii) Effects of Oxygen Concentration and Particle Size. With the use of Table 2 for the kinetic constants one can solve for the ignition temperature $\overline{\theta}_{\infty,I}$ for bituminous, lignite and anthracite coals. Figures (12a) and (12b) show the variation of HIT with oxygen concentration and particle size. Since an adsorption control mechanism was assumed for heterogeneous reaction (normally true at normal pressures and low oxygen concentration) an increase in oxygen concentration increases surface coverage and hence increases the reaction rate. Note that only overall kinetics are involved including the oxidation of solid volatile left in the coal. Similarly it was assumed that only a surface reaction exists which is true at low oxygen concentrations and higher temperatures. Hence any increase in particle size decreases heat loss per unit area and hence lowers the HIT. A comparison is made between solutions of nonsteady state theory, present steady state theory and experimental results. It is found that for low reactive anthracite coals the deviation between steady state and nonsteady state solutions is minor. A comparison with experimental results does not show appreciable deviation. Thus, it is concluded that the steady state solutions for the ignition problem are good approximations to the experimental conditions under which the results were obtained.

Figure 12a. Variation of HIT with Oxygen Concentration;
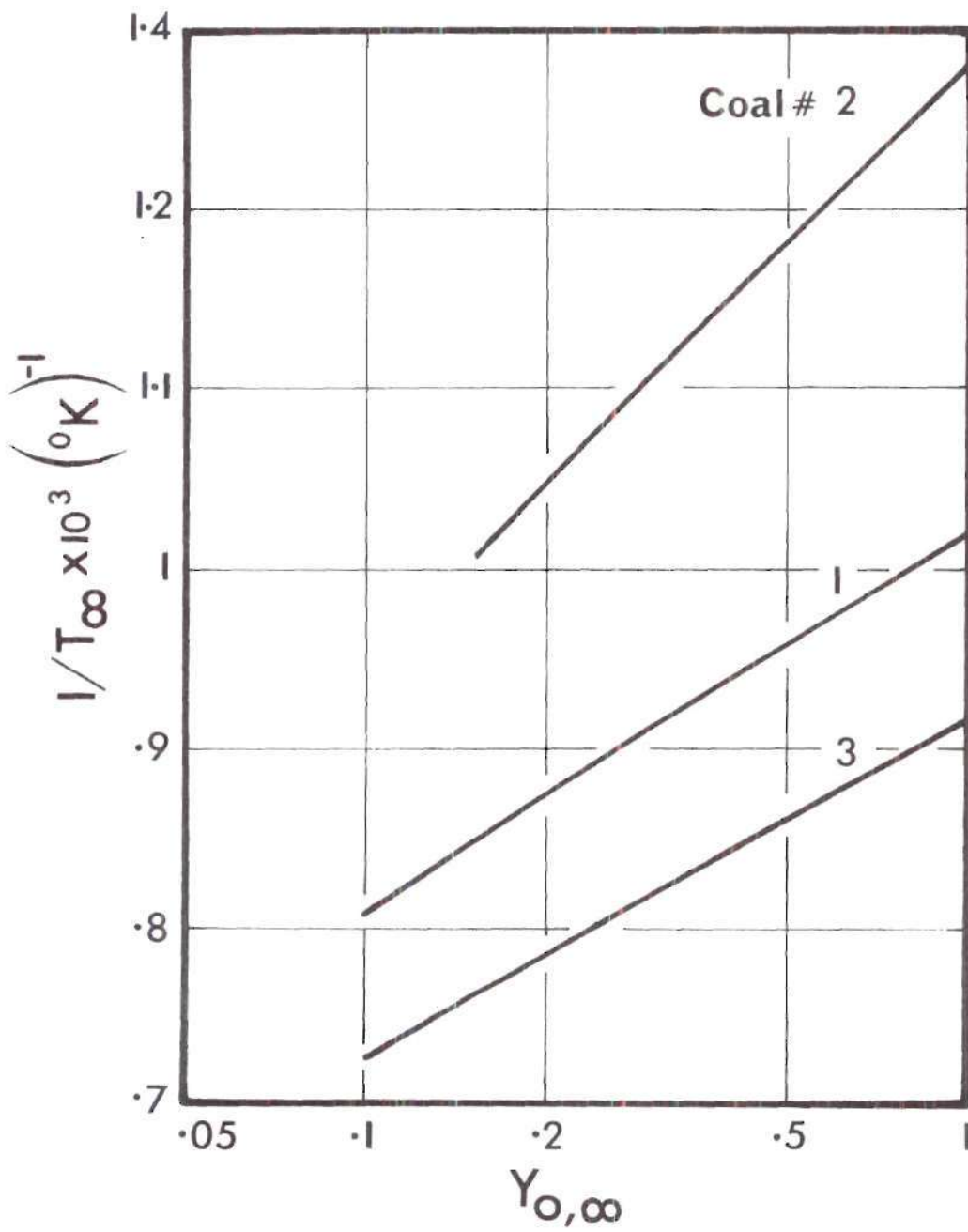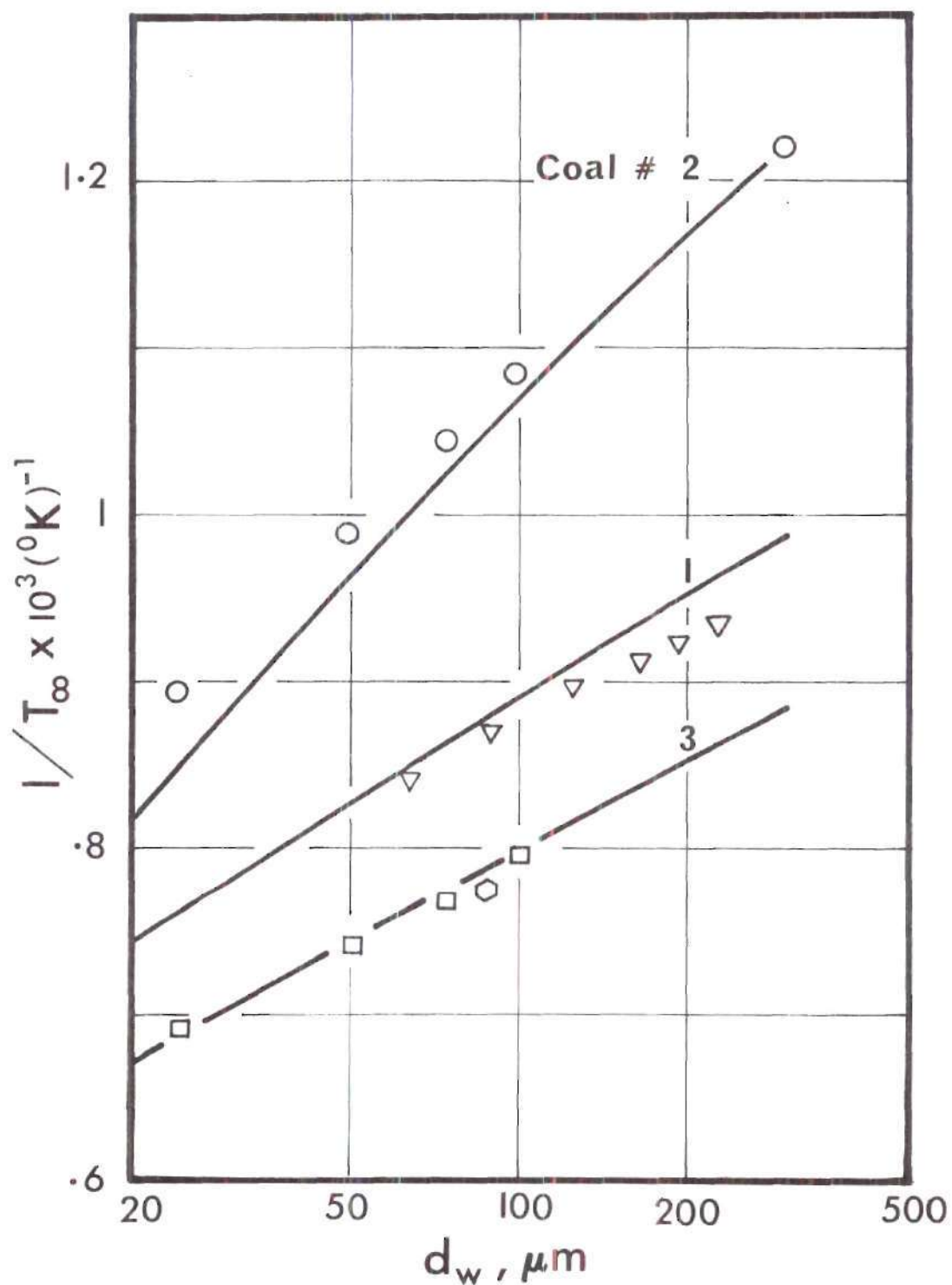Critical Concentrations $Y_{O,\infty}$: .04 Coal No.
2, .05 Coal No. 1, .064 Coal No. 3

Figure 12b. Variation of HIT with Particle Size; ▽ Coal No. 1 (experiment), ○ Coal No. 2 (nonsteady state theory), □ Coal No. 3 (nonsteady state theory), ⬡ Coal No. 3 (experiment); ——Present Steady State Theory; Critical Sizes d_w: 3.5 μm Coal No. 1, 3 μm Coal No. 2, 13.5 μm Coal No. 3.

(iii) Critical Parameters for Heterogeneous Ignition.
When oxygen concentration or the particle size is reduced
below a certain value, there appears to be no solution for
HIT. An investigation carried out to find the cause,
resulted in a set of equations (62) (see Section 4.5.3).
Figure 13a is a familiar curve of the reaction rate versus
surface temperature for a specified set of chemical constants
and $Y_{0,\infty} = .15$. The slopes of this curve at every $\bar{\theta}_w$ are
plotted in Figure 13b for different oxygen concentrations.
Needless to say, this curve has a maximum. On the same
diagram, the heat loss curve (properly accounted for $Q^+_{w,h}$)
is plotted. We observe that when the maximum slope falls
below the line AB, then steady state heat loss always exceeds
the heat liberation rate. One is interested to know the
oxygen concentration or the particle size (the critical
parameters) at which the peak slope touches the slope of the
heat loss curve. The resulting solutions are presented in
Figures 14a and 14b. These universal plots are useful when
arbitrary set of physical and chemical parameters are
involved in the ignition problem. Given $Y_{0,\infty}$, ν_s and
$Q^+_{w,h}$, one can find a critical particle radius. Figures 12a
and 12b indicate such a set of critical values for selected
coals. Figure 14b gives the wall temperatures corresponding
to the critical conditions. It is found that an increased
oxygen mass fraction lowers the critical particle size,
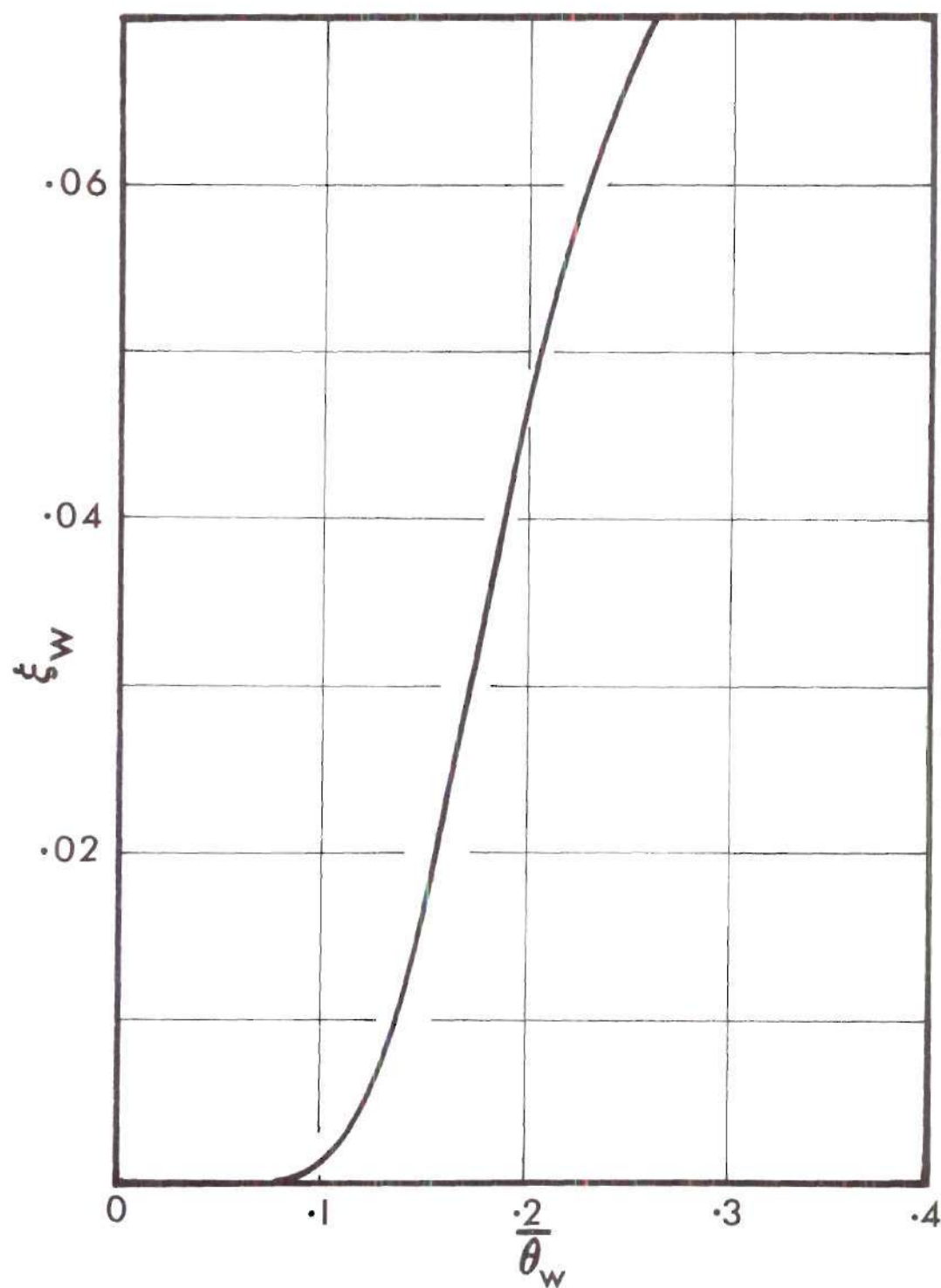since the heat liberation rate is increased. Similarly an

Figure 13a.   Burning Rate versus Surface Temperature;
$(D_{III,w})_h = 10.0$, $Y_{0,\infty} = .15$.
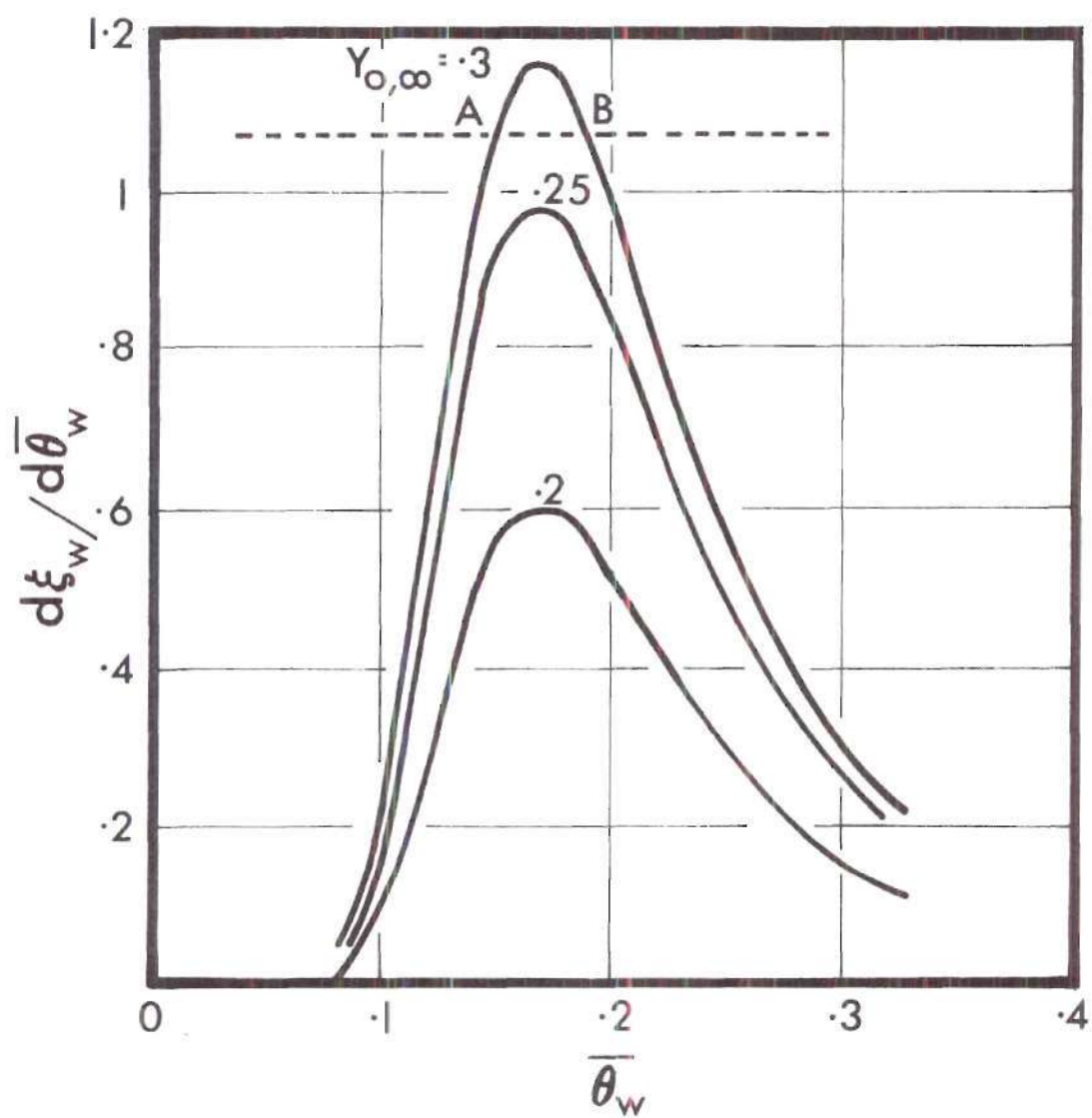
Figure 13b.   Burning Rate Slope versus Surface Temperature
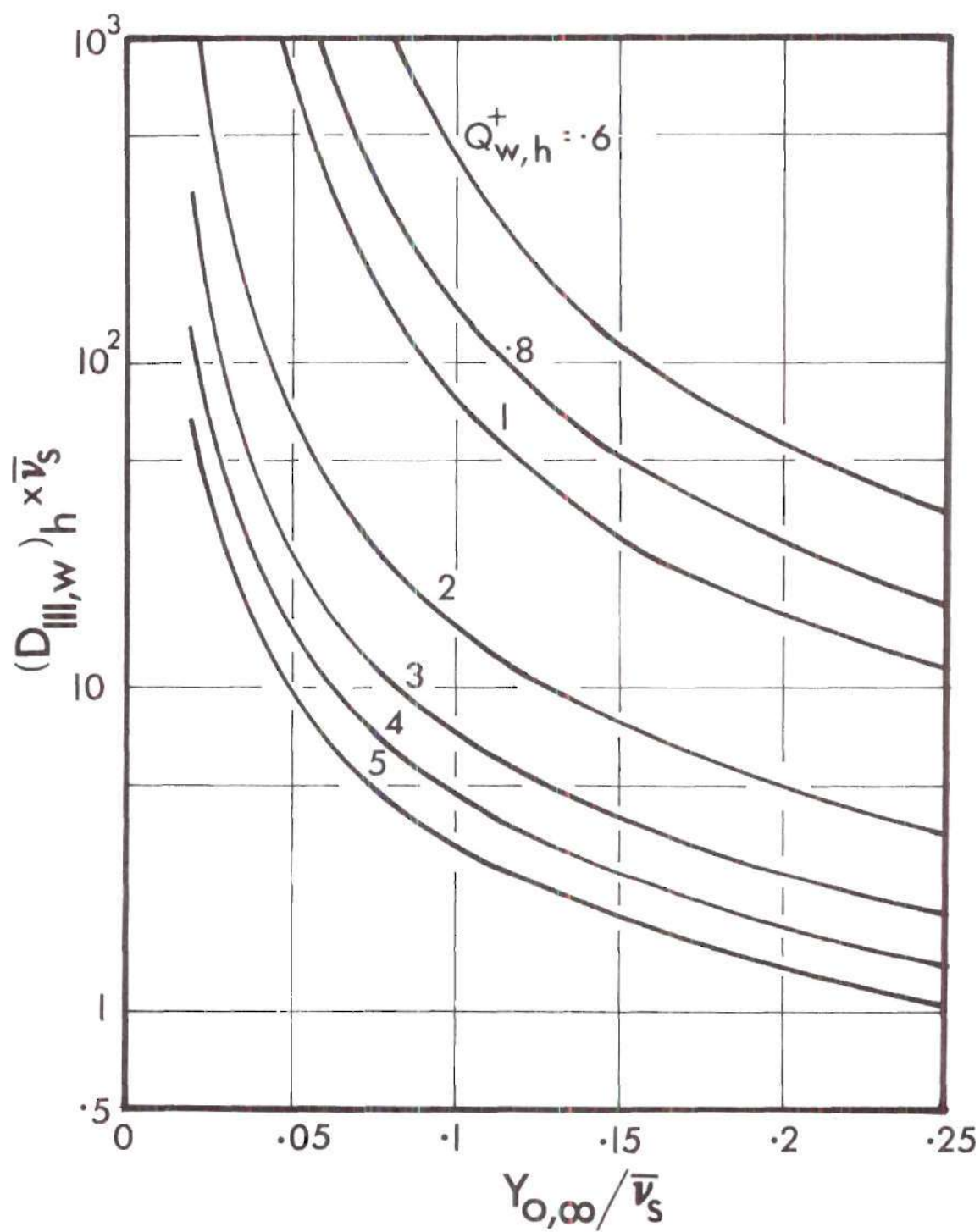
Figure 14a. Critical Values for Slow Burning
of Coals
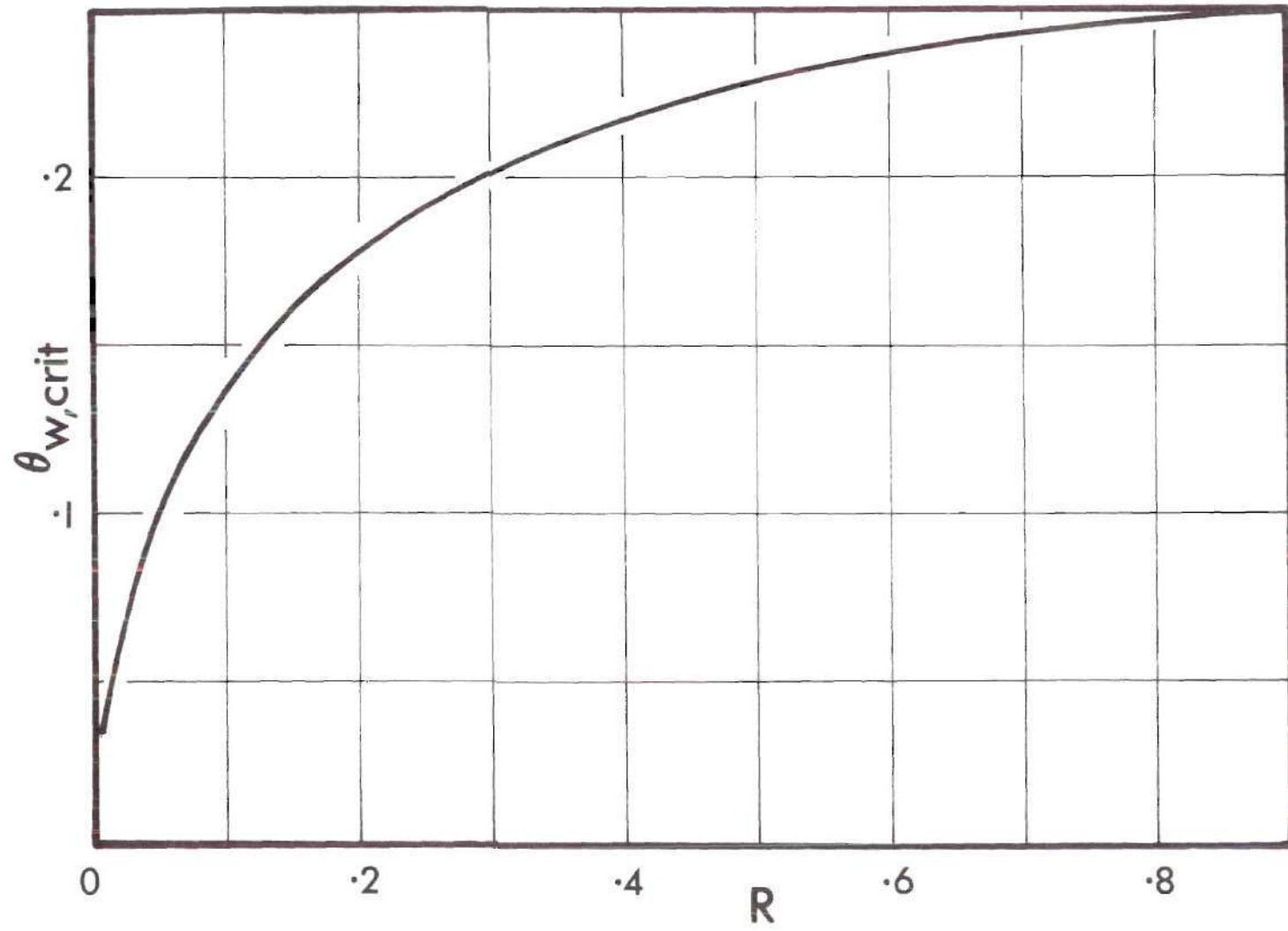
Figure 14b.   Critical Surface Temperatures

increase in particle size lowers the critical oxygen concentration.

5.3.2. Comparison Between Approximate and Exact Solutions

Equations (61) and equation (63c) were used to obtain the exact and approximate results, respectively, for IIIT and then are compared in Figure 15a. It is found that though both the exact and the approximate results give a similar qualitative picture, the quantitative accuracy is not satisfactory. Hence the constants $\bar{a}$ and $\bar{b}$ in equation (63d) were modified after fitting the exact results with a least squares fit. Thus,

$$(1-\bar{a})^{-1} = 1.4332$$

$$\bar{b} = e^{4.57}$$

Then

$$D_{c,h} = e^{4.57} (D_{IV,w})_h Y_{0,\infty} \tag{67c}$$

and

$$1/\bar{\theta}_{\infty,I} = 1.433 \ln (D_{c,h}).$$

The dark line in Figure 15a shows the second approximation. The usefulness of the first approximation lies in the fact

Figure 15a.   Fitting a Straight Line to Iterative Results of HIT;
    -·-·First Approximate Solution,
    ——Second Approximate Solution;
    $\triangle$ $(D_{IV,w})_h$ = 8.8, $\bigcirc$ 47.0, $\square$ 175.0.

that it resulted in obtaining a correlating group for HIT.
Figure 15b compares the approximate results (hereafter,
the approximate results for HIT means only a second approxi-
mation) with the results from nonsteady state theory and
with the experimental results obtained elsewhere [17]. The
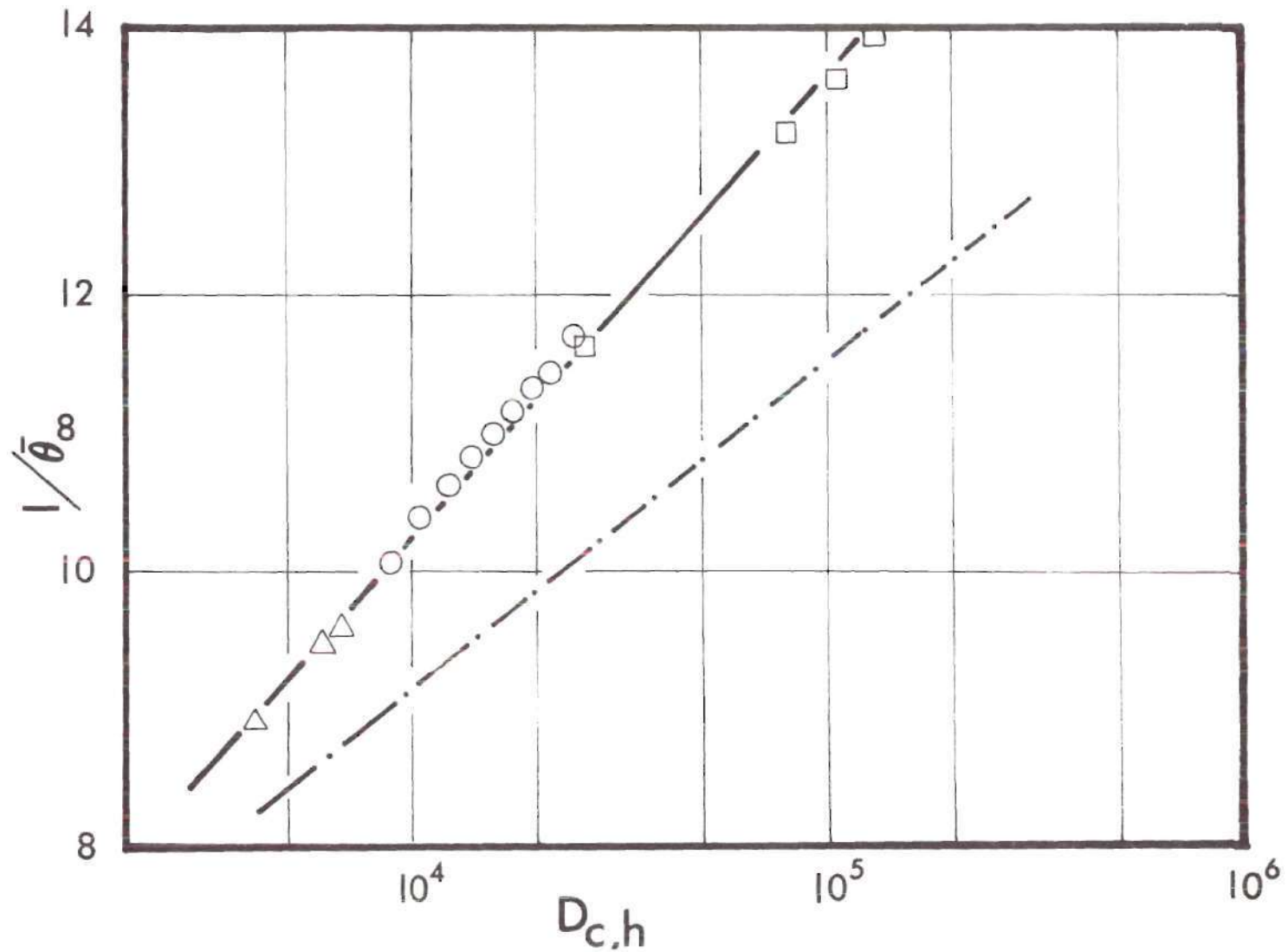approximate results are found to correlate well for a wide
range of conditions.

5.4. A TIP Diagram for Estimation of TIP Parameters

As discussed in Sections 5.2 and 5.3, the GIT and
HIT vary very differently for variation with ambient oxygen
mass fraction. Similarly, they vary to a different order of
magnitude with respect to the variation in particle size.
Hence transition of ignition phase (TIP) will occur if the
above two curves do not appreciably change when both processes
occur simultaneously (see Section 4.6). Thus superimposing
Figures 12a on Figure 4 and Figures 12b, 6a and 6b appropri-
ately, one obtains the transition points [59]. For bituminous
coal particles (coal number 1 and coal number 11) of 100 μm
in diameter, for oxygen concentration below about 0.21,
ignition is likely to occur in the gas phase and vice versa.
Large sized bituminous particles and increased volatile
content increases the TIP oxygen concentration. Solutions
could not be obtained for the GIT with coals number 15, 21
and 31 at particle diameters of about 100 μm. From Figure 6a
it is noticed that ignition is likely to occur on the surface
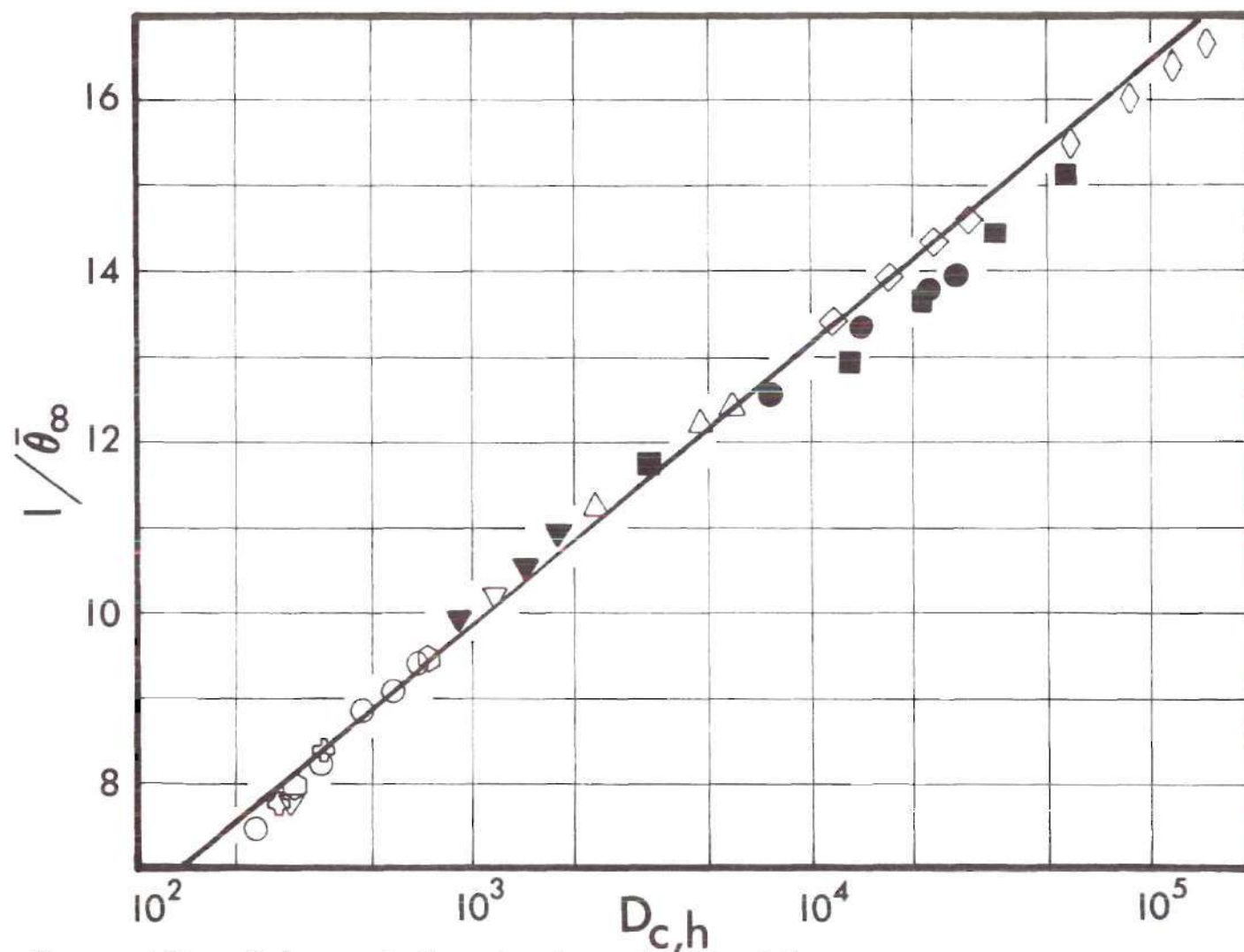
Figure 15b. Universal Correlation of HIT with a Correlating Group $D_{c,h}$; —Approximate Solution; Iterative Solutions: ✿ $(D_{IV,w})h = 4.5$, ◯ 6.0, ⬡ 7.5, ▽ 15.0, △ 60.0, ◇ 300.0, ◊ 1500.0; Experimental and Unsteady State Solution: ● Coal No. 1, ▼ Coal No. 2, ■ Coal No. 3.

for bituminous coals combination number 1 and number 11 for
diameter less than 140 μm, and for number 1 and number 15
for diameters less than 350 μm. Here it is worth mentioning
that Howard [20] could not obtain gas phase ignition for coal
number 15 when he used a size range up to 60 μm. The theory
proves that it is impossible to attain such gas phase
ignition at these particle sizes. An increase in volatile
content or a decrease in oxygen concentration up to a
certain low limit can lower the TIP size. Figure 6b shows
that for lignite particles because of higher surface
reactivity, the HIT is always lower than GIT even when
particles size is increased up to 1000 μm. No solution could
be obtained for coal number 31 at $Y_{0,\infty}$ = .23.

It is of interest to estimate the TIP size and TIP
concentration for any coal of interest. Also the procedure
so far used is a graphical procedure. Using equations in
Section 4.6, one can obtain TIP points through approximate
results for GIT and HIT. Such equations are similar to
those obtained for estimation of critical parameters for
gas phase ignition on the surface. Hence, Figures 8a and
8b give the TIP diagrams for the estimation of TIP points
given the values for chemical kinetics at the surface for
pyrolysis and heterogeneous oxidation and gas phase oxida-
tion of the pyrolysate. The corresponding definitions for
α, M and x are given in Table 3. For this problem normally
M is less than zero. Hence Figure 8b is most frequently

used for the estimation of TIP points.

As an example the procedure to find the TIP size for the coal combination number 1 and number 11 is outlined below.

$$m = 2, \text{ for volumetric pyrolysis,}$$

$$n = 1, \text{ for gas phase oxidation of the pyrolysate,}$$

$$n_0 = 1.4,$$

$$\nu_s = 4.0,$$

$$Y_{0,\infty} = 0.23,$$

$$\bar{Q}_w^+ = .035.$$

$$E_g = 38,000.0 \text{ cal/mole,}$$

$$E_w = 17,700 \text{ cal/mole,}$$

$$E_{w,h} = 29,600 \text{ cal/mole,}$$

$$\left.\begin{array}{l} \overset{o}{D}_{III,w} = 260.0, \\[4pt] \overset{o}{D}_{III,g} = 588.0, \\[4pt] (\overset{o}{D}_{III,w})_h = 380.0, \end{array}\right\} \quad \begin{array}{l} \text{based on a reference particle} \\ \text{size of 100 } \mu m \end{array}$$

$$Q_{w,h}^+ = 1.29,$$

$$E_w^+ = E_w/E_g, \; = .466,$$

Hence, $M = -1.22$ (equation (65b)),

$$\xi^* = .0565 \text{ (equation (45)),}$$

$$\alpha_g = 226.0 \text{ (equation (65d)),}$$

$$\alpha_h = 159.5 \text{ (equation (65e)),}$$

$$\alpha_4 = .422 \times 10^{-5} \text{ (equation (65c)).}$$

Thus,

$$\left\{\frac{d_w^+}{\sqrt{\xi^*}}\right\}^{-1.22} = .422 \times 10^{-5} \; \ell n \; \left\{\frac{d_w^+}{\sqrt{\xi^*}}\right\}^2$$

Using Figure 8b for $\alpha_4 = .422 \times 10^{-5}$, one solves for $(d_w^+/\sqrt{\xi^*})$ (BC). Hence,

$$d_w^+/\sqrt{\xi^*} \simeq 70.0$$

$$d_w^+ \simeq 16.6$$

Using equations (54b) to find the TIP point,

$$d_w \simeq 103 \; \mu m$$

An exact solution by graphical procedure gives,

$$d_w = 140 \; \mu m$$

It is found that the approximate result for TIP size deviates by about 25 percent from the exact results.

Applying a similar procedure to find the TIP concentration of oxygen (line AD in Figure 8b), for given $d_w = 100 \; \mu m$

$$d_w^+/\sqrt{\xi^*} \simeq 60.0$$

$$\xi^* \simeq .072$$

Hence,

$$Y_{0,\infty} \simeq .288$$

An exact solution for TIP is given as

$$Y_{0,\infty} \simeq .210$$

This gives an error of about 38 percent compared to exact results. This error is more than the one encountered for the TIP size. One reason that can be attributed to this increased error for TIP concentration is that more approximations have been introduced for this procedure (i.e. $1-e^{-\xi^*} \simeq \xi^*$, see Appendix C.1).

CHAPTER VI

COMBUSTION ANALYSIS OF A HARD PRESSED
GRAPHITE OR CHAR PARTICLE

In this section an analysis is carried out to explain
the occurrence of peak erosion rate of solid carbon. A
hypothesis for the occurrence of the peak even under normal
pressures is proposed in Section 6.1 and explained. Suitable
assumptions for this analysis consistent with the above
hypothesis are presented in Section 6.2. In Section 6.3
simplified conservation equations including both the gas
phase and the interface are presented. Two numerical
methods are proposed in Section 6.4 to obtain a solution
for the nondimensional bulk velocity at the surface as an
eigenvalue of the problem (for a given surface temperature
of the particle).

6.1. A Hypothesis for the Occurrence
of the Peak Erosion Rate

A carbon particle, uniformly heated by some external
source (e.g. induction heating or direct heating in the
case of carbon rods) to different surface temperatures is
considered. Two possible situations arise:

(i) Given a char particle which produces only CO at
the surface and the gas phase oxidation of CO is almost

frozen. Then if the surface reaction is very fast, for every mole of diffusion of oxidant there are two carbon atoms removed from the surface. This will be called a CO dominated case (CO-DC).

(ii) Given that the gas phase oxidation of CO is also fast. With the production of CO from the surface oxidation there is associated an immediate oxidation of CO to CO_2 at the surface. Then for every mole of O_2 diffusing to the surface there is only one atom of carbon removed from the surface. This will be called CO_2 dominated case (CO_2-DC).

Since the gas phase oxidation rate of CO is proportional to the square of the particle diameter while for heterogeneous oxidation (a surface reaction) it is proportional to the particle diameter, then there is some particle diameter for a given surface temperature at which the gas phase reaction oxidation is almost frozen until some temperature which corresponds to CO-DC (AB in Figure 16a). However as the surface temperature is increased, the erosion rate shifts to CO_2-DC. The same qualitative behavior is true if the gas phase oxidation of CO is of the order of two and if the surface oxidation is of the order of one. Depending upon the relative rates of production of CO and oxidation of CO_2, a maximum could exist. This means that a maximum could exist only between the two limiting diffusion rates corresponding to CO-DC and CO_2-DC. This has been verified experimentally at normal pressures for some char particles [6]
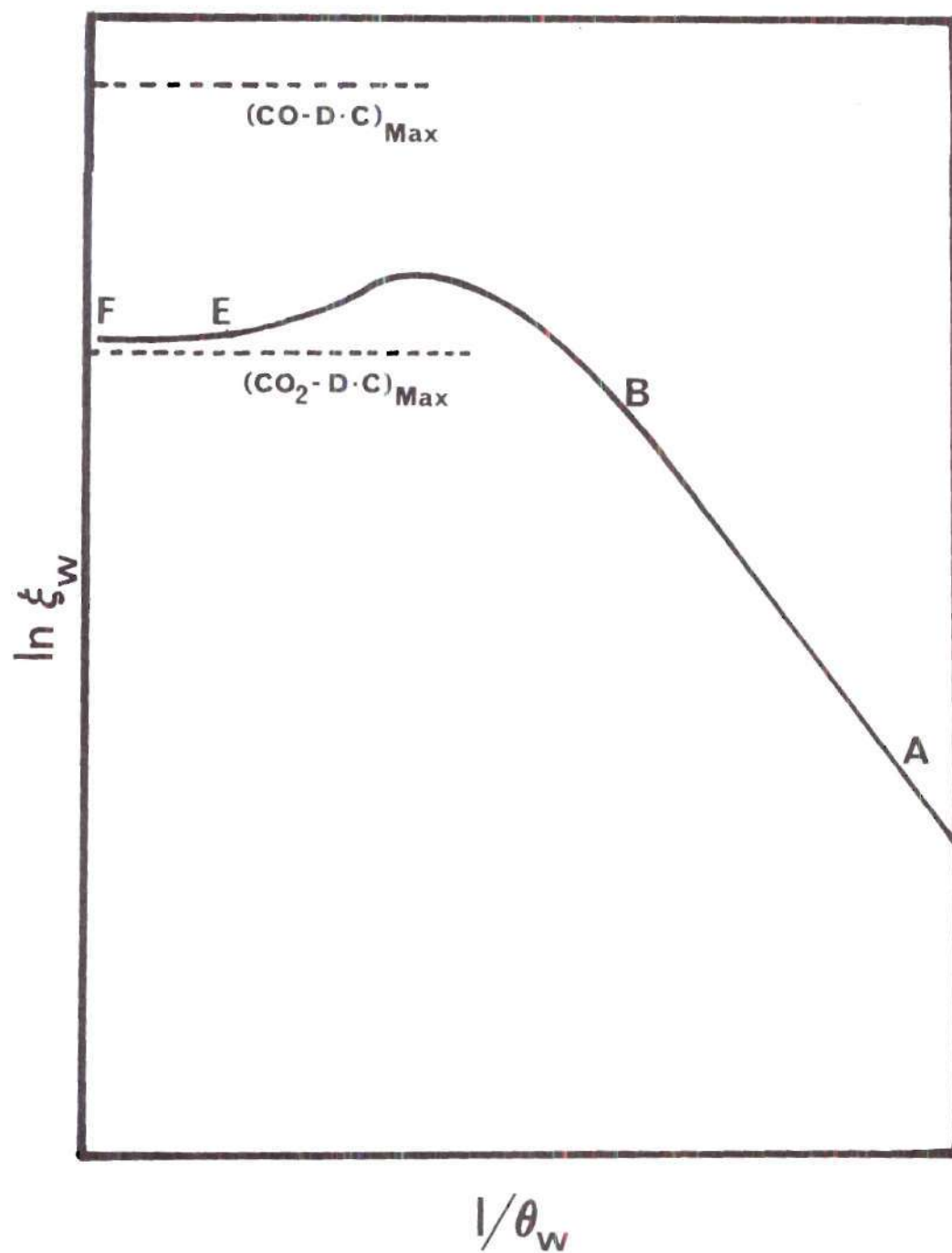
Figure 16a. Variation of Dimensionless Erosion Velocity at the Surface with Dimensionless Surface Temperatures (not to scale); AB: CO Rate controlled; EF: CO_2 Rate Controlled.

at normal pressures. Also the ratio of the maximum erosion rate to the asymptotic erosion rate could not be greater than about two according to this hypothesis. This is not confirmed at low pressures thus indicating that there exists a variation of activation energy at least at low pressures (see References [36] and [37]) for experimental results at low pressures). This hypothesis involves finite chemical kinetics for all reactions. Also, it is experimentally determined that carbon or hard char particles indeed burn under finite chemical kinetics control [33,3] even under ambient pressures. It is then expected that a maximum could occur under these pressures. Sometimes beyond this maximum erosion point, the rate instead of approaching the value corresponding to the asymptotic value of CO_2-DC, may again start increasing towards the rate corresponding to CO-DC, if there is a strong reduction process. In order to obtain all these characteristics one has to resort to a numerical procedure for this finite kinetic, boundary value and eigenvalue problem.

6.2. Assumptions

The governing equations already presented in general form in Section 3 must be reduced for this problem with the following assumptions.

(i) Normally CO_2 is produced at the surface only at low surface temperatures [60,61]. This is confirmed by the

following equation for the experimental results [27,33].

$$\dot{m}_{CO}/\dot{m}_{CO_2} = 2500 \; e^{-12000/R°T}$$

Hence all surface reactions including the reduction of solid carbon produce only CO. The surface reactions mostly follow a first order law in the temperature range considered here [3,60,61,35]. (Also see references 62 and 63 for kinetics of reduction of carbon with CO_2.)

(ii) The surface reactions are described by an Arrhenius type of expression. If the reduction process at the surface is neglected, the solutions can be generalized for known surface temperatures even for non-Arrhenius behavior of oxidation of hard solid carbon; also, a monotonic linearly varying activation energy can be accommodated (see Appendix E.1).

(iii) The oxidation reaction in the gas phase follows a general order with respect to CO and O_2. The order appears to be two when $Y_O < 5$ percent while first order prevails at higher oxygen mass fractions [65]. The kinetic values of oxidation of CO for various combustion systems are tabulated in Reference [64].

(iv) No sublimation occurs in the temperature range of interest.

(v) The particle is heated by an external source to a set temperature. The ambient temperature is arbitrary.

6.3. Governing Equations and Boundary Conditions

The governing equations necessary for this problem are equations (29) through (33) and (35). No interface energy balance (equation 34) at the surface is required since the surface temperature is specified. The principal species is considered to be CO.

Equations:

$$\frac{d^2 Y_{CO}}{d\eta^2} + \xi_w \frac{dY_{CO}}{d\eta} = D_{III,g} \; e^{-\frac{1}{\theta}} \; Y_0^{n_0} \; Y_{CO}^{n_{CO}}/\eta^4 \theta^n \tag{68}$$

where

$$\eta = \xi/\xi_w \tag{68a}$$

$$D_{III,g} = \nu_{CO} W_{CO} A_g r_w^2 \; (\frac{p}{E_g})^n / \rho D \tag{68b}$$

Chemical Kinetics:

Oxidation at the surface:

$$C(s) + \frac{1}{2} O_2 \rightarrow CO \qquad (a) \tag{68c}$$

Reduction at the surface:

$$C(s) + CO_2 \rightarrow 2CO \qquad (b) \tag{68c}$$

Oxidation of CO in the gas phase:

$$CO + \frac{1}{2} O_2 \rightarrow CO_2 \qquad (g) \qquad (68c)$$

Boundary Conditions

Species balance are made for the species CO, CO_2 and O_2 at the surface using equation (35) and the assumptions presented in Section 6.2. Thus the mass and flux fractions of CO at the surface are derived in terms of ξ_w and θ_w using the above species balance. The details of the derivation are shown in Appendix E.1. The results are presented below. As $\eta \rightarrow 1$,

$$Y_{CO,w} = [(1+\nu_b)(1-e^{-\xi_w}) + e^{-\xi_w}(Y_{CO,\infty} - Y_{0,\infty}/\nu_g)$$

$$+ \frac{\xi_w}{\Gamma_a} \frac{1}{\nu_g} - \frac{(1+\nu_g+\nu_g\nu_b)}{\nu_g}(1-e^{-\xi_w})\frac{\Gamma_b}{\Gamma_a}$$

$$- \frac{e^{-\xi_w}}{\nu_g}\frac{\Gamma_b}{\Gamma_a}\{(1+\nu_g) Y_{CO,\infty} + Y_{CO_2,\infty}\}]/[1 - \frac{1+\nu_g}{\nu_g}\frac{\Gamma_b}{\Gamma_a}] \qquad (68d)$$

$$\varepsilon_{CO,w} = [(1+\nu_a)-(1+\nu_b)\frac{1+\nu_g}{\nu_g}\frac{\Gamma_b}{\Gamma_a} - \{\nu_b-\nu_a\}\{\frac{\nu_b\Gamma_b}{\xi_w} \text{ x}$$

$$(1-e^{-\xi_w}) - e^{-\xi_w}(\frac{1+\nu_g}{\nu_g}Y_{0,\infty} + Y_{CO_2,\infty})\Gamma_b\}]/[1 - \frac{1+\nu_g}{\nu_g}\frac{\Gamma_b}{\Gamma_a}] \qquad (68e)$$

where

$$\Gamma_a = E^+_{w,a} \ (D_{III,w})_a \ e^{-E^+_{w,a}/\theta_w}/\theta_w \qquad (69a)$$

$$\Gamma_b = E^+_{w,b} \ (D_{III,w})_b \ e^{-E^+_{w,b}/\theta_w}/\theta_w \qquad (69b)$$

$(D_{III,w})_a$ = the third Damkohler number for the reaction "a" (see equation 68c) based on carbon consumption,

$$r_w \ A_{w,a} \ (p/E_{w,a})/\rho D, \qquad (69c)$$

$(D_{III,w})_b$ = the third Damkohler number for the reaction "b" (see equation 68c) based on carbon consumption,

$$r_w \ A_{w,b} \ (p/E_{w,b})/\rho D, \qquad (69d)$$

$E^+_{w,a}$ = $E_{w,a}/E_g$, a ratio of activation energy of surface reaction "a" to the gas phase activation energy,

$E^+_{w,b}$ = $E_{w,b}/E_g$

ν_a = $(\nu_0 W_0/\nu_c W_c)_a$, stoichiometric consumption of oxygen per unit mass of carbon for reaction "a",

$$\nu_b = (\nu_{CO_2} W_{CO_2} / \nu_c W_c)_b, \text{ stoichiometric consumption}$$

of CO_2 per unit mass of carbon for the

reaction "b" (69e)

$Y_{CO,w}$ = mass fraction of CO at the surface,

$\varepsilon_{CO,w}$ = flux fraction of CO at the surface,

$A_{w,a}, A_{w,b}$ = pre-exponential factors for reactions "a"

and "b", respectively.

As $\eta \to 0$,

$$Y_{CO} = Y_{CO,\infty} \qquad (70)$$

Since there are three boundary conditions for the second
order ordinary nonlinear differential equation, the nondimen-
sional bulk velocity at the surface ξ_w is solved as an
eigenvalue of the problem. Note that Y_0 and θ in equation
(68) can be brought in terms of Y_{CO} and η using equations
(29), (24), (23a) and (23b).

6.4. Numerical Methods of Solution

Essentially two methods were originally adopted.
Section 6.4.1 deals with the sandwich method and Section
6.4.2 deals with the initial value method with Nachsteim's
modification [66]. The latter method is dealt with more
detail as this was found to be the better method. A
general subroutine is presented for the initial value
method for use in the particle burning problem.

6.4.1. Sandwich Method

First an eigenvalue is selected such that the mass fractions of all the species of interest at the surface are between zero and one. Then the integrals of the two first order differential equations are obtained (i.e. the second order differential equation (68)). The boundary condition at $\eta = 0$ is checked (equation 70). If it is not matched, an increment $+\Delta\xi_w$ to the eigenvalue ξ_w is taken and the procedure is repeated. Now if the difference between the mass fraction thus obtained by integration at $\eta = 0$ $((Y_{CO,\infty})_i)$ and the actual mass fraction of CO ($Y_{CO,\infty}$, see equation (70)) is increasing, then the increment $-\Delta\xi_w$ is given to the engenvalue ξ_w and the procedure is once more repeated. Now the difference $((Y_{CO,\infty})_i - Y_{CO,\infty})$ may continue to decrease and eventually change in sign as more decrements are given. At this time, the interval is subdivided and the decrements are given in small amount. The procedure is thus repeated until the proper eigenvalue is found which can satisfy the boundary condition given by equation (70).

The convergence rate is very slow for this method. However, this method appeared to work well for a problem with no chemical kinetics [67].

6.4.2. Initial Value Method

The method adopted here is a modified initial value method. The method is illustrated in detail for this

problem.

(i) First consider the following two first order differential equations:

$$\frac{dY(1)}{d\eta} = D_{III,g} \ e^{-1/Y(3)} \ Y_0^{n_0} \ \{Y(2)\}^{n_{CO}}/\eta^4 \ Y(3)^{n} \qquad (71)$$

$$\frac{dY(2)}{d\eta} = Y(1) - Y(2) \ \xi_w \qquad (72)$$

where

$$Y(1) = \frac{dY(2)}{d\eta} + \xi_w \ Y(2) \qquad (73a)$$

$$Y(2) = Y_{CO} \qquad (73b)$$

$$Y(3) = \theta \qquad (73c)$$

and $Y(3)$ and Y_0 are given in terms of $Y(2)$ and η with the use of equations (29), (24), (23a) and (23b):

$$\frac{dY(3)}{d\eta} = \left\{ \frac{\xi_w e^{-\eta \xi_w}}{1-e^{-\xi_w}} \right\} \left\{ h_{T,w}^+ + (Y_{CO,w} - Y_{CO,\infty})Q_g^+ \right\}$$

$$- Q_g^+ \ \frac{dY(2)}{d\eta} \qquad (74a)$$

$$Y_0 = \left\{ \frac{1-e^{-\eta \xi_w}}{1-e^{-\xi_w}} \right\} \left\{ Y_{0,w} - Y_{CO,w} \nu_g + Y_{CO,\infty} \nu_g - Y_{0,\infty} \right\}$$

$$+ Y(2)\nu_g - (Y_{CO,\infty}\nu_g - Y_{0,\infty}) \qquad (74b)$$

where

$$Y_{0,w} = [\frac{\xi_w}{\Gamma_a} + \nu_b(1-e^{-\xi_w}) \frac{\Gamma_b}{\Gamma_a}$$

$$- e^{-\xi_w} \frac{\Gamma_b}{\Gamma_a} \{ \frac{1+\nu_g}{\nu_g} Y_{0,\infty} + Y_{CO_2,\infty} \}] / [1 - \frac{1+\nu_g}{\nu_g} \frac{\Gamma_b}{\Gamma_a}] \qquad (74c)$$

The integrals of equations (71), (72), and (74a) are obtained with the use of the following initial conditions:

At $\eta = 1$,

$$Y(1) = \xi_w \varepsilon_{CO,w} \qquad \text{(see equation (68e))}$$

$$Y(2) = Y_{CO,w} \qquad \text{(see equation (68d))} \qquad (74d)$$

$$Y(3) = \theta_w \qquad \text{(specified for given surface temperature)}$$

Also a value for ξ_w is assumed such that $0 \leq Y_{i,w} < 1$.

(ii) The equations (71), (72) and (74a) are differential with respect to the eigenvalue. Thus the following

perturbation equations are obtained:

$$\frac{dY(4)}{d\eta} = \frac{dY(1)}{d\eta}\left[Y(6)\left\{\frac{1}{(Y(3))^2} - \frac{n}{Y(3)}\right\} + n_{CO}\frac{Y(5)}{Y(2)} + \frac{n_0}{Y_0}\frac{\partial Y_0}{d\xi_w}\right] \quad (74e)$$

$$\frac{dY(5)}{d\eta} = Y(4) - Y(5)\,\xi_w - Y(2) \quad (74f)$$

and the integral of the perturbation equation obtained from (74a) is given as,

$$Y(6) = \left\{\frac{1}{1-e^{-\xi_w}}\right\}\{h_{T,w}^+ + (Y_{CO,w} - Y_{CO,\infty})Q_g^+\}\{\eta e^{-\eta\xi_w} - e^{-\xi_w}$$

$$\times(1-e^{-\xi_w})\} + \frac{dY_{CO,w}}{d\xi_w}Q_g^+\left\{\frac{1-e^{-\eta\xi_w}}{1-e^{-\xi_w}}\right\} - Y(5)Q_g^+ \quad (74g)$$

where,

$$Y(4) = \frac{\partial Y(1)}{\partial\xi_w}$$

$$Y(5) = \frac{\partial Y(2)}{\partial\xi_w} \qquad\qquad (75)$$

$$Y(6) = \frac{\partial\theta}{\partial\xi_w}$$

$$\frac{\partial Y_0}{\partial\xi_w} = Y(5)v_g - \left\{\frac{\eta e^{-\eta\xi_w}}{1-e^{-\eta\xi_w}} - \frac{(1-e^{-\eta\xi_w})e^{-\xi_w}}{(1-e^{-\xi_w})^2}\right\}x$$

$$x \left\{ Y_{CO,w} \nu_g - Y_{0,w} + Y_{0,\infty} - Y_{CO,\infty} \nu_g \right\}$$

$$- e^{-\xi_w} \frac{1 - e^{-\eta \xi_w}}{1 - e^{-\xi_w}} \left\{ (1 + \nu_b) \nu_g + (Y_{0,\infty} - Y_{CO,\infty} \nu_g) \right\} \qquad (76a)$$

$$\frac{dY_{CO,w}}{d\xi_w} = [e^{-\xi_w} (1 + \nu_b) - e^{-\xi_w} (Y_{CO,\infty} - \frac{Y_{0,\infty}}{\nu_g}) + \frac{1}{\Gamma_a} \frac{1}{\nu_g}$$

$$- e^{-\xi_w} \frac{(1 + \nu_g + \nu_g \nu_b)}{\nu_g} \frac{\Gamma_b}{\Gamma_a} +$$

$$\frac{e^{-\xi_w}}{\nu_g} (1 + \nu_g) Y_{CO,\infty} + Y_{CO_2,\infty} \frac{\Gamma_b}{\Gamma_a}] / [1 - \frac{1 + \nu_g}{\nu_g} \frac{\Gamma_b}{\Gamma_a}] \qquad (76b)$$

$$\frac{dY_{0,w}}{d\xi_w} = [\frac{1}{\Gamma_a} + \nu_b e^{-\xi_w} \frac{\Gamma_b}{\Gamma_a} + e^{-\xi_w} \frac{1 + \nu_g}{\nu_g} Y_{0,\infty} + Y_{CO_2,\infty} \frac{\Gamma_b}{\Gamma_a}] /$$

$$[1 - \frac{1 + \nu_g}{\nu_g} \frac{\Gamma_b}{\Gamma_a}] \qquad (76c)$$

$$\frac{\partial \varepsilon_{CO,w}}{d\xi_w} = \frac{\Gamma_a}{\xi_w^2} (\nu_b - \nu_a) Y_{0,w} - \frac{\Gamma_a}{\xi_w} (\nu_b - \nu_a) \frac{dY_{0,w}}{d\xi_w} \qquad (76d)$$

The integrals of equations (74e) and (74f) are obtained
with the use of the following known initial conditions:
At $\eta = 1$,

$$Y(4) = \varepsilon_{CO,w} + \xi_w \frac{d\varepsilon_{CO,w}}{d\xi_w} \tag{77a}$$

$$Y(5) = \frac{dY_{CO,w}}{d\xi_w} \tag{77b}$$

$$Y(6) = 0 \tag{77c}$$

(iii) The integrals of equations (71), (72), (74a), (74e) and (74f) are obtained with the use of initial conditions (74d) and (77). For integration the Adams-Moulton integration schemes are used and the necessary subroutine was taken from Reference [66].

(iv) The boundary condition (70) is expanded around the value of $Y(2)$ thus obtained with an assumed eigenvalue, using Taylor's expansion:

$$Y_{CO,\infty} = Y(2)_{\eta=0} + Y(5)_{\eta=0} \Delta\xi_w \tag{78a}$$

where

$$\Delta\xi_w = \xi_{w,new} - \xi_{w,old} \tag{78b}$$

(v) The value $Y(5)$ at $\eta = 0$ is obtained from the integral of equation (74f). The value $Y(2)$ at $\eta = 0$ is obtained from integral of equation (72). Thus $\Delta\xi_w$ is estimated and a new eigenvalue is found. Steps (i) to (v)

thus constitute the initial value method. The following additional steps are necessary if Nachsteim's modification is incorporated in the above method.

(vi) Note that ordinarily equation (78a) consists of a remainder term. Also for an asymptotic problem (for example a boundary layer problem), a desired parameter (velocity) must approach the proper value asymptotically (i.e. the velocity gradient must approach zero). Nachsteim used both the above boundary conditions (velocity and velocity gradient) and found the two corresponding remainder terms. He selected the eigenvalue such that the sum of the squares of the two remainder terms is a minimum. A corresponding situation exists here since as $Y_{CO} \to 0$, $\theta \to \theta_\infty$. However these two boundary conditions are linearly dependent on each other and thus Nachsteim's procedure does not make any difference. Since it was intended to form a general subroutine for this method, for a system of N unknowns at the start of the integration of a system of differential equations, the procedure is explained for this problem. Let there be N unknowns at the start of the integration (for example for this problem N = 1). At the other boundary (i.e. $\eta = 0$) there are 2N conditions to be satisfied (i.e. for this problem N = 2, $Y_{CO} = Y_{CO,\infty}$ and $\theta = \theta_\infty$). Hence one must have 2N remainder terms (i.e. 2 remainder terms here: $\delta_1 = \{Y(2)\}_{\eta=0} - Y_{CO,\infty} + \{Y(5)\}_{\eta=0} \Delta \xi_w$, $\delta_2 = \{Y(3)\}_{\eta=0} - \theta_\infty + \{Y(6)\}_{\eta=0} \Delta \xi_w$). The increment for the N initial values

values is obtained by having the sum $(\delta_1{}^2 + \delta_2{}^2 \ldots + \delta_{2N}{}^2)$ a minimum. Thus using the least squares method, (see Appendix E.2) the following results are obtained:

For minimum $\sum\limits_{j=1}^{2N} \delta_j^2$,

$$[F] \ [s] = [M] \tag{79a}$$

and hence,

$$[s] = [F]^{-1} \ [M] \tag{79b}$$

where,

$$
F = \begin{vmatrix}
\sum\limits_{j=1}^{2N} a_{j1}a_{j1} & \sum\limits_{j=1}^{2N} a_{j2}a_{j1} & \cdots & \sum\limits_{j=1}^{2N} a_{jN}a_{j1} \\[2em]
\sum\limits_{j=1}^{2N} a_{j1}a_{j2} & \sum\limits_{j=1}^{2N} a_{j2}a_{j2} & \cdots & \sum\limits_{j=1}^{2N} a_{jN}a_{j2} \\[2em]
\cdot \cdot \cdot \cdot \cdot \cdot \cdot \cdot \cdot \cdot \\[2em]
\sum\limits_{j=1}^{2N} a_{j1}a_{jN} & \sum\limits_{j=1}^{2N} a_{j2}a_{jN} & \cdots & \sum\limits_{j=1}^{2N} a_{jN}a_{jN}
\end{vmatrix} \tag{80a}
$$

$$s = \begin{vmatrix} s_1 \\ s_2 \\ .. \\ s_N \end{vmatrix} \qquad (80b)$$

$$M = \begin{vmatrix} \sum\limits_{j=1}^{2N} a_{j1} a_{10} \\ \\ \sum\limits_{j=1}^{2N} a_{j2} a_{j0} \\ \\ \cdots \\ \\ \sum\limits_{j=1}^{2N} a_{jN} a_{j0} \end{vmatrix} \qquad (80c)$$

where,

$$\delta_j = a_{j0} + \sum_{i=1}^{N} a_{ji} s_i \qquad (81)$$

a_{j0} = the difference between the actual jth boundary
condition at $\xi = 0$ and the condition obtained
by iteration at the same location (e.g.:
$\{Y(2)\}_{\eta=0} - Y_{CO,\infty}$).

a_{ji} = the first partial derivative of jth boundary
condition with respect to the ith initial value

which occur in the Newton Raphson technique.
(e.g.: $\{Y(5)\}_{\eta=0}$ in equation (78a)).

s_i = the increment in the ith initial value or the eigenvalue as in this problem (e.g.: $\Delta\xi_w$ in equation (78b).

δ_j = the error introduced by Taylor series when the series is expanded up to first order, i.e. the remainder term.

Equation (79a) is solved by using the Gauss-Jordan elimination method (GJEM). A subroutine for GJEM is presented in Reference [52].

(vii) Many times the integration breaks down at some intermediate point where the mass fraction of some species or the temperature becomes less than zero and this is not permissible. To avoid this the following procedure is introduced:

If the iterated quantity $(Y_{j,\infty})$ is very near the proper boundary condition, then expanding in Taylor's series around $\eta = \eta_{stop}$,

$$Y_{j,\infty} = (Y_{j,\infty})_i + (\frac{\partial Y_j}{\partial \eta})_{\eta_{stop}} (0 - \eta_{stop}) + (\frac{\partial Y_j}{\partial \xi_w})_{\eta_{stop}} \Delta\xi_w \qquad (82)$$

The term $(\frac{\partial Y_j}{\partial \xi_w})_{\eta_{stop}}$ is evaluated from the integrals of the perturbation equations at $\eta = \eta_{stop}$. The term $(\frac{\partial Y_j}{\partial \eta})_{\eta_{stop}}$ is known from the integrals of the original differential

equations at $\eta = \eta_{stop}$. Thus the necessary increment $\Delta\xi_w$ is found by repeating the procedure (vi) so that the integration could be continued from $\eta = \eta_{stop}$ to $\eta = 0$. A subroutine for this initial value method including Nachsteim's modification along with step (vi) is presented in Appendix E.3.

CHAPTER VII

RESULTS AND DISCUSSION FOR THE

COMBUSTION CHARACTERISTICS

The equations presented in Section 6.3 are solved using the numerical schemes presented in Section 6.4.2. Section 7.1 presents a table listing the chemical kinetics constants for some chars and cokes. Since the main parameter of interest here is the burning rate, its variation with particle surface temperature, particle size and pressure are presented and discussed in Section 7.2. Each computation on the average took about 1 second of CPU time. The particle temperature at which there is maximum erosion rate of carbon is found. Since this indicates the existence of considerable levels of CO, a general relation, for this particle temperature at peak burning condition, in terms of particle size and pressure is desirable. Such a relation is presented in Section 7.3 and is used to correlate the data obtained in Section 7.2.

7.1. Selection of Chemical Kinetics Constants

For the surface heated carbon or hard char particles, one requires the quantitative kinetics of the three reactions for determining the combustion characteristics: (i) heterogeneous oxidation of carbon, (ii) heterogeneous

reduction of carbon at the surface, and (iii) gas phase oxidation of CO. Various mechanisms for these reactions are well explained in the literature survey by Walker et al. [35] and Howard et al. [64].

The chemical kinetic constants for the heterogeneous oxidation are tabulated in Table 4 along with the references. The method of conversion to the present form using data found in the literature is explained in Appendix D. The reduction kinetics of carbon with CO_2 was selected from reference [63] where they conducted experiments for a pitch coke. The order of reaction was found to be complex at low temperature while at higher temperatures the order approaches unity. Here it has been assumed that the order is unity and the kinetics of reduction are the same for all chars (normally char is relatively hard compared to coke; coke is the product from the high temperature distillation of moisture and volatiles while char is a product from low temperature carbonization of coal). The gas phase oxidation kinetics of CO are very well collected by Howard et al. [64]. The kinetic constants quoted by Sobolev [65] have been selected here. It is found that the order with respect to CO remains almost near unity while with oxygen, the order appears to vary from 0 to 1, the former value being a good approximation to the values quoted in several references. Also, Sobolov presents results only for monomolecular oxidation of CO though he found that the order with respect

Table 4. Chemical Kinetics Constants for CO Production
and Oxidation for Selected Coals

No.	Reaction Equation	n_F	n_0	D_{III}	E	Reacting Species	References	Remarks
1	$C + \frac{1}{2} O_2 \rightarrow CO$	0	1.0	47.0	13550.0	Brown Coal	[8]	--
		0	1.0	23.0	18200.0	Petroleum Coke	[34]	--
		0	1.0	13.0	16700.0	Anthracite Char	[34]	--
		0	1.0	11.0	16000.0	Bituminous Char	[34]	--
		0	1.0	12.6	16200.0	Brown Coal Char	[3]	--
	$C + CO_2 \rightarrow 2CO$	0	1.0 ($>1000°K$)	0.590	40200.0	Petroleum Coke	[63]	--
	$CO + \frac{1}{2} O_2 \rightarrow CO_2$	1.0	0.0 ($Y_0 > 5\%$)	68.00	30000.0	CO gas	[65]	Assumed $n = 1.0$ in the calculation
		1.0	1.0 ($Y_0 < 5\%$)	1.00 to 6.00	30000.0	CO gas	[65]	

All Damkohler numbers are evaluated for a particle size of 100μm based on carbon consumption.

Overall order of reaction $n = n_F + n_0$

to oxygen approaches unity when the oxygen concentration
falls below 5 percent (volumetric). However an attempt was
made to extract the kinetics of CO oxidation with overall
order as two from the figure given by Sobolov (see Appendix
D); this calculation is subject to an error of about 600
percent. Such results are also listed in Table 4. For
detailed calculations for many char particles, only mono-
molecular oxidation was assumed since the kinetics are
readily available.

7.2. Variation of Burning Rates
7.2.1. Effect of Particle Temperature

Figure 16b presents results for burning rate versus
surface temperature for petroleum coke, anthracite and
bituminous char particles while Figure 17 gives the corre-
sponding curves for brown coal particles with a high carbon
content. Though the analysis is doubtful for the brown
coals, still the results are included for the reason that
this coal exhibits a rather pronounced peak so that one can
obtain the results for a wide range of parameters which then
lead to the prediction of characteristics of burning for any
char particle with a similar behavior. As mentioned
earlier there are three regions (see Figure 17).

Region I corresponds to a situation of CO-DC. One
can obtain the activation energy for the production of CO
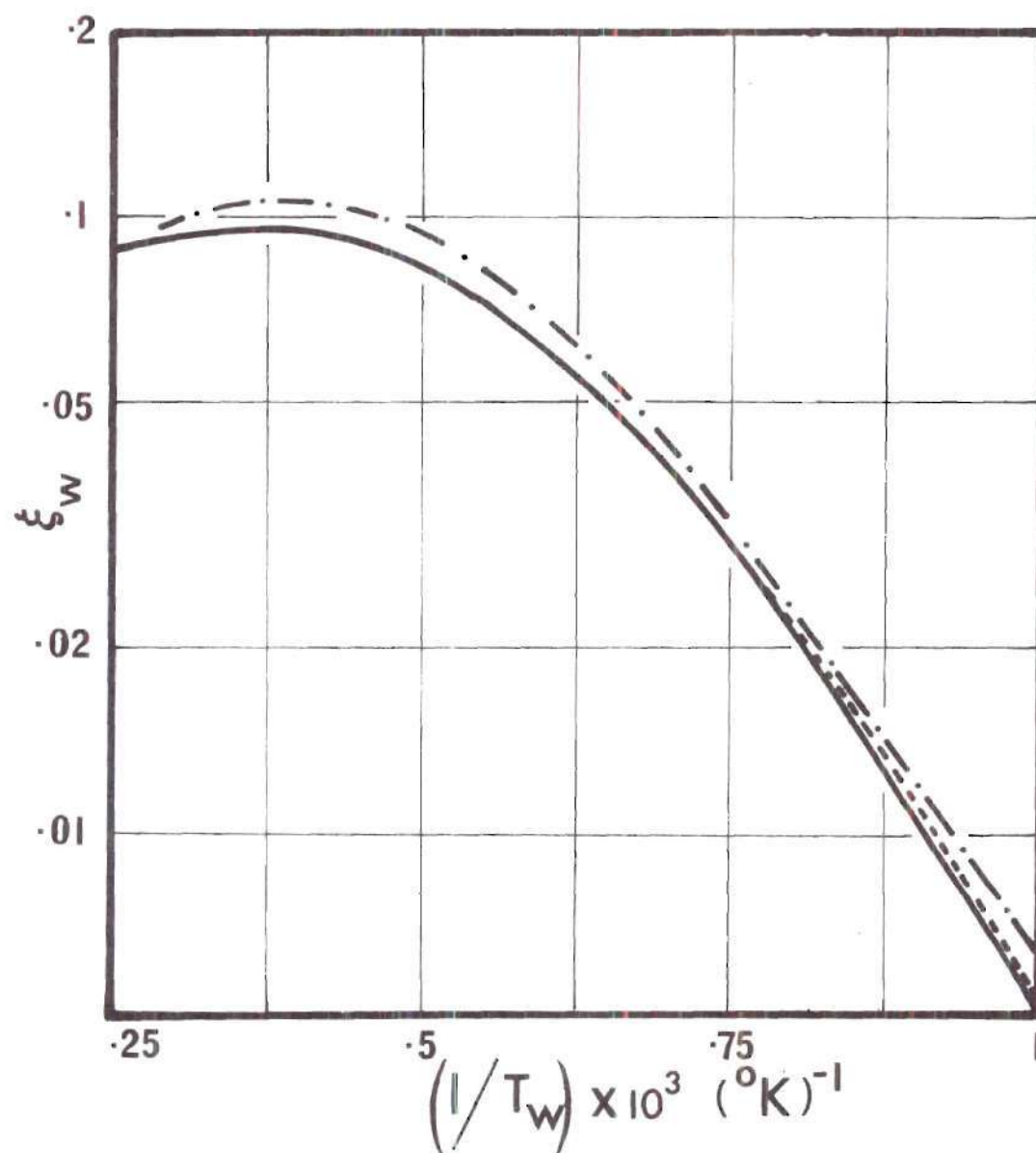in this region since the plot of burning rate versus

Figure 16b. ξ_W versus $1/T_W$ for Chars and Cokes

——— Petroleum Coke
- - - - Anthracite Char
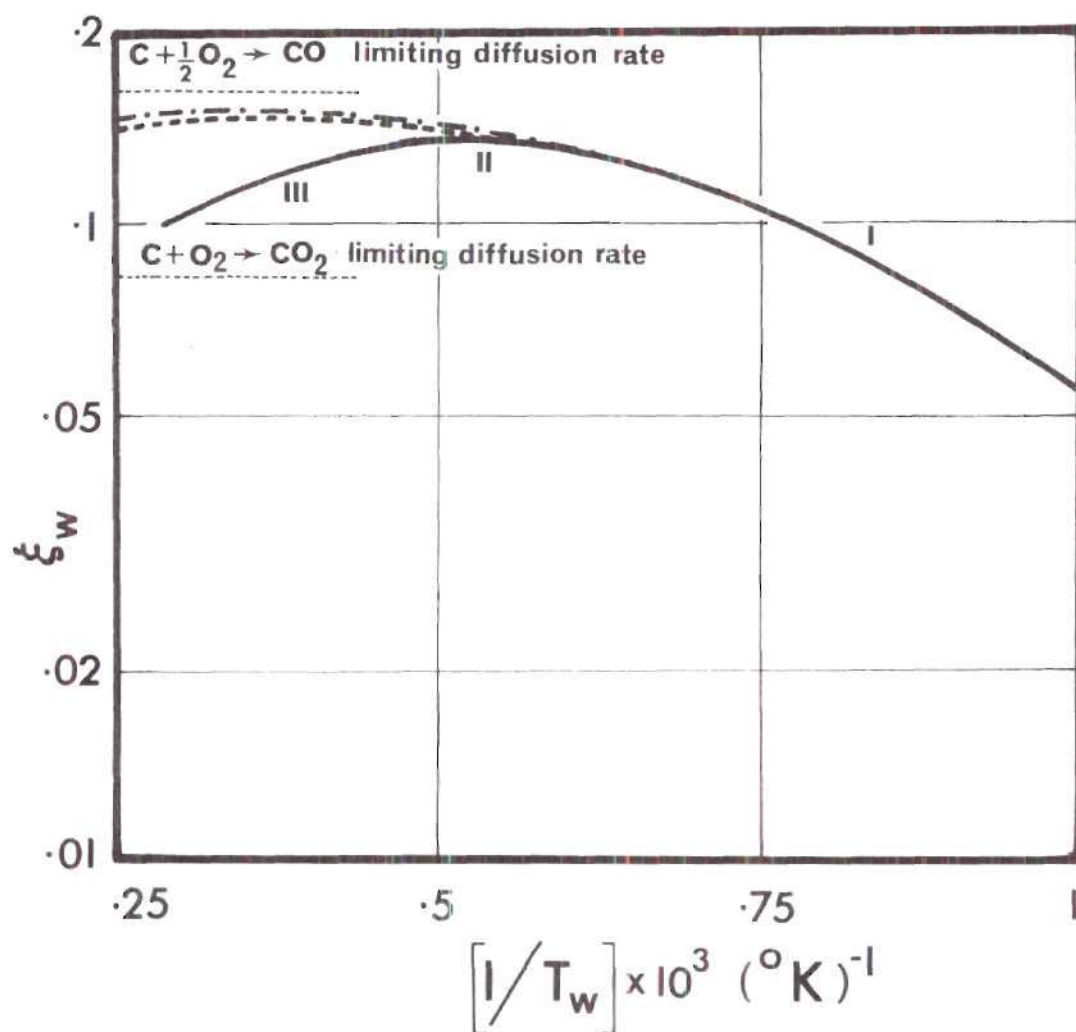-·-·· Bituminous Char

Figure 17. ξ_w versus $1/T_w$, Brown Coal, 100 μm

——— $n_{CO} = 1.0$, $n_0 = 0$, $D_{III,g} = 68.0$

- - - - $n_{CO} = 1.0$, $n_0 = 1.0$, $D_{III,g} = 6.0$

-・-・ $n_{CO} = 1.0$, $n_0 = 1.0$, $D_{III,g} = 1.0$

$(1/T_w)$ exhibits almost a linear behavior (see Figure 16). Here the oxidation of CO is almost frozen. Brown coal exhibits less steepness compared to other char particles because the activation energy is low. All the results are carried out for a particle of 100 μm in diameter and at a pressure of 1 atm.

Region II exhibits the influence of gas phase oxidation of CO on the burning rate. Here the reduction of $Y_{0,w}$ (wall mass fraction of oxygen) occurs both due to heterogeneous oxidation and the gas phase oxidation of CO. The increase in the rate due to heterogeneous production of CO dominates the gas phase oxidation of CO.

Region III shows the dominance of gas phase oxidation of CO over the production of CO at the surface. Here the burning rate approaches a value similar to the diffusion limit for the direct CO_2 product at the surface. Thus the peak occurrence is an indication that the particle is still producing a significant amount of CO. Figure 17 also shows the consequence of assumption of second order gas phase reaction with a corresponding reduction in Damkohler number selected in Table 5.

Since the CO oxidation becomes rapid at some temperature, one should expect that the wall mass fraction of CO should also show a peak. Figure 18a shows a plot of wall mass fractions of CO, CO_2 and O_2 versus surface temperature and such a peak is exhibited for CO. Also, it is found that
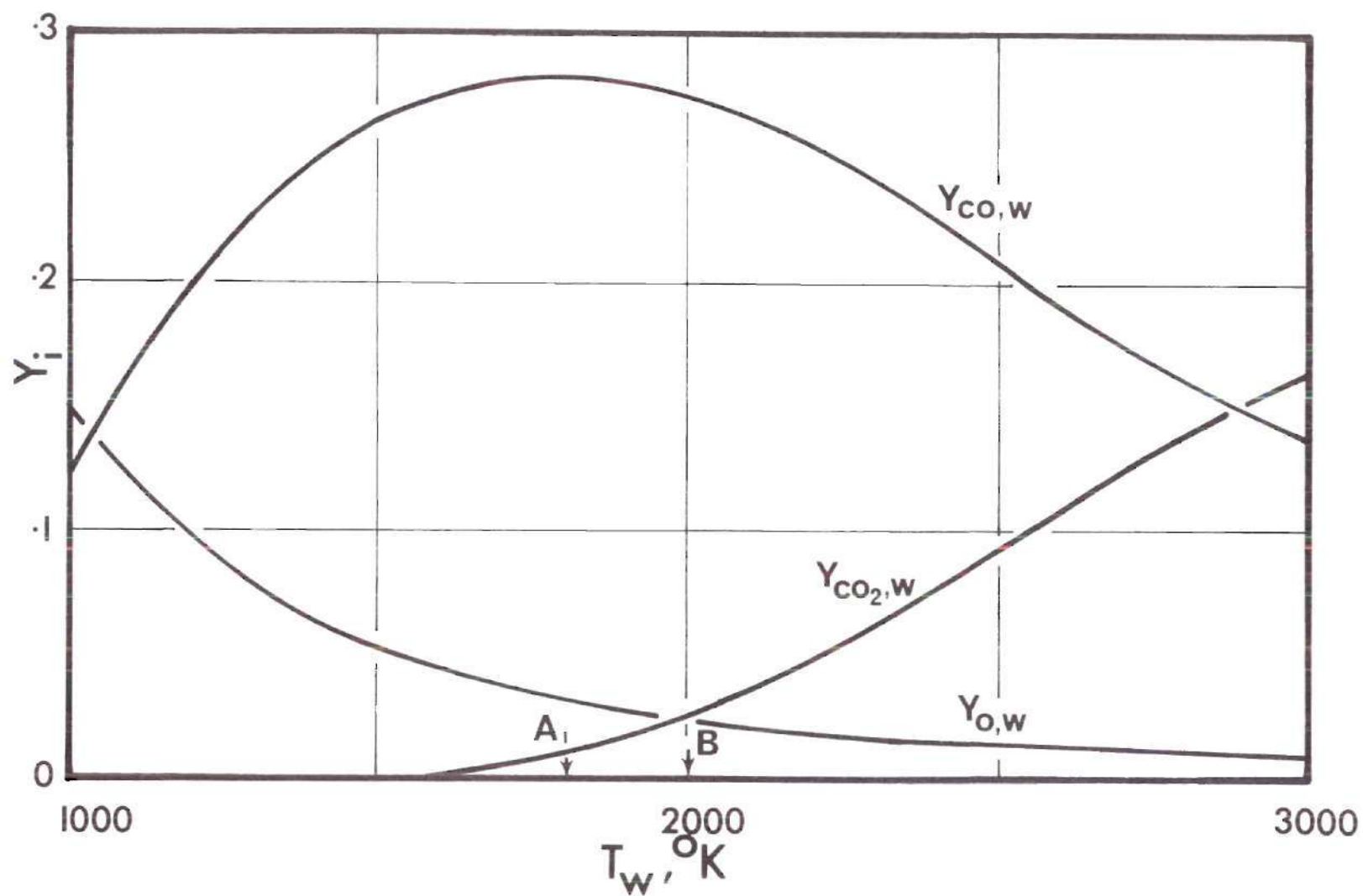
Figure 18a. Wall Mass Fraction of Species versus T_w, Brown Coal;
A: T_w corresponding to maximum $Y_{CO,w}$, B: T_w
corresponding to maximum burning rate.

the temperature corresponding to the peak burning rate is always higher than the one corresponding to the peak wall mass fraction of CO. This is expected since this is just a precursory event of impending occurrence of peak burning rate. Also, this is a point at which the intensive oxidation of CO is about to start. A plot of the flux fractions of CO and CO_2 at a large distance from the particle (see Figure 18b) versus the surface temperature reveal such a behavior. Figure 18c shows the temperature profiles at four surface temperatures: (i) 1000°K, almost frozen gas phase oxidation, (ii) 1800°K, peak $Y_{CO,w}$ point, (iii) 2000°K, peak burning point, and (iv) 2800°K, very fast gas phase oxidation. These were plotted to reveal the contribution of heat to the gases due to exothermic oxidation of CO. Due to cold surroundings, such a contribution is not significant. A temperature peak appears to be improbable for steady state burning, since the surface reaction is exothermic. Also notice that one has almost a linear plot for the frozen case. This too is expected for the coordinates selected here.

7.2.2. Effect of Particle Size

Figure 19a shows curves for burning rate versus inverse of the surface temperature, for brown coals of particle size ranging from 25 μm to 200 μm. As particle size is increased, the CO oxidation increases more rapidly than the corresponding increase in CO production rate and hence the peak burning point moves toward a lower surface
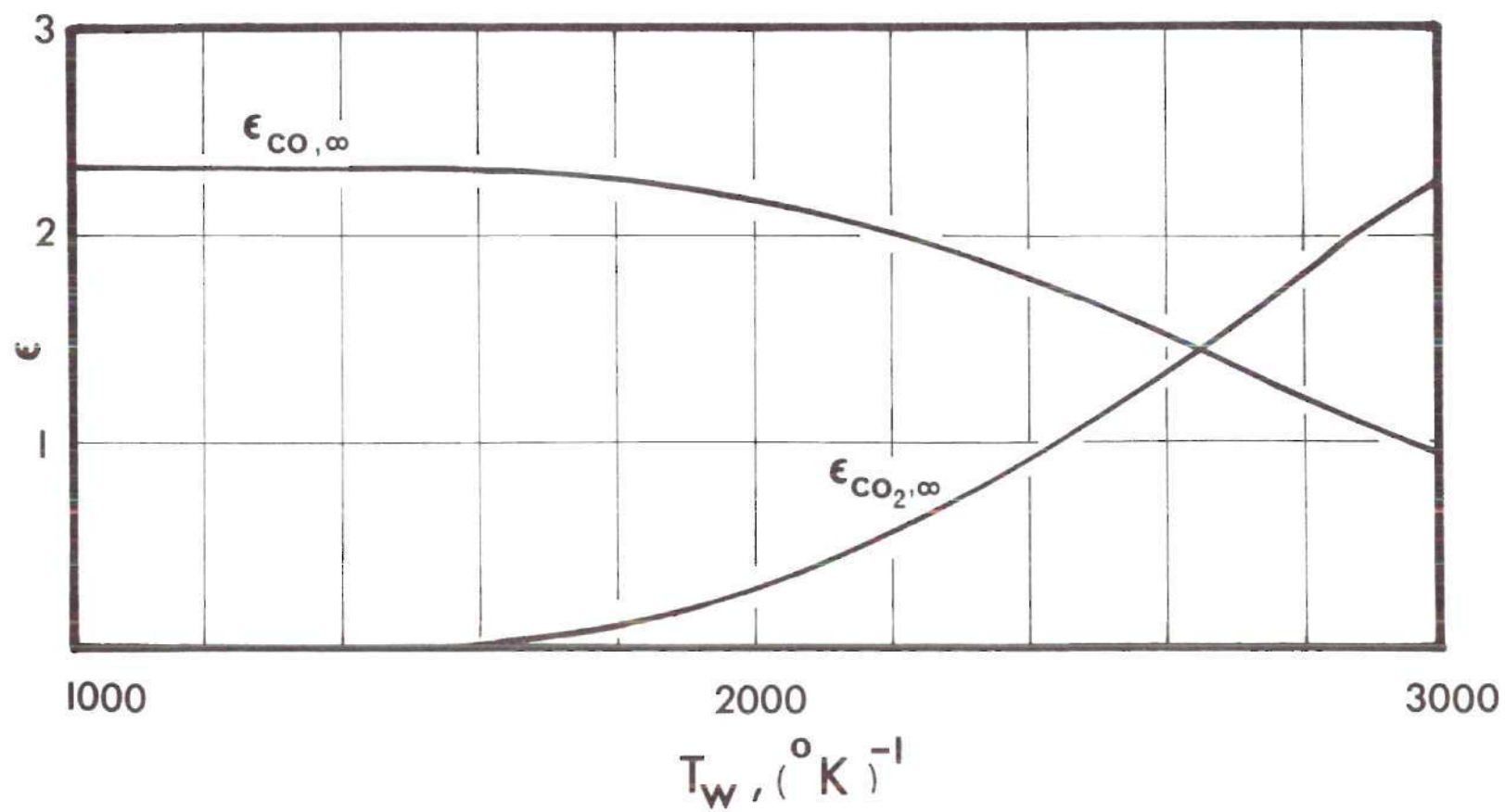
Figure 18b. Flux Fractions of CO and CO_2 at Infinity versus T_w
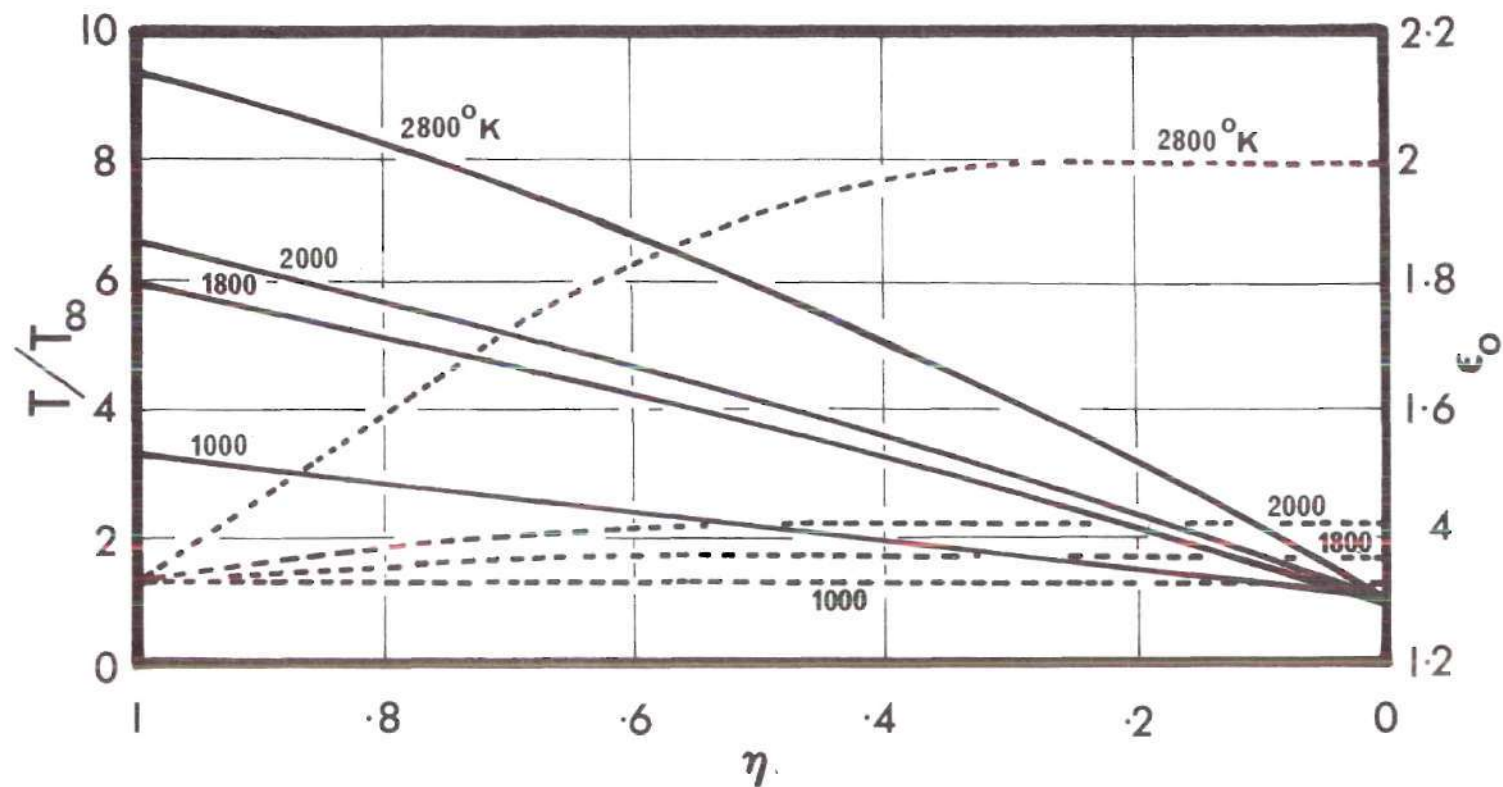
Figure 18c.   Temperature and Flux Fraction Profile

——— T/T_∞

--- ε_i

1800°K   Temperature Corresponding to Peak Wall
         Mass Fraction of CO

2000°K   Temperature Corresponding to Peak
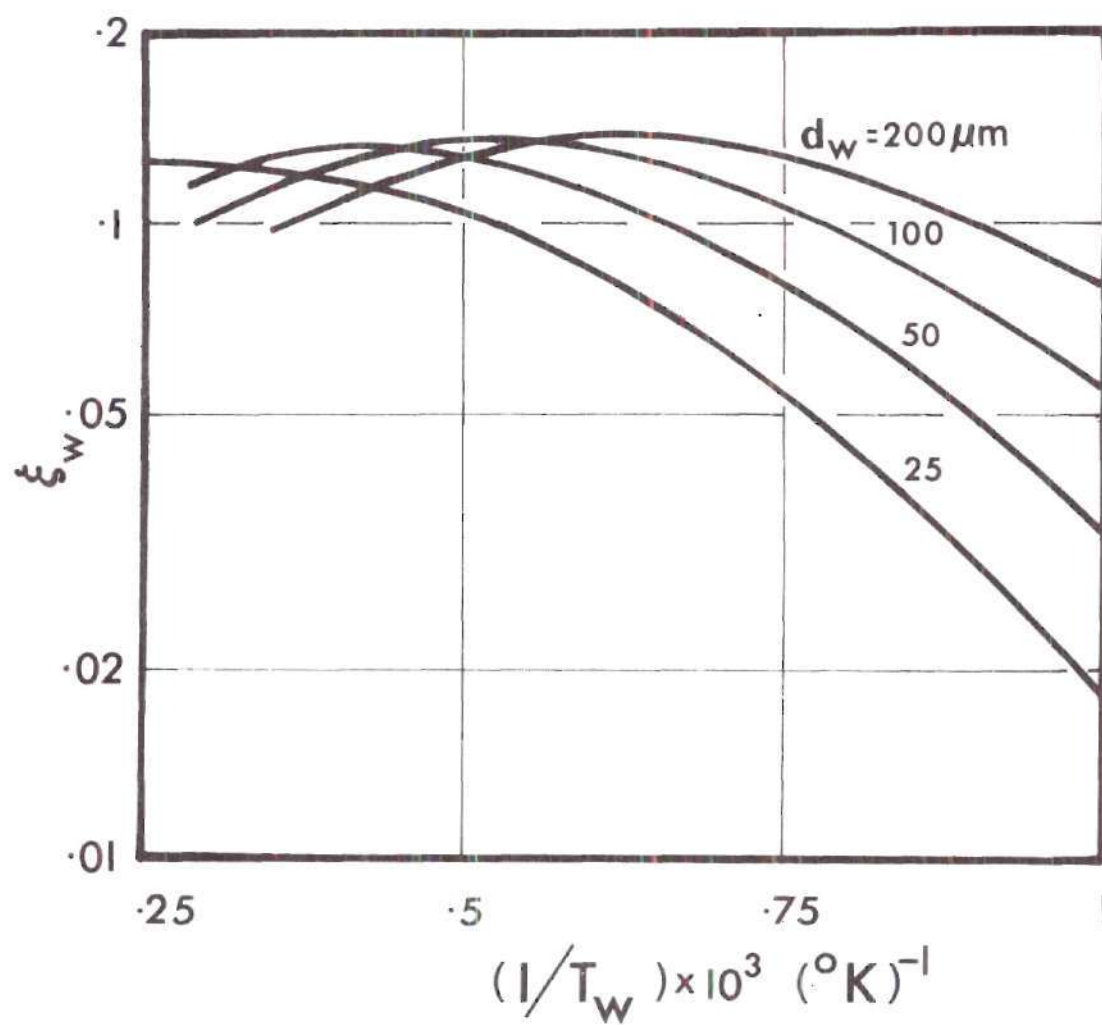   Burning Rate.

Figure 19a. Effect of Particle Size on Burning Rate versus $(1/T_w)$ Curves; Brown Coal

temperature. This is due to the fact that the gas phase reaction rate is proportional to the square of particle size while the surface reaction rate is proportional to the particle size. A reverse trend is exhibited when the particle size is decreased. Figure 19b shows a plot of inverse of peak burning temperature versus ln (particle size) and the plot appears to be linear. On the same plot the temperatures corresponding to peak $Y_{CO,w}$ were plotted. Both appear to have the same slopes. The points were indicated by short vertical lines to indicate the order of fluctuation in fixing the point since the iterative procedure was not carried out for every degree interval of surface temperature. The results will be discussed further in Section 7.3.

7.2.3. Effect of Pressure

Figure 20 shows the effect of increase in the pressure from about 0.1 atm to 10.0 atm, a hundred fold increase. The gas phase reaction and the surface reactions are proportional to the pressure. Since at higher pressures the approach to CO-DC will be faster (if activation energy for CO production is less), one should expect a lower peak burning temperature. Such a trend is shown in Figure 20.

7.3. General Correlation for Peak Burning
Particle Temperatures

Figure 21a shows a semilog plot of $(1/T_{w,p})$ versus d_w with pressure p as a parameter. Figure 21b shows the
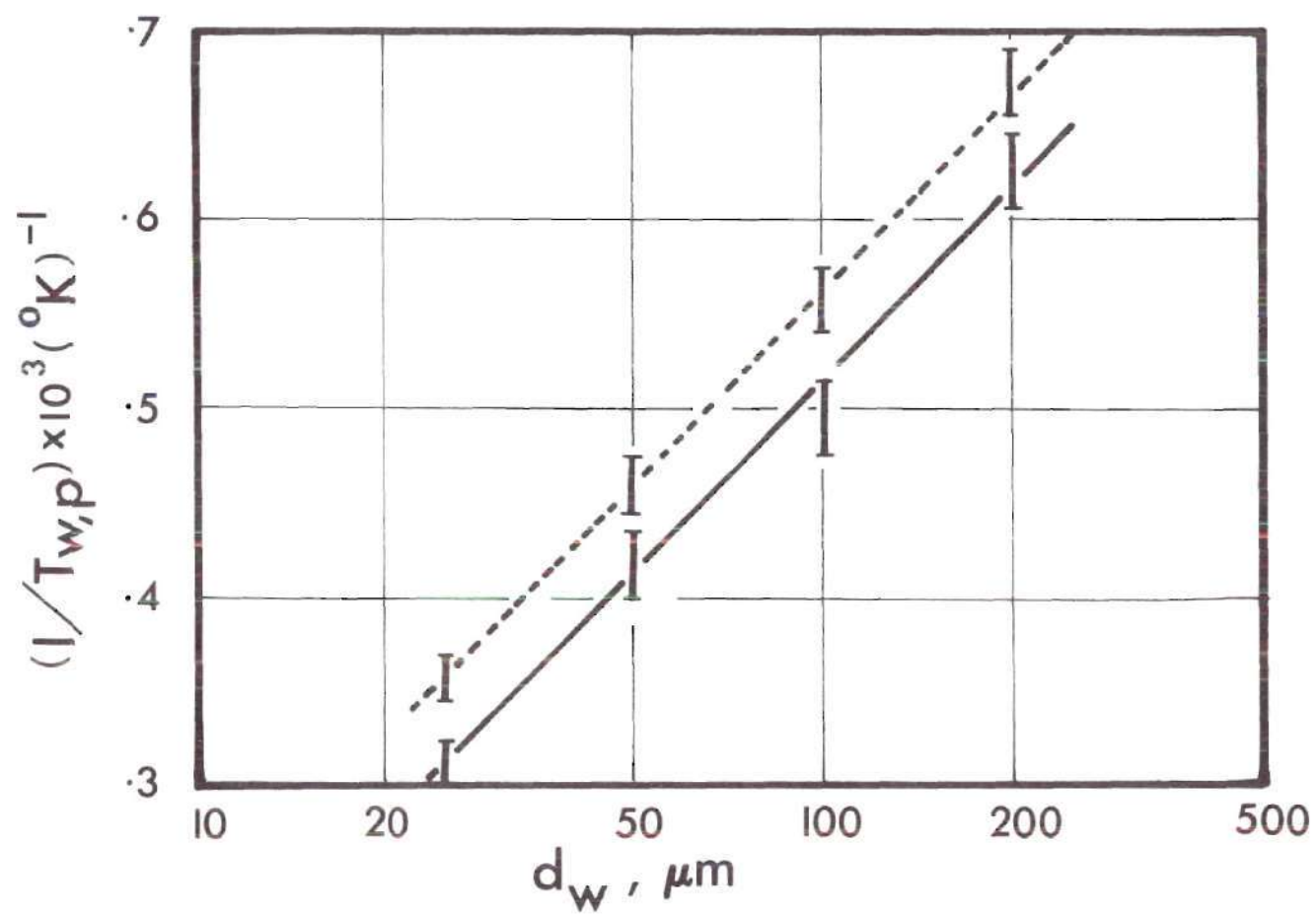
Figure 19b. $1/T_{w,p}$ versus d_w at Peak Points; Brown Coal; $\mathbf{I}$:

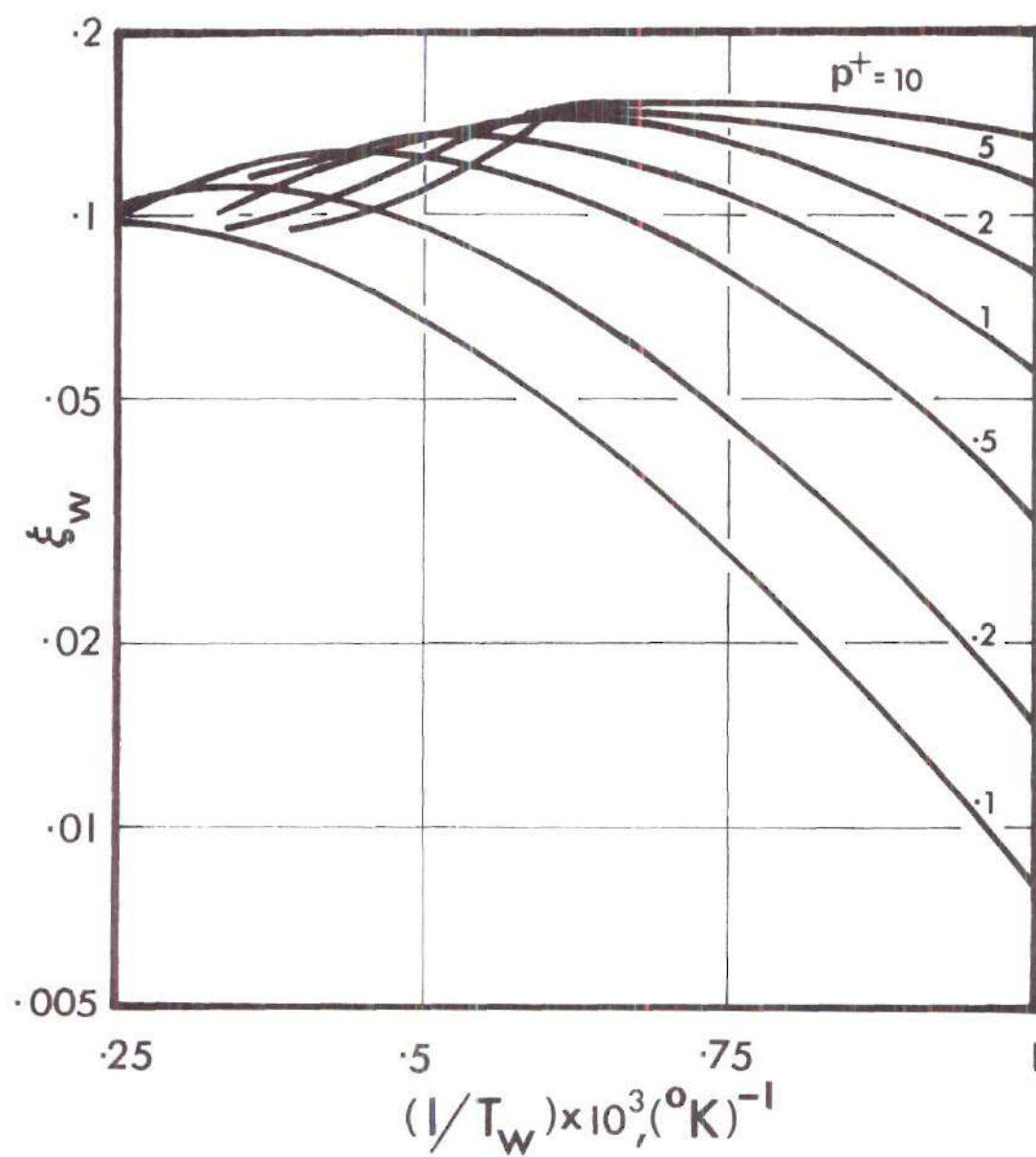Range of Possible Error in Fixing the Peak
Temperatures.

Figure 20. Effect of Pressure on Burning Rate versus $(1/T_w)$ Curves; Brown Coal
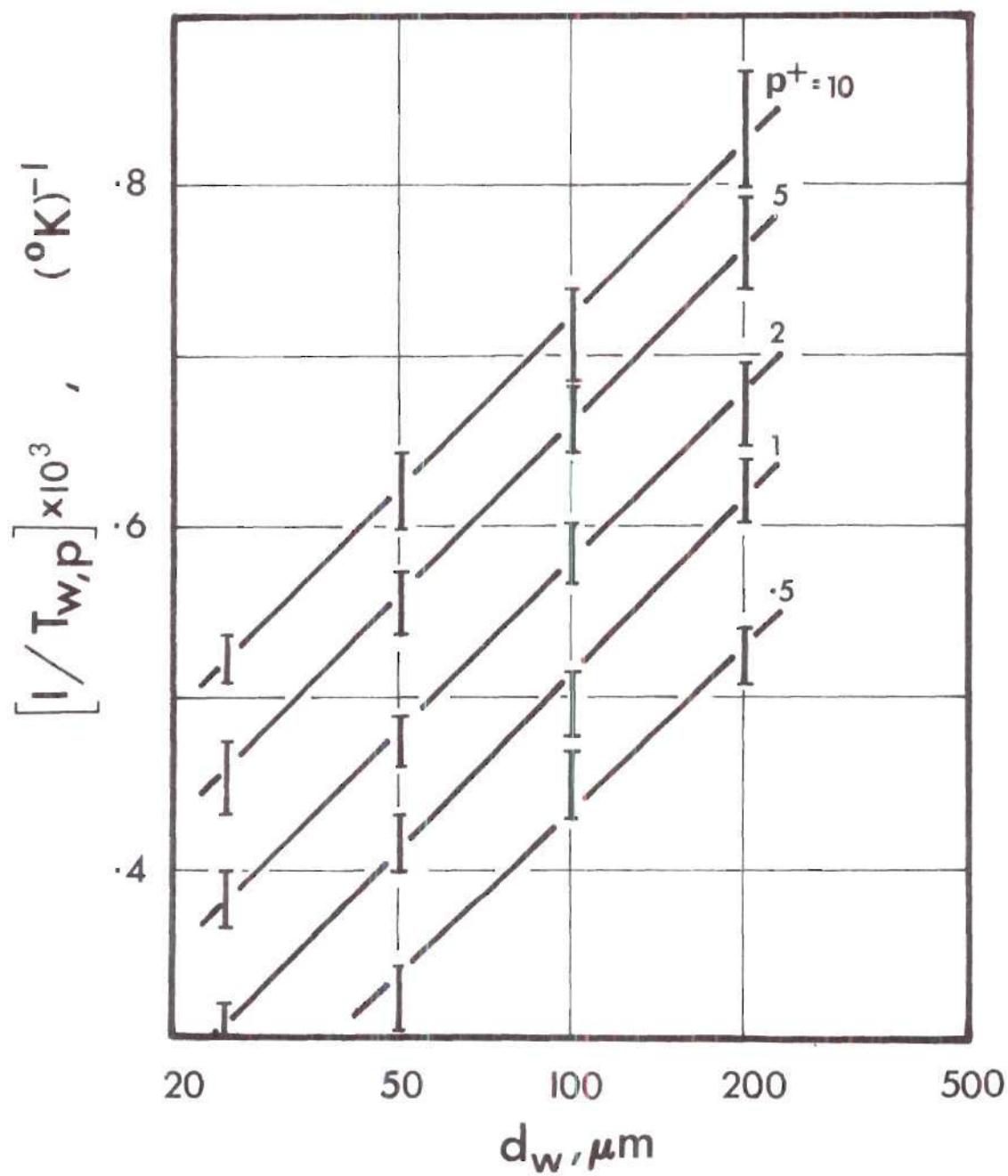
Figure 21a. Plot of $(1/T_{w,p})$ versus d_w with p^+ as Parameter
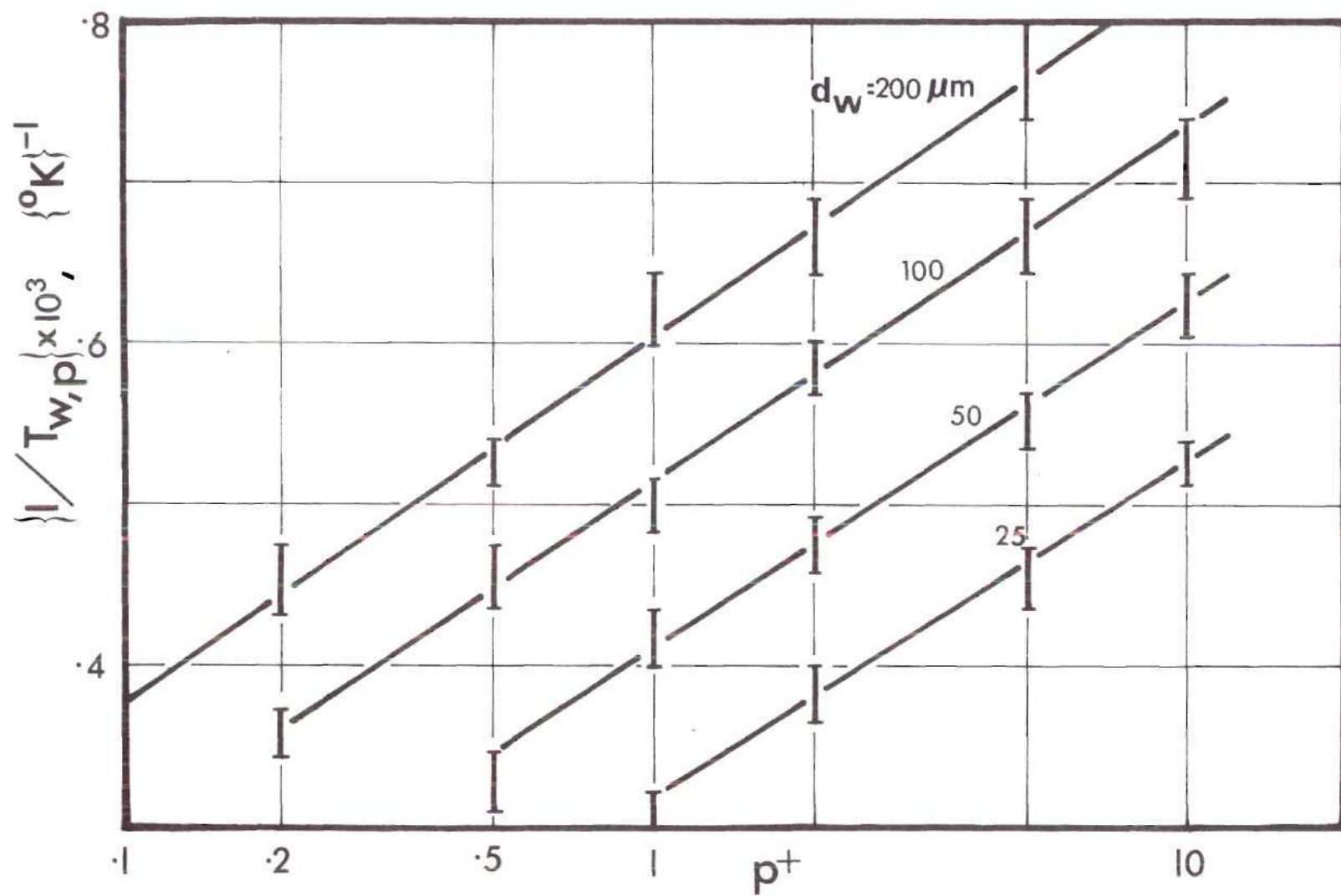
Figure 21b. Peak Burning Temperature versus p^+ with d_w as Parameter

same plot but with p as an independent variable and d_w as a parameter. It is observed that the peak burning temperatures are more sensitive to the particle size than to the pressure. Also all the plots were almost linear. A single curve is more desirable than parametric plots. When one is interested in finding a range of temperatures for a given size distribution of coal char or coal particles, beyond which a furnace with cold surroundings has to be operated for minimum production of CO, a general correlation or general plot is more desirable. Since the particle is surface heated, one expects that most of the CO oxidation occurs near the surface. Then imposing such an assumption, one can show at the time of peak burning (see Appendix E.4), that, (reduction process is also regligible)

$$D_{III,g} \frac{e^{-1/\theta_{w,p}}}{\theta_{w,p}^n} (D_{III,w})_a \frac{e^{-E_{w,a}^+/\theta_{w,p}}}{\theta_{w,p}} \simeq const. \qquad (83)$$

Assuming a general overall order of reaction as unity for the gas phase oxidation,

$$D_{III,g} \propto d_w^2 (p^+) \qquad (84a)$$

and assuming general power law for particle size for surface reaction

$$(D_{III,w})_a \; \alpha \; d_w^{m_1} \; p^+ \tag{84b}$$

Then, considering the dominant exponential terms only

$$1/T_{w,p} = \frac{R^\circ}{E_g(E_{w,a}^+ + 1)} \; \ln \; (d_w^{m_1+2} \; p^{+2}) + \text{constant} \tag{85}$$

For the brown coal $m_1 = 1$ and hence all the results obtained for particle temperatures at peak burning conditions are plotted against $d_w^3 p^{+2}$ on a semilog plot. Such a correlation appears to fit this example very well as seen in Figure 22, for pressures varying from 0.1 atm to 10 atm and particle size ranging from 25 μm to 200 μm. Also, a comparison is made for the theoretical slope as obtained in equation (85) with the slope obtained from the least squares fit of the points in Figure 22. This relation is very useful since with a single point for the peak burning temperature for any selected char (such as petroleum coke, bituminous char, anthracite char, etc. as given in Figure 16a) a wide range of characteristics for different conditions are predicted.
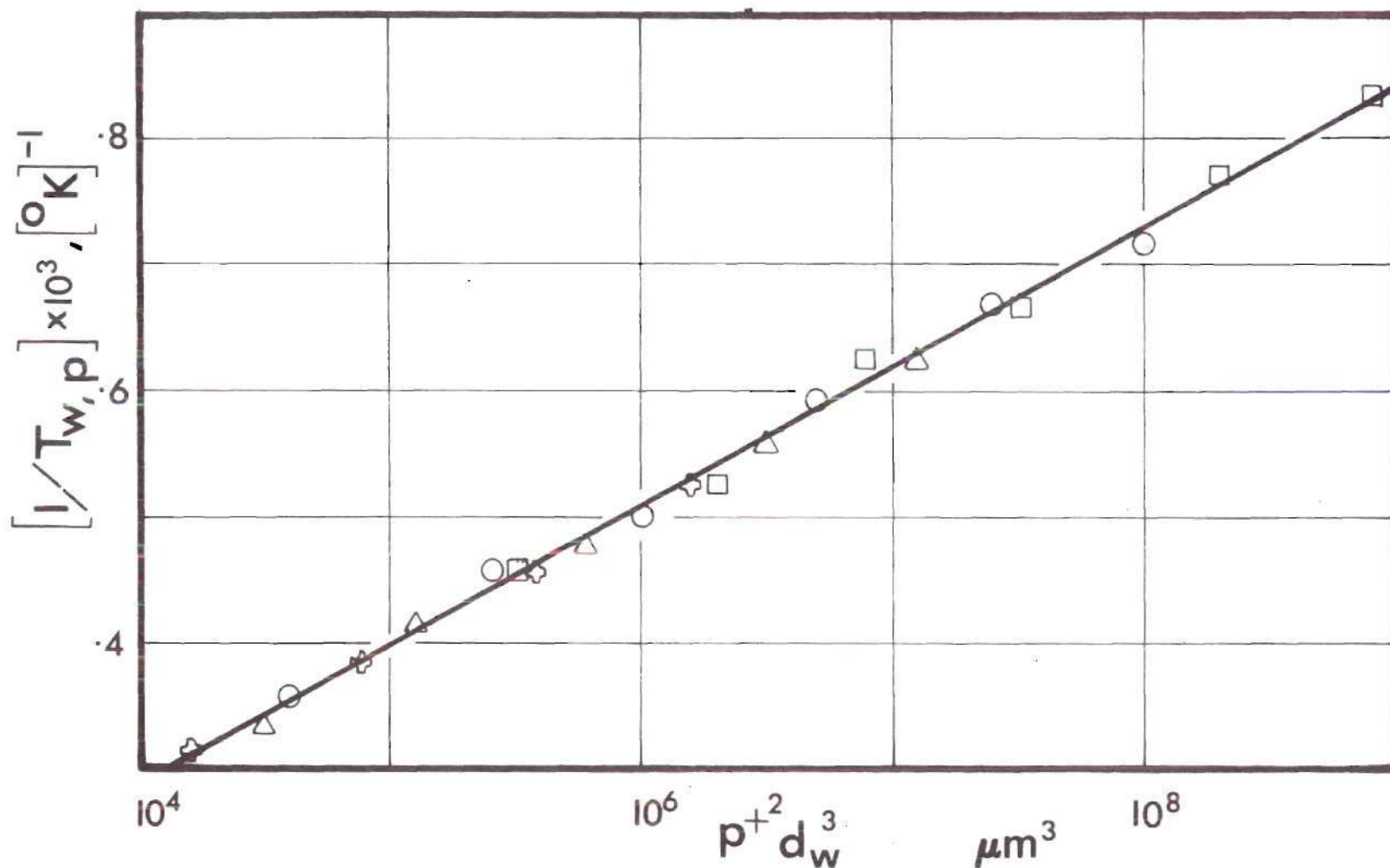
Figure 22. Peak Burning Temperatures versus $p^{+2} d_w^3$; ——Approximate Theory; Numerical Results: □ 200 μm, ○ 100 μm, △ 50 μm, ⟡ 25 μm; $\frac{1}{T_{w,p}} = -.151425 \times 10^{-3} + .109985 \times 10^{-3} \log d_w^3 p^{+2}$; Slope (fit) = $.10999 \times 10^{-3}$, Slope (theory) = $.105 \times 10^{-3}$.

CHAPTER VIII

CONCLUSIONS

8.1. Ignition

Based on the ignition model presented here the following conclusions are drawn:

(i)   Ignition occurs on the surface for a non-pyrolyzing solid particle while for totally pyrolyzing materials ignition occurs normally in the gas phase.   Thus the present thesis presents a transitional volatile content above which the ignition occurs in the gas phase and vice versa.

(ii)   Smaller coal particles are more likely to ignite on the surface while larger particles ignite in the gas phase.   This explains in part the recent results of Howard and Essenhigh, who obtained ignition on the surface while the earlier experimenters conducted experiments on large particles and obtained ignition in the gas phase.

(iii)   Coal particles in large oxygen concentration are found to ignite on the surface; for low oxygen concentration, they are found to ignite in the gas phase.

(iv)   Not all coal particles exhibit transitional behavior where change of ignition phase occurs.   Thus the coals could be classified according to their ignition modes:

(a)   Coals with ignition through heterogeneous mode
      of oxidation,

(b)   Coals with gas phase ignition only, and

(c)   Coals with hybrid behavior where transition of
      ignition phase occurs.

(v)   Critical conditions for gas ignition exist
beyond which the ignition occurs only on the surface. Thus
there exists a minimum particle size, a minimum volatile
content and maximum oxygen concentration at which ignition
occurs on the surface (due to gas ignition).

(vi) Steady state heterogeneous ignition theory is
sufficient to predict the ignition temperature.

(vii) Radiation does not appear to play a signifi-
cant role in determining the ignition temperature though it
involves serious error in the computation of ignition time.

(viii) There exists a minimum particle size and oxygen
concentration below which there is neither gas ignition nor
heterogeneous ignition in a rigorous sense. There is only
incipient combustion.

Note the following limitations with the gas ignition
model:

(a)   Imposition of volume reaction to a single surface
is doubtful for particles below about 100 microns if the
flame velocity of the pyrolysate is of the order of about
35 cm/sec (e.g.: if methane is the pyrolysate). Also the
flame thickens at low oxygen concentrations.

(b) An absolute ignition criterion which takes into account all heat losses to the pyrolyzing surface and to the surrounding ambient atmosphere, is preferable compared to an adiabatic ignition criterion which takes into account heat loss to the particle surface only. A consequence of this adiabatic criterion is that the model fails at low oxygen concentrations where the flame appears to move away from the particle surface thus increasing the heat loss to the ambient atmosphere. Since this was neglected, the result gives rise to lower ignition temperatures even at very low oxygen concentrations. Thus the results are not reliable at low oxygen concentrations.

(c) Neglect of unsteady state terms is severe for very small particles. Not only that the particle size may decrease appreciably before ignition, but also the rate of heating changes so much that the volatile content and the kinetics of pyrolysis are likely to be different since they are dependent upon the rate of heating.

8.2. Combustion

(i) A low activation energy for the heterogeneous production of CO and relatively a high activation energy for the gas phase activation energy for oxidation of CO results in a peak for the burning rate versus surface temperature curve. This effect is found to be due to cumulative reduction of oxygen concentration near the surface as a

result of the heterogeneous and gas phase oxidation processes.

(ii) Large particles and high pressures give rise to the peak burning rate at lower surface temperatures. The peak burning surface temperatures are found to be strong functions of both pressure and particle size. Thus the inverse of peak burning surface temperature was found to be proportional to the logarithm of {(particle size)^3 x (pressure)^2} for the systems considered here. However this relation is generally applicable to other chars and graphite particles.

(iii) Along with the occurrence of a peak burning rate, there is always associated a peak wall mass fraction for CO gas. The characteristics of the corresponding temperatures are similar to the ones given in (i) and (ii).

Note the following limitations for the combustion model considered here.

    (a) The present results can not be directly applied to furnace conditions for the following reasons.

        (i) The ambient temperature is normally closer to the surface temperature.

        (ii) Diffusion model is inadequate since the velocity of injection is normally high which creates a boundary layer around the particle.

    (b) The activation energies may not remain constant throughout the temperature range considered here.

APPENDIX A

A.1. Derivation for the Deflagration Rate
of Coal Under Pyrolysis

Using equations (29) and (24) with $j = T$ and $p = 0$, (25), (39) and (41),

$$\xi_w = \ell n \left\{ 1 + \frac{\dfrac{\theta_\infty - \theta_w}{Q_g^+} + \dfrac{Y_{0,\infty} - Y_{0,w}}{\nu_s}}{\dfrac{Q_w^+}{Q_g^+} + \dfrac{Y_{0,w}}{\nu_s}} \right\} \tag{A.1}$$

where

$$Q_g^+ = (q^\circ / \nu_V W_V) / (C_p E_g / R^\circ),$$

From equations (A.1) and (40a,b), one can solve for ξ_w as a function of $Y_{0,w}$ only. The solution is possible if $Y_{0,w}$ is obtained as a function of known conditions and ξ_w from equation (37). Integrating equation (37) between $0 \leq \xi \leq \xi_w$ one gets,

$$\frac{Y_0 - Y_0^*}{Y_{0,w} - Y_0^*} = \frac{e^{-\xi^*} - e^{-\xi}}{e^{-\xi^*} - e^{-\xi_w}}, \quad \xi^* < \xi \leq \xi_w \tag{A.2}$$

$$\frac{Y_0 - Y_{0,\infty}}{Y_0^* - Y_{0,\infty}} = \frac{1 - e^{-\xi}}{1 - e^{-\xi*}}, \quad 0 \le \xi < \xi* \tag{A.3}$$

Integrating between ξ^*_- and ξ^*_+,

$$(\varepsilon_0)_{\xi^*_+} - (\varepsilon_0)_{\xi^*_-} = D_{III,g} \frac{Y_V^* Y_0^* \xi_w^2 e^{-\frac{1}{\theta*}}}{\xi^{*4}(\theta*)^2} \tag{A.4}$$

From equation (29) at stoichiometric surface (where $Y_V = Y_0/\nu_s$),

$$1 - (\phi_{V0})^*(1 - e^{-\xi_w}) = e^{-\xi*} \tag{A.5}$$

From the definition of ϕ_{V0} (equation (24) with j = V, and p = 0),

$$(\phi_{V0})^* = \frac{Y_{0,\infty}/\nu_s}{Y_{V,w} - \frac{Y_{0,w}}{\nu_s} + \frac{Y_{0,\infty}}{\nu_s}} \tag{A.6}$$

Differentiating equation (29), then using equation (24) with j = V and p = 0 and making use of equations (40a) and (42),

$$Y_{V,w} - \frac{Y_{0,w}}{\nu_s} = (1 - e^{-\xi_w}) - \frac{Y_{0,\infty} e^{-\xi_w}}{\nu_s} \tag{A.7}$$

Hence from equations (A.5), (A.6) and (A.7),

$$\xi^* = \ln \left\{ 1 + \frac{Y_{0,\infty}}{\nu_S} \right\} \tag{A.8}$$

and

$$(\phi_{VO})^* = \frac{Y_{0,\infty}/(\nu_0 W_0/\nu_V W_V)}{(1-e^{-\xi_W})(1 + \frac{Y_{0,\infty}}{\nu_S})} \tag{A.9}$$

Equation (A.8) shows that the position of the stoichiometric surface is directly proportional to the mass burning rate. From equation (A.3) $(\varepsilon_0)_{\xi^*-}$ can be obtained. From equation (41), $(\varepsilon_0)_{\xi^*+}$ is known to be equal to zero. Then using equation (A.4),

$$D_{III,g} = \frac{\frac{Y_{0,\infty}-Y_0^*}{(1-e^{-\xi_W})\nu_S} - \frac{Y_{0,\infty}}{\nu_S}}{\frac{\xi_W^2 e^{-\frac{1}{\theta^*}}}{\xi^{*4}\theta^{*n}} \left\{\frac{Y_0^*}{\nu_S}\right\}^n \nu_S^{n_0-1}} \tag{A.10}$$

Since, $(\varepsilon_0)_+ = 0$, from equation (A.2),

$$Y_{0,w} = Y_0^* e^{\xi^*-\xi_W} \tag{A.11}$$

From equations (29) and (24) with j = T, and p = 0 and equation (25),

$$\theta^* = \theta_\infty + \frac{Y_{0,\infty} - Y_0^*}{\nu_s} - \frac{1-e^{-\xi^*}}{1-e^{-\xi_w}}(\theta_\infty - \theta_w + Q_g^+ \frac{Y_{0,\infty} - Y_0^*}{\nu_s}) \qquad (A.12)$$

Similarly differentiating equation (29) and (24) with j = T, and p = 0 and using equations (25), (A.3) and (A.12), we get

$$\theta_0' = (\theta')_{\xi=0} = (\frac{\theta^* - \theta_\infty}{1-e^{-\xi^*}}) \qquad (A.13)$$

A.2. Pyrolysis in Absence of Gas Phase Oxidation

Using equation (29) and (24) with $\beta = \theta$ for no heat release in the gas phase,

$$\frac{\tilde\theta - \tilde\theta_\infty}{\tilde\theta_w - \tilde\theta_\infty} = \frac{1-e^{-\tilde\xi}}{1-e^{-\tilde\xi_w}} \qquad (A.13a)$$

Using equations (A.13a) and (39),

$$e^{\tilde\xi_w} = 1 + \frac{\tilde\theta_\infty - \tilde\theta_w}{\tilde Q_w^+} \qquad (A.13b)$$

where

$$\tilde{\xi}_W = \dot{m}/4\pi\rho Dr_W$$

(A.13c)

$$\tilde{\theta} = T/(E_W/R°)$$

Then solving for $\tilde{\xi}_W$,

$$\tilde{\xi}_W = \ln \left(1 + \frac{\tilde{\theta}_\infty - \tilde{\theta}_W}{\tilde{Q}_W^+} \right)$$

(A.13d)

where $\tilde{\theta}_W$ is obtained from equation (40b); then,

$$\tilde{\xi}_W = \ln \left\{ 1 + \frac{\tilde{\theta}_\infty}{\tilde{Q}_W^+} - \frac{1}{\tilde{Q}_W^+ \, \ln \left(\dfrac{D_{III,W}}{\tilde{\xi}_W}\right)} \right\}$$

(A.13e)

A.3. Ignition Conditions for a Coal Under Pyrolysis

Equation (A.13) shows that θ'_o is solely a function of $\theta*$ for given ambient temperature and ambient mass fraction of oxygen. Invoking the Van't Hoff criterion (see Section 4.2) and denoting the ignition condition as I, we obtain,

$$\theta* = \theta_{\infty,I}$$

(A.14)

Using this result in equation (A.12), making use of equation (A.1) to eliminate ξ_w, and equation (A.8) to eliminate $Y_{0,\infty}$, one gets,

$$\frac{Y_0^*}{\nu_S} = (1-e^{-\xi^*}) \left\{1-\left(\frac{\theta_\infty+Q_w^+-\theta_w}{Q_g^+}\right)\right\}$$

(A.15)

From equations (A.1), (A.11) and (A.14), then

$$\left(\frac{\theta_{\infty,I}-\theta_w}{Q_w^+}\right) + 1 = e^{\xi_w-\xi^*}$$

(A.16)

Note: As $\xi^* \to \xi_w$, $\theta_{\infty,I} \to \theta_w$ which checks with the physics of the problem. From equations (A.15) and (A.16), one gets,

$$\frac{Y_0^*}{\nu_S} = (1-e^{-\xi^*})(1 - \frac{Q_w^+}{Q_g^+} e^{\xi_w-\xi^*})$$

(A.17)

Using equation (40b) in equation (A.16), one has

$$\theta_{\infty,I} = Q_w^+ (e^{\xi_w-\xi^*}-1) + \frac{E_w^+}{\ln \frac{D_{III,w}}{\xi_w}}$$

(A.18)

As

$$\xi^* \to \xi_w, \quad \theta_{\infty,I} = E_w^+/\ln D_{III,w}/\xi^*$$

(A.18a)

Using equations (A.14), (A.17) and (A.18) in equation (A.10), we obtain an explicit relation for $D_{III,g}$ at the time of ignition (or an implicit relation for ξ_w for given $D_{III,g}$),

$$D_{III,g} = \nu_s^{1-n_0} \frac{\dfrac{Q_w^+}{Q_g^+} e^{\xi_w - \xi^*} \xi^{*4}}{\xi_w^2} \times e^{\dfrac{1}{Q_w^+(e^{\xi_w - \xi^*} - 1) + \dfrac{E_w^+}{\ln(D_{III,w}/\xi_w)}}}$$

$$\times \left[\frac{Q_w^+(e^{\xi_w - \xi^*} - 1) + \dfrac{E_w^+}{\ln(D_{III,w}/\xi_w)}}{(1 - \dfrac{Q_w^+}{Q_g^+} e^{\xi_w - \xi^*})(1 - e^{-\xi^*})} \right]^n \qquad (A.19)$$

Since ξ_w can be found from equation (A.19) for specified values of $D_{III,g}$ and $D_{III,w}$, then $\theta_{\infty,I}$ is obtained from equation (A.18).

A.4. Critical Parameters for Gas Phase Ignition

(i) Critical Size:

    (a) $m \neq 0$, $n \neq 0$

Let

$$d_w^+ = d_w / (d_w^o / (D_{III,w}^o)^{1/m}) \qquad (A.20)$$

Then,

$$D_{III,w} = (d_w^+)^m \qquad (A.21)$$

Also

$$D_{III,g} = D^O_{III,g} \, d_w^{\,2} / (D^O_{III,w})^{2/m} \tag{A.22}$$

Substituting (A.20), (A.21) and (A.22) in (53b), then multiplying both sides of the equation by $\xi^{*\,(\frac{2}{m}-\frac{1}{E^+_w})}$ and rearranging we obtain equation (54a).

(b) $m \neq 0$, $n = 0$

Raise the whole equation (24a) to the power n and let $n \rightarrow 0$. Then redefine M, and x as shown in Table 3.

(c) $m = 0$, $n = $ arbitrary

Since the reference particle diameter was based on the particle size dependent surface Damkohler number, one can not use the above relations directly. However the gas phase Damkohler number is dependent on the particle size. Rewriting equation (53b) for this case,

$$\frac{D_{III,g}}{\xi^*} = \xi^* v_s^{1-n} {}_0\bar{Q}^+_w \left(\frac{D_{III,w}}{\xi^*}\right)^{\frac{1}{E^+_w}} \left\{ \frac{E^+_w}{\ln\left(\frac{D_{III,w}}{\xi^*}\right)(1-\bar{Q}^+_w)(1-e^{-\xi^*})} \right\}^n \tag{4.23}$$

one can obtain the critical particle size since $D_{III,g} \propto d_w^2$. Letting $n \rightarrow 0$ in equation (A.23) the case for $n = 0$ and $m = 0$ is obtained.

(ii)   Critical Volatile Content:

(a) $n \neq 0$

Since $D_{III,g}$ is not dependent on the volatile content, one can solve for $(D_{III,w}/\xi^*)$; i.e. from equation (53b), rearranging, one obtains the equation as shown in Table 3.

(b) $n = 0$

A similar procedure as in case (i)b is adopted.

(iii)   Critical Oxygen Mass Fraction:

(a)   m = arbitrary, $n \neq 0$

Use the expansion for $(1-e^{-\xi^*}) \simeq \xi^*$, then multiply equation (54b) by $D_{III,w}^{(\frac{1}{E_w^+}-2+n)}$ and then rearrange the resulting equation to obtain equation (55b).   Note that

$$\frac{D_{III,w}}{\xi^*} \equiv d_w^{+\frac{m}{2}}/\sqrt{\xi^*}$$

(b)   m = arbitrary, $n = 0$

Adopt a similar procedure as in case (i)b.

APPENDIX B

B.1. Heterogeneous Ignition--Exact Solution

From Semanov's steady state thermal theory of ignition at the time of ignition,

$$\dot{Q}_L = \dot{Q}_{chem}$$

$$\frac{d\dot{Q}_L}{d\bar{\theta}_w} = \frac{d\dot{Q}_{chem}}{d\bar{\theta}_w} \tag{B.1}$$

where

$$\dot{Q}_L = \text{heat loss rate,} = -k(\frac{dT}{dr})\xi_w 4\pi r_w^2$$

$$= -k(\frac{d\bar{\theta}}{d\xi})_w \xi_w 4\pi E_{w,h}/R^\circ \tag{B.2}$$

$$\dot{Q}_{chem} = \dot{m} \, Q_{w,h}, \text{ the heat liberation rate,}$$

$$= \xi_w 4\pi\rho D \, r_w \, Q_{w,h} \tag{B.3}$$

Applying the interface mass conservation equation,

$$\xi_w = (D_{III,w})_h \, r_w \, \frac{e^{-1/\bar{\theta}_w}}{\bar{\theta}_w} Y_{0,w} \tag{B.4}$$

Also

$$\varepsilon_0 = -\overline{\nu}_s$$

Using equation (60b) and definition for ε (equation (26)), one obtains,

$$Y_{0,w} = Y_{0,\infty} \; e^{-\xi_w} - \frac{1-e^{-\xi_w}}{Y_{0,\infty}/\overline{\nu}_s} \tag{B.5}$$

Using equations (B.2) and (B.3) in (B.1) and with the assumption of Le = 1, we obtain equations (61a) to (61c).

B.2. Critical Parameters for the
Heterogeneous Ignition

Using the following approximation consistently for all exponential functions in equations (61a) to (61c),

$$e^{-\xi_w} \simeq 1-\xi_w \tag{B.6}$$

and solving for ξ_w,

$$\xi_w \simeq g_1/(1+g_1\beta) \tag{B.7}$$

where

$$g_1 = \bar{\nu}_s \; (D_{III,w})_h \; \frac{e^{-1/\bar{\theta}_w}}{\bar{\theta}_w} \; \frac{Y_{0,\infty}}{\bar{\nu}_s} \qquad (B.8)$$

$$\beta = (1+1/(Y_{0,\infty}/\bar{\nu}_s)) \qquad (B.9)$$

The slope of the heat liberation rate curve versus surface temperature (see Figures 13a and 13b) will be a maximum when,

$$\frac{d^2 \xi_w}{d\bar{\theta}_w^2} = 0 \qquad (B.10)$$

Differentiating equation (B.7) twice,

$$\frac{d\xi_w}{d\bar{\theta}_w} = \frac{g_1'}{(1+g_1\beta)^2} \qquad (B.11)$$

and

$$\frac{d^2 \xi_w}{d\bar{\theta}_w^2} = \frac{2g_1'^2}{g_1(1+g_1\beta)^3} + \frac{g_1'^2}{(1+g_1\beta)^2} - \frac{2g_1'^2}{g_1(1+g_1\beta)^2} \qquad (B.12)$$

where

$$g_1' = g_1 \; (\frac{1}{\bar{\theta}_w^2} - \frac{1}{\bar{\theta}_w}) \qquad (B.13)$$

$$g_1'' = g_1 \left(\frac{1}{\overline{\theta}_w^2} - \frac{2}{\overline{\theta}_w^3}\right) + g_1 \left(\frac{1}{\overline{\theta}_w^2} - \frac{1}{\overline{\theta}_w}\right)^2 \tag{B.14}$$

Using equations (B.13), (B.8), (B.9), and (B.12) in (B.10),

$$2\overline{\theta}_w^2 + 1 - 4\overline{\theta}_w = (\widetilde{D}_{III,w})_h \frac{e^{-1/\overline{\theta}_w}}{\overline{\theta}_w} \left(1 + \frac{Y_{0,\infty}}{\overline{\nu}_s}\right) \tag{B.15}$$

Substituting for g_1 and β from equations (B.8) and (B.9) in (B.11),

$$\left(\frac{d\xi_w}{d\overline{\theta}_w}\right)_{max} = \frac{(\widetilde{D}_{III,w})_h \frac{Y_{0,\infty}}{\overline{\nu}_s} \frac{e^{-1/\overline{\theta}_w}}{\overline{\theta}_w} \left(\frac{1}{\overline{\theta}_w^2} - \frac{1}{\overline{\theta}_w}\right)}{1 + (\widetilde{D}_{III,w})_h \left(1 + \frac{Y_{0,\infty}}{\overline{\nu}_s}\right) \frac{e^{-\frac{1}{\overline{\theta}_w}}}{\overline{\theta}_w}} \tag{B.16}$$

Thus substituting solutions for $\overline{\theta}_w$ from equation (B.15) in (B.16) one can obtain the maximum $(d\dot{Q}_{chem}/d\overline{\theta}_w)$. But

$$\left(\frac{d\dot{Q}_{chem}}{d\overline{\theta}_w}\right)_{max} = \left(\frac{d\xi_w}{d\overline{\theta}_w}\right)_{max} \left(Q_{w,h}^+ 4\pi\rho D \, C_p r_w \frac{E_{w,h}}{R^\circ}\right) \tag{B.17}$$

Similarly for the heat loss curve,

$$\left(\frac{d\dot{Q}_L}{d\bar{\theta}_w}\right) = 4\pi\rho D C_p r_w \frac{E_{w,h}}{R^6} \tag{B.18}$$

which happens to be a constant (see line AB in Figure 13b). Hence using equations (B.17) and (B.18) at the critical condition,

$$\left(\frac{d\xi_w}{d\bar{\theta}_w}\right)_{max} Q^+_{w,h} = 1.0 \tag{B.19}$$

Thus equations (B.15), (B.16) and (B.19) give the solutions for the critical parameters. First use equation (B.19) in (B.16). Then solve for the group $(e^{-1/\bar{\theta}_w}/\bar{\theta}_w)$. Substitute this group in (B.15). Obtain equation (62b).

B.3. Heterogeneous Ignition--Approximate Solution

When the mass consumption rate of coal is small or/and $Y_{0,\infty}$ is large and also $\bar{\nu}_s$ (the stoichiometric requirement of oxygen per unit mass of coal) is small, then from equation (B.7),

$$\xi_w = g_1 \tag{B.20}$$

Hence the heat generation rate and heat loss rate at the time of ignition under the above conditions,

$$\frac{\overset{\circ}{Q}_{chem}}{(4\pi\rho D\ C_p\ E_{w,h}/R^\circ)\,r_w} = \xi_w\ Q^+_{w,h} \tag{B.21}$$

$$\overset{\circ}{Q}_L/(4\pi\rho DC_p r_w E_{w,h}/R^\circ) = (\overline{\theta}_w - \overline{\theta}_\infty) \tag{B.22}$$

Using the ignition criterion given by the set of equations (B.1) and equations (B.21) and (B.22),

$$Y_{0,\infty}\ (D_{III,w})_h\ Q^+_{w,h}\ \frac{e^{-1/\overline{\theta}_w}}{\overline{\theta}_w} = (\overline{\theta}_w - \overline{\theta}_\infty) \tag{B.23}$$

and

$$Y_{0,\infty}\ (D_{III,w})_h\ Q^+_{w,h}\ \frac{e^{-1/\overline{\theta}_w}}{\overline{\theta}_w} = \frac{\overline{\theta}_w^2}{(1-\overline{\theta}_w)} \tag{B.24}$$

From equations (B.23) and (B.24) one can solve for $\overline{\theta}_w$,

$$\overline{\theta}_w = \frac{1+\overline{\theta}_\infty}{4} \left\{ 1 \pm \left(1 - \frac{8\overline{\theta}_\infty}{(1+\overline{\theta}_w)^2}\right)^{1/2} \right\} \tag{B.25}$$

Selecting the negative sign corresponding to the ignition condition and for small $\overline{\theta}_\infty$,

$$\overline{\theta}_w = \overline{\theta}_\infty\ (1+\overline{\theta}_\infty) \tag{B.26}$$

Substituting (B.26) in equation (B.23) and expanding $(1+\overline{\theta}_\infty)^{-1} \simeq (1-\overline{\theta}_\infty)$ for small $\overline{\theta}_\infty$, one obtains

$$1 \simeq \frac{(D_{III,w})_h \; Q_{w,h}^+ \; e^{1-1/\overline{\theta}_\infty} \; Y_{0,\infty}}{\overline{\theta}_\infty^3} \qquad\qquad (B.27)$$

APPENDIX C

TIP PARAMETERS FOR COAL PARTICLES

(i) TIP size:

(a) $m \neq 0,\ n \neq 0$

The derivation uses the same definitions as given in equations (A.20) to (A.22). Using equations (A.20) to (A.22) in equation (56d),

$$D_{c,g} = \alpha_g \left\{ \frac{d_w^+}{\sqrt{\xi^*}} \right\}^{\frac{m}{2} \cdot \frac{2(2m+2)}{m}} \ell n \left\{ \frac{d_w^+}{\sqrt{\xi^*}} \right\}^{\frac{m}{2} \cdot 2} \tag{C.1}$$

where α_g is defined by equation (65d). Similarly,

$$(D_{III,w})_h = (D^o_{III,w})_h \ (d_w/d_w^o) \tag{C.2}$$

and making use of equations (54b), (C.2) and (63f) and after some rearrangement,

$$D_{c,h} = \alpha_h \left\{ \frac{d_w^+}{\sqrt{\xi^*}} \right\}^{\frac{m}{2} \cdot \frac{2}{m}} \tag{C.3}$$

where α_h is defined by equation (65e). Now using equations (C.1) and (C.3) in (64b), for the TIP size, equation (65a) is obtained.

(b) $m \neq 0$ and $n = 0$

Adopt a similar procedure as given in Appendix (A.4) and case (i)b.

(c) $m = 0$ and $n = $ arbitrary

Since the surface Damkohler number is independent of the particle size, equations (A.20) to (A.22) cannot be used.

Define,

$$D_{III,g} = d_w^{+^2} \qquad (C.4)$$

where

$$d_w^+ = d_w / (d_w^o / (D_{III,g})^{1/2} \qquad (C.5)$$

Using these definitions in equation (56d),

$$D_{c,g} = \frac{D_{III,g}}{1-n_0} \frac{D_{III,w}^2}{\xi^{*4}} \frac{1}{Q_w^+} \left\{ \frac{(1-e^{-\xi^*})}{E_w^+} (1-\bar{Q}_w^+) \ell n \frac{D_{III,w}}{\xi^*} \right\}^n \qquad (C.6)$$

Similarly,

$$(D_{Iv,w})_h = (D_{IV,w}^o)_h \, d_w^+ \, (D_{III,g})^{1/2} \qquad (C.7)$$

Using equation (C.7) in equation (63f),

$$D_{c,h} = \sqrt{D_{III,g}} \; e^{4.57} \; Y_{0,\infty} \; (D_{IV,w})_h / (D^o_{III,g})^{1/2} \qquad (C.8)$$

Substituting equations (C.6) and (C.8) in equation (64b), the resulting equation as tabulated in Table 3 is obtained. The terms α_g' and α_h' are defined as follows:

$$\alpha_g' = \frac{D_{III,w}^{\;2}}{\nu_s^{\;1-n_0}} \; \frac{1}{Q_w^+} \; \frac{1}{\xi^{*3}} \; x$$

$$x \left\{ \frac{(1-e^{-\xi^*})(1-\bar{Q}_w^+)}{E_w^+} \; \ln \frac{D_{III,w}}{\xi^*} \right\}^n \qquad (C.9)$$

$$\alpha_h' = \frac{(D^o_{IV,w})_h}{D^o_{III,g}} \; e^{4.57} \; \sqrt{\xi^*} \; Y_{0,\infty} \qquad (C.10)$$

(ii) TIP oxygen Mass Fraction:

  (a)   m = arbitrary and $n \neq 0$

  Here we have to use two approximations: (i) $1-e^{-\xi^*} = \xi^*$ and (ii) $Y_{0,\infty} = \nu_s \xi^*$. Using the first approximation in equation (56d),

$$D_{c,g} = \gamma_g \; \left(\frac{D_{III,w}}{\xi^*} \right)^{(4-n)} \; \ln \left(\frac{D_{III,w}}{\xi^*} \right) \qquad (C.11)$$

where γ_g is defined in equation (66d). Similarly using the second approximation in equation (63f),

$$D_{c,h} = (D_{IV,w})_h \; e^{4.57} \; \xi^* \; \nu_s \qquad (C.12)$$

Using these relations (C.11) and (C.12) in equation (64b), the relation as tabulated in Table 3 is obtained.

(ii) m = arbitrary and n = 0.

Adopt the same procedure as in Appendix (A.4) and case (i)b.

APPENDIX D

ESTIMATION OF DAMKOHLER NUMBERS

1. Surface Pyrolysis

According to our definition

$$\dot{m}_V = A_w \, e^{-E_w/R^\circ T_w} \, f(r_w)(V^* - V)^\ell \tag{D.1}$$

From the literature

$$\frac{dV}{dt} = k_o \, (V^* - V)^\ell \, e^{-E_w/R^\circ T_w} \tag{D.2}$$

where

V^* = fraction of vapor attainable at $t \to \infty$

V = fraction of vapor at $t = t$

ℓ = order of reaction

k_o = frequency factor, $\sec^{-1}$

Hence, for volumetric pyrolysis,

$$\dot{m}_V = \frac{dV}{dt} \, \frac{4}{3} \, \pi r_w^3 \rho_o \tag{D.3}$$

where

ρ_o = density of solid coal, $\simeq .8 \; gm/cm^3$

Comparing equations (D.1) and (D.3)

$$A_w = k_o \rho_o$$

$$f(r_w) = \frac{4}{3} \pi r_w^3$$

(D.4)

From the definition of $D_{III,w}$,

$$D_{III,w} = \frac{A_w \ f(r_w) (V^* - V)^\ell}{4\pi r_w \ \rho D}$$

(D.5)

Also $V \simeq 0$ before ignition and $\ell = 1.0$, and ρD for air at about 1300°K,

$$\rho D = .67 \times 10^{-3} \ gm/cm\text{-}sec$$

References 42 and 57 give values of V^* and k_o for various types of coal. Thus for coal number 15 with a particle diameter of 100μm,

$$A_w = 706 \times .8 = 565 \ gm/cm^3 sec$$

$$V^* = .3981$$

$$D_{III,w} = 565 \times \frac{\frac{1}{3} \times (50 \times 10^{-4})^2}{.67 \times 10^{-3}} \times .3981$$

$$= 2.80$$

A similar procedure is used for evaluation of the surface Damkohler number for other coals.

2. Gas Phase Reactions

Methane oxidation:

$$\frac{\dot{w}_F}{\nu_F W_F} = \frac{\dot{w}_O}{\nu_O W_O} = A_g \ C_F^{n_F} \ C_O^{n_O} \ e^{-E_g/R^\circ T} \tag{D.6}$$

Hence,

$$\dot{w}_O = \nu_O W_O \ A_g \ e^{-E_g/R^\circ T} \ C_F^{n_F} \ C_O^{n_O} \tag{D.7}$$

From the results of reference [58] for methane oxidation and with the assumption of equal molecular weights,

$$\nu_O W_O A_g = 2.48 \times 10^{10} \ \text{gm/sec-mole}$$

$$n_V = -.4$$

$$n_O = 1.4$$

$$n = n_F + n_O = 1.0$$

From the definition (see equation (37b) for $D_{III,g}$, the Damkohler number is evaluated. For a particle size of $100\mu m$

in diameter, p = 1 atm, E_g = 38000 cal/g mole, J = 42700 gm_F cm/cal, n = 1.0, $\rho D_{1300°K}$ = .67x10^{-3} gm/cm-sec, r_w = 50μm,

$$D_{III,g} = \frac{2.48x10^{10} \times (50x10^{-4})^2}{.67x10^{-3}} \times (\frac{1035}{38000x42700})$$

$$= 588.0$$

3. CO Oxidation

Turning the attention towards CO oxidation and with the assumption of equimolecular weights,

$$\dot{w}_F = A_g \ \nu_F W_F \ e^{-E_g/RT} \ \rho^n \ Y_F^{n_F} \ Y_O^{n_O} \tag{D.8}$$

From Sobolev's results (reference [65]) for CO oxidation,

$$\frac{\Delta C_{CO_2}}{\Delta t \ C_{CO}} = k_{o_1} \ e^{-E_g/R°T} \ sec^{-1} \tag{D.9}$$

where C_{CO_2} is the molal concentration of CO_2. From the reaction,

$$CO + \frac{1}{2} O_2 \rightarrow CO_2$$
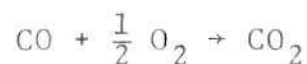
one obtains:

$$\frac{\Delta C_{CO}}{\Delta t} = \frac{\Delta C_{CO_2}}{\Delta t} \times 1.0 \tag{D.10}$$

Hence using equations (D.8) to (D.10)

$$A_g \nu_{CO} W_{CO} = k_{o1} \, W_{CO} \qquad \text{(D.11)}$$

Using Sobolev's values

$$k_{o1} = 9.5 \times 10^7 \, \text{sec}^{-1},$$

$$A_g = 2.66 \times 10^9 \, \text{gm/sec mole},$$

$$E_g = 30,000 \, \text{cal/gm mole},$$

and using the definition for $D_{III,g}$ from equation (37b) and letting $n_0 \simeq 0$ (actually $n_0 \sim .20$ to $.25$ for $Y_0 > 5\%$ and $= 1.0$ for $Y_0 < 5\%$), $\rho D)_{2000°K} \simeq .79 \times 10^{-3}$ gm/cm sec.[†] Thus using equation (37b) $D_{III,g}$ is estimated

$$D_{III,g} = 2.66 \times 10^9 \times \frac{(50 \times 10^{-6})^{2.0}}{.79 \times 10^{-3}} \times \frac{1035}{30000 \times 42700}$$

$$= 68.0$$

If $n_0 = 1.0$ and $n_F = n_{CO} = 1.0$, and $E_g = 30000$ cal/gm mole, then estimating the frequency factor from the figure given in reference [65], (reproduced here)

[†]The property selections at different temperatures are due to tabulation of kinetic constants at different temperatures.
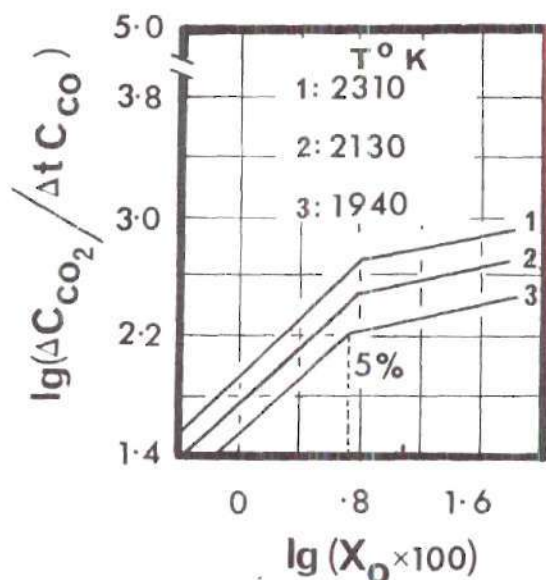
Figure D.1. Variation of Reaction Rate with Oxygen Concentration

$$A_g \nu_{CO} W_{CO} = 4.29 \times 10^{13} \text{ cm}^6 \text{gm/mole}^2 \text{ cm}^3 \text{ sec}$$

Then for $n = 2$, using equation (37b),

$$D_{III,g} = .88, \text{ say } 1.0$$

In order to check this estimation, we carried out a similar estimation for region II where Y_0 is greater than .05 and thus obtained $D_{III,g}$ as 13.6 which is five times lower than the value quoted by Sobolov. Thus the order of error for the above calculation ($Y_0 < .05$) should be about 500%.

4. Heterogeneous Surface Reactions

For solids undergoing reaction under constant density,

for first order reaction,

$$\frac{\dot{w}_O}{\nu_O W_O} = \frac{\dot{w}_C}{1.0} = A_{w,h} \; 4\pi r_w^2 C \; e^{-E_{w,n}/R^\circ T} \; Y_{0,w} \tag{D.12}$$

Hence,

$$\dot{W}_C = A_{w,n} \; 4\pi r_w^2 C \; e^{-E_{w,n}/R^\circ T} \; Y_{0,w} \tag{D.13}$$

where,

$$C = P/R^\circ JT \tag{D.14}$$

Therefore,

$$\dot{w}_C'' = (\dot{w}_C/4\pi r_w^2) = A_{w,h} \; \frac{P}{R^\circ JT} \; e^{-E_{w,h}/R^\circ T} \; Y_{0,w} \tag{D.15}$$

From Bhaduri's equation [17]

$$\dot{w}_C'' = \beta \rho_o k_o \; e^{-E_{w,h}/R^\circ T} \; \{O_2\} \tag{D.16}$$

where

   $\{O_2\}$ = volume fraction of oxygen.

Also,

$$\rho_0 \{O_2\} \simeq W_0 \; C \; Y_0 \tag{D.17}$$

Hence

$$\dot{w}_c'' \simeq (\beta W_0 k_0) \, e^{-E_{w,h}/R^\circ T} \, C \, Y_{0,w} \qquad (D.18)$$

Comparing equations (D.18) and (D.15)

$$A_{w,h} = \beta W_0 k_0 \quad \text{gm cm/mole sec} \qquad (D.19)$$

Using various values of β, k_0 for each coal, $A_{w,h}$ was computed. From equation (60j), $(D_{III,w})_h$ could be estimated. Thus $\rho D \simeq .67 \times 10^{-3}$ gm/cm sec. For anthracite coal [17]

$$\beta = .53$$
$$k_0 = 4.5 \times 10^7 \text{ cm/sec}$$
$$E_{w,h} = 33500 \text{ cal/gm mole}$$

and letting

$$r_w = 50 \mu m$$

$$(D_{III,w})_h = \frac{7.64 \times 10^8 \times 50 \times 10^{-4}}{.67 \times 10^{-3}} \times \frac{1035}{33500 \times 42700}$$

$$= 418.0$$

Thus using a similar procedure to bring the equation in the literature to our form, the Damkohler numbers were estimated for surface reactions.

APPENDIX E

E.1. Details of Derivations for Combustion

Characteristics

Mass and Flux Fractions at the Surface

Apply species balance equations at the interface
(see equations (35) and (36)).

CO

$$\varepsilon_{CO,w} = \frac{(1+\nu_a)\Gamma_a}{\xi_w} Y_{0,w} + \frac{(1+\nu_b)\Gamma_b}{\xi_w} Y_{CO_2,w} \qquad (E.1)$$

where Γ_a, Γ_b, ν_a and ν_b are defined in equations (69). (Note
that the Damkohler numbers are based upon the consumption
of carbon).

O_2

$$\varepsilon_{0,w} = -\nu_a\Gamma_a Y_{0,w}/\xi_w \qquad (E.2)$$

CO_2

$$\varepsilon_{CO_2,w} = -\nu_b\Gamma_b Y_{CO_2,w}/\xi_w \qquad (E.3)$$

Overall Mass Conservation. Since net mass flow out of
the carbon surface must have come from the interior solid

carbon,

$$1 = \varepsilon_{CO,w} + \varepsilon_{0,w} + \varepsilon_{CO_2,w} \tag{E.4}$$

Using equations (E.1) through (E.4),

$$Y_{CO,w} = \frac{\xi_w}{\Gamma_b} - \frac{\Gamma_a}{\Gamma_b} Y_{0,w} \tag{E.5}$$

Substituting (E.5) in (E.1) and (E.3),

$$\varepsilon_{CO,w} = (1+\nu_b) - \Gamma_a(\nu_b-\nu_a) Y_{0,w}/\xi_w \tag{E.6}$$

$$\varepsilon_{CO_2,w} = -\nu_b + \nu_b\Gamma_a Y_{0,w}/\xi_w \tag{E.7}$$

Adding equations (E.2), (E.6) and (E.7) one finds that the sum is equal to unity. From equations (29) and (24) with $j = 0$ and $p = CO$ and then with $j = CO_2$ and $p = CO$, we obtain the flux fractions of the species 0 and CO_2 in the gas phase.

$$\varepsilon_{0,w} = \nu_g (\varepsilon_{CO,w}-Y_{CO,w}) + Y_{0,w}$$

$$- \frac{e^{-\xi_w}}{1-e^{-\xi_w}} \{\nu_g(Y_{CO,w}-Y_{CO,\infty}) + Y_{0,\infty}-Y_{CO,w}\} \tag{E.8}$$

$$\varepsilon_{CO_2,w} = - (1+\nu_g)(\varepsilon_{CO,w}-Y_{CO,w}) + Y_{CO_2,w}$$

$$+ \frac{e^{-\xi_w}}{1-e^{-\xi_w}} \{(1+\nu_g)(Y_{CO,w}-Y_{CO,\infty}) + (Y_{CO_2,w}-Y_{CO_2,\infty})\} \qquad (E.9)$$

Substituting for $\varepsilon_{0,w}$, $Y_{CO_2,w}$, $\varepsilon_{CO_2,w}$ and $\varepsilon_{CO,w}$ in equations (E.8) and (E.9) from equations (E.2), (E.5), (E.6) and (E.7) respectively (thus matching the mass of species consumed at the surface with species flux that has to be maintained in the gas phase), the following two equations are obtained:

$$- \frac{\nu_a \Gamma_a Y_{0,w}}{\xi_w} = \nu_g[(1+\nu_b) - \frac{\Gamma_a}{\xi_w}(\nu_b-\nu_a)Y_{0,w}] - \frac{\nu_g Y_{CO,w}}{1-e^{-\xi_w}}$$

$$+ \frac{Y_{0,w}}{(1-e^{-\xi_w})} + \frac{e^{-\xi_w}}{1-e^{-\xi_w}} [\nu_g Y_{CO,\infty}-Y_{0,\infty}] \qquad (E.10)$$

$$- \nu_b + \nu_b \frac{\Gamma_a}{\xi_w} Y_{0,w} = - (1+\nu_g)[(1+\nu_b) - \frac{\Gamma_a}{\xi_w}(\nu_b-\nu_a)Y_{0,w}]$$

$$+ (1+\nu_g) \frac{Y_{CO,w}}{1-e^{-\xi_w}} + \frac{1}{1-e^{-\xi_w}} [\frac{\xi_w}{\Gamma_b} - \frac{\Gamma_a}{\Gamma_b} Y_{0,w}]$$

$$- \frac{e^{-\xi_w}}{1-e^{-\xi_w}} [(1+\nu_g) Y_{CO,\infty}+Y_{CO_2,\infty}] \qquad (E.11)$$

Solving for $Y_{CO,w}$ in terms of $Y_{0,w}$ from equation (E.10),

$$Y_{CO,w} = \frac{1-e^{-\xi_w}}{\nu_g} \left[\nu_g(1+\nu_b) + \frac{e^{-\xi_w}}{1-e^{-\xi_w}} (\nu_g Y_{CO,\infty} - Y_{0,\infty}) \right.$$

$$\left. + \frac{Y_{0,w}}{1-e^{-\xi_w}} + \frac{\Gamma_a Y_{0,w}}{\xi_w} (\nu_a + \nu_a \nu_g - \nu_b \nu_g) \right] \tag{E.12}$$

There are two unknowns $Y_{0,w}$ and $Y_{CO,w}$ for given ξ_w and θ_w and these two equations (E.11) and (E.12). Thus solving for $Y_{CO,w}$

$$Y_{CO,w} = \left[(1+\nu_b)(1-e^{-\xi_w}) + \frac{\Gamma_b}{\xi_w} \bar{\nu}(1-e^{-\xi_w})^2 (1+\nu_b) \right.$$

$$+ e^{-\xi_w} (Y_{CO,\infty} - \frac{Y_{0,\infty}}{\nu_g}) + e^{-\xi_w}(1-e^{-\xi_w})(Y_{CO,\infty} - \frac{Y_{0,\infty}}{\nu_g})\frac{\Gamma_b}{\xi_w} \bar{\nu}$$

$$+ (\frac{1-e^{-\xi_w}}{\nu_g})\bar{\nu} - \Gamma_b \bar{\nu}(1-e^{-\xi_w})(1+\nu_g+\nu_g\nu_b)/\nu_g$$

$$+ \frac{\xi_w}{\Gamma_a \nu_g} - \frac{\Gamma_b}{\Gamma_a} (1-e^{-\xi_w})(1+\nu_g+\nu_g\nu_b)/\nu_g$$

$$- \frac{e^{-\xi_w}}{\nu_g} \frac{\Gamma_b}{\Gamma_a} \{ (1+\nu_g)Y_{CO,\infty} + Y_{CO_2,\infty} \} \right]/\left[1 - \frac{1+\nu_g}{\nu_g} \frac{\Gamma_b}{\Gamma_a} \right.$$

$$\left. - \frac{1+\nu_g}{\nu_g} \frac{\Gamma_b}{\xi_w} \bar{\nu} (1-e^{-\xi_w}) + \frac{(1-e^{-\xi_w})\Gamma_b}{\xi_w} \bar{\nu} \right] \tag{E.13}$$

where

$$\bar{\nu} = \nu_a + \nu_g \nu_a - \nu_g \nu_b \qquad (E.13a)$$

Since for the three reactions considered here, $\bar{\nu} = 0$, setting $\bar{\nu} = 0$ in equation (E.13), equation (67) is obtained for $Y_{CO,w}$. Substituting (67) and (E.13a) in equation (E.12), $Y_{0,w}$ is obtained (see equation (74c)). Using the results for $Y_{0,w}$, in equations (E.2), (E.6) and (E.7), $\varepsilon_{0,w}$, $\varepsilon_{CO,w}$ and $\varepsilon_{CO_2,w}$ are obtained.

$$\varepsilon_{0,w} = -\nu_a[1 + \frac{\Gamma_b}{\xi_w} \nu_b (1-e^{-\xi_w} \frac{\Gamma_b}{\xi_w} \{(\frac{1+\nu_g}{\nu_g}) Y_{0,\infty}$$

$$+ Y_{CO_2,\infty}\}] / [1 - (\frac{1+\nu_g}{\nu_g}) \frac{\Gamma_b}{\Gamma_a}] \qquad (E.14)$$

$$\varepsilon_{CO,w} = \text{see equation (68)}$$

$$\varepsilon_{CO_2,w} = \nu_b[\frac{1+\nu_g}{\nu_g} \frac{\Gamma_b}{\Gamma_a} + \frac{\nu_b \Gamma_b}{\xi_w} (1-e^{-\xi_w}) - e^{-\xi_w} \frac{\Gamma_b}{\xi_w} \{(\frac{1+\nu_g}{\nu_g}) Y_{0,\infty}$$

$$+ Y_{CO_2,\infty}\}] / [1 - (\frac{1+\nu_g}{\nu_g}) \frac{\Gamma_b}{\Gamma_a}] \qquad (E.15)$$

Using equation (E.15) in equation (E.3), $Y_{CO_2,w}$ is obtained:

$$Y_{CO_2,w} = [e^{-\xi_w} \{ (\frac{1+\nu_g}{\nu_g}) Y_{0,\infty} + Y_{CO_2,\infty} \} - \frac{\xi_w}{\Gamma_a} (\frac{1+\nu_g}{\nu_g})$$

$$- \nu_b (1-e^{-\xi_w})] / [1 - (\frac{1+\nu_g}{\nu_g}) \frac{\Gamma_b}{\Gamma_a}] \qquad (E.16)$$

In order to check the derivations, we obtain the wall mass fraction of inert gas N_2; remembering that the flux fraction of N_2 is equal to zero, the following differential equation is obtained:

$$\frac{dY_{N_2}}{d\xi} + Y_{N_2} = 0 \qquad (E.17)$$

with the boundary condition,

as $\xi \to 0$, $\qquad\qquad Y_{N_2} = Y_{N_2,\infty} \qquad (E.18)$

Thus integrating equation (E.17) with boundary condition (E.18)

$$Y_{N_2} = Y_{N_2,\infty} e^{-\xi_w} \qquad (E.19)$$

At $\xi = \xi_w$, then $\quad Y_{N_2,w} = Y_{N_2,\infty} e^{-\xi_w} \qquad (E.20)$

Adding equations (E.20), (E.16), (74c) and (67), we verified that the sum is indeed equal to unity.

Comments. (i) For the numerical method, differentiation of wall mass fractions and flux fractions with respect to ξ_w are obtained from the above equations. (ii) For no reduction process let $\Gamma_b \to 0$ in the concerned equations and obtain the results.

Flux Fractions of Species at $\xi = 0$

CO_2

Remembering the definition of flux fraction (see equation (26)), and using the coupling functions (24) and equation (29) ($j = CO_2$, $p = CO$),

$$[\frac{dY_{CO_2}}{d\xi} + \frac{dY_{CO}}{d\xi} (1+\nu_g)]_{\xi=0} =$$

$$[Y_{CO_2,w} + Y_{CO,w}(1+\nu_g) - Y_{CO_2,\infty} - Y_{CO,\infty}(1+\nu_g)] \frac{1}{1-e^{-\xi_w}} \qquad (E.21a)$$

But

$$\varepsilon_i = \frac{dY_i}{d\xi} + Y_i \qquad (E.21b)$$

Hence,

$$\varepsilon_{CO_2,\infty} = \frac{1}{1-e^{-\xi_w}} [Y_{CO_2,w} + Y_{CO,w}(1+\nu_g)] -$$

$$- \frac{e^{-\xi_w}}{1-e^{-\xi_w}} [Y_{CO_2,\infty} + Y_{CO,\infty}(1+\nu_g)] - \varepsilon_{CO,\infty}(1+\nu_g) \qquad (E.22)$$

Similarly, for $\varepsilon_{0,\infty}$,

$$\varepsilon_{0,\infty} = \frac{1}{1-e^{-\xi_w}} [Y_{0_2,w} - Y_{CO,w}\nu_g] - \frac{e^{-\xi_w}}{1-e^{-\xi_w}} [Y_{0_2,\infty} - Y_{CO,\infty}\nu_g]$$

$$+ \varepsilon_{CO,\infty}\nu_g \qquad (E.23)$$

Adding equations (E.22) and (E.23), it is verified that the sum is equal to unity.

Limiting Diffusion Rates and Other Conditions

At limiting diffusion rates in absence of gas phase oxidation,

$$Y_{0,w} \to 0 \qquad (E.24a)$$

Also

$$\varepsilon_0 = \varepsilon_{0,w} = (\varepsilon_0)_{\xi=0} = -\nu_s \qquad (E.24b)$$

Hence using equation (29) with $\beta = Y_0$, and equation (E.21b),

$$(\frac{dY_0}{d\xi}) = \varepsilon_0 - Y_0 = \frac{e^{-\xi}}{1-e^{-\xi_w}}(Y_{0,w} - Y_{0,\infty}) \qquad (E.25)$$

Using equations (E.25) and (E.24a and b), at $\xi = \xi_w$,

$$\xi_w = \ln(1 + \frac{Y_{0,\infty}}{\nu_s})$$ (E.26)

where $\nu_s = \frac{1}{2} W_{0_2}/W_C$, if CO is the product of heterogeneous reaction at the surface and $\nu_s = W_{0_2}/W_C$, if CO is the product and if CO_2 is produced by the gas phase oxidation instantaneously; i.e. as though CO_2 is produced at the surface.

Again using equations (29) and (E.21b) with $\beta = Y_{pr}$,

$$(\frac{dY_{pr}}{d\xi}) = \varepsilon_{pr} - Y_{pr} = \frac{e^{-\xi}}{1-e^{-\xi_w}}(Y_{pr,w} - Y_{pr,\infty})$$ (E.27a)

where

$$\varepsilon_{pr} = (1+\nu_s), \text{ the flux fraction of the product. (E.27b)}$$

From equations (E.26), (E.27a) and (E.27b),

$$Y_{pr,w} = \frac{(1+\nu_s)\frac{Y_{0,\infty}}{\nu_s}}{(1 + \frac{Y_{0,\infty}}{\nu_s})}$$ (E.28)

If CO is the final product, then with $Y_{0,\infty} = .23$, $W_{0_2} = 32.0$, and $W_C = 12.0$,

$$\xi_w = .159, \quad \xi_{CO,w} = 2.333, \quad Y_{CO,w} = .343$$ (E.29)

If CO_2 is the final product, then

$$\xi_w = .083, \quad \varepsilon_{CO_2,w} = 3.667, \quad Y_{CO_2,w} = .291 \qquad (E.30)$$

Variable Activation Energy Modification

If activation energy at the surface or in the gas phase varies linearly with temperature,

$$E = a + b\,T \qquad (E.31)$$

then,

$$e^{-E/R°T} = e^{-b/R°} \, e^{-a/R°T} \qquad (E.32)$$

One can associate the term $\{e^{-b/R°}\}$ with the corresponding Damkohler numbers. For example Tesner found that surface activation energy decreases linearly with temperature [58]. Then b is less than zero.

E.2. Initial Value Method with Nachsteim's Modification for a System of Ordinary Differential Equations

Let

$$\delta_j = a_{j0} + \sum_{i=1}^{N} a_{ji}s_i, \quad j = 1\ldots 2N \qquad (E.33)$$

One is interested in determining s_i such that the sum $\sum_{j=1}^{2N} \delta_j^2$ is a minimum. Then,

$$\frac{\partial}{\partial s_k} \left\{ \sum_{j=1}^{2N} a_{j0}^2 + 2 \sum_{j=1}^{2N} \left(\sum_{i=1}^{N} a_{ji} s_i \right) a_{j0} \right.$$

$$\left. + \sum_{j=1}^{2N} \left(\sum_{\ell=1}^{N} \sum_{m=1}^{N} a_{j1} a_{jm} s_1 s_m \right) \right\} = 0$$

$$k = 1 \ldots N \qquad (E.34)$$

After differentiation one obtains

$$2 \sum_{j=1}^{2N} a_{j0} \left[\sum_{i=1}^{N} a_{ji} \delta_{ik} + \sum_{=1}^{N} (a_{j1} a_{jm} s_1 \delta_{mk}) \right.$$

$$\left. + \sum_{m=1}^{N} (a_{j1} a_{jm} s_m \delta_{1k}) \right] = 0 \qquad (E.35)$$

Simplifying equation (E.35), we get

$$\sum_{j=1}^{2N} \sum_{\ell=1}^{N} a_{j1} a_{jk} s_1 = - \sum_{j=1}^{2N} a_{j0} a_{jk}, \quad k = 1 \ldots N \qquad (E.36)$$

The N equations given by equation (E.36) are solved and the solutions for s_i are given by equation (79b).

```
 1          SUBROUTINE PERTM(N,A,B,XT,P,ITRB,LMT,IC,DELTA,ER,JJ,X,BB)
 2     C    THIS SUBROUTINE EVALUATES THE NECESSARY INCREMENT IN THE INITIAL
 3     C    VALUES OF A       SYSTEM OF NON-LINEAR DIFFERENTIAL EQUATIONS
 4     C    USING THE INTEGRALS OF THE PERTURBATION EQUATIONS AND
 5     C    METHOD OF LEAST SQUARES FOR THE MINIMUM ERROR BETWEEN
 6     C    PIVOTAL AND AUXILIARY PARAMETERS
 7          N2        = 2*N
 8          DIMENSION A(N2,N2),B(N2,N2),XT(N),P(N2),X(N) ,BB(N2,N2)
 9          KK        = 7
10          JL        = 0
11          LMT  = LMT-1
12          IF(LMT.LT.0) GO TO 130
13          JM        = 0
14          N1        = N+1
15          GO TO (10,90,110,125),ITRB
16     10   CONTINUE
17          DO 30 K=1,N
18          DO 30 L=1,N1
19          B(K,L)  = 0.0
20     30   CONTINUE
21          DO 40 K=1,N
22          DO 40 L=1,N1
23          DO 40 J=1,N2
24          B(K,L)  = A(J,L)*A(J,K)+B(K,L)
25     40   CONTINUE
26          DO 45 K=1,N
27     45   B(K,N1) = -B(K,N1)
28          LL        = 0
29          CALL GJEM(N,N1,B,X,BB)
30          IC   = IC+1
31          DO 80 I=1,N
32          XT(I)    = XT(I) + X(I)
33          IF((ABS(X(I)/XT(I))).LT.ER) JL = 1
34          IF((ABS(X(I)/XT(I))).GT.ER) JM = 2
35     80   CONTINUE
36          JJ        = 2
37          IF(N.GT.1.AND.JL.EQ.1.AND.JM.EQ.2) JJ= 1
38          IF(N.EQ.1.AND.JL.NE.1) JJ=1
39          RETURN
40     90   CONTINUE
41          IF(IC.EQ.1) IC=0
42          ETAST1   = ABS(DELTA)
43          DO 100 L=1,N2
44          A(L,N1) = A(L,N1)+P(L)*DELTA
45     100  CONTINUE
46          GO TO 10
47     110  LL        = LL+1
48          IF(LL.EQ.KK) GO TO 140
49          DO 120 I=1,N
50          XT(I)    = XT(I)-X(I)/KK
51     120  CONTINUE
52          JJ        = 1
53          RETURN
54     125  CONTINUE
55          IF(LL.GE.1) ETAST3 = ETAST2
56          ETAST2   = ABS(DELTA)
57          IF(ETAST2.GT.ETAST1) GO TO 150
58          IF(ETAST2.LT.ETAST3.AND.ETAST2.GT.0.07) GO TO 110
59          GO TO 90
60     130  JJ        = 3
61          RETURN
62     140  JJ        = 4
63          WRITE(6,145)
64     145  FORMAT(/,4X,'FIGURE OUT BETTER GUESS FROM LIST')
65          RETURN
66     150  WRITE(6,160)
67          GO TO 110
68     160  FORMAT(/,5X,'INTEGRATION STOPS EARLIER.')
69          END
```

Explanation

N, number of initial values assumed at start of integration, (for example in the thesis, N = 1); specify.

A, a matrix of order (2N, N+1). First N columns contain the derivatives of boundary conditions with respect to the initial values (see a_{ji} after equation (81)), while (N+1)th column contains the 2N boundary conditions to be satisfied at other end (see a_{j0} after equation (81));

B, a matrix of order (N,N+1).

XT, a matrix or order (N,1), specify first set of values only. This matrix contains the next set of initial values when coming out of subroutine.

P, a matrix or order (2N,1); must contain spatial derivatives of 2N boundary conditions, if integration trouble in between the boundaries is to be avoided.

ER, maximum permissible error for the boundary conditions; specify (not a matrix).

LMT, maximum number of iterations; specify.

IC, an iteration counter; specify = 1, for first iteration.

DELTA, (Integration distance to be reached--distance actually so far integrated); must be specified; equal to zero if there is no integration trouble

or specify actual value if there is integration

trouble (for e.g.: $0 - \eta_{stop}$ in the thesis).

X, a matrix of order (N,1) containing the increments.

BB, a matrix or order (2N,2N) for use in GJEM.

ITRB, = 1, means integration reached the boundary; next
step is guessed automatically.

= 2, integration breaks down for the first itera-
tion; subroutine attempts to guess next set of
values so that integration could be continued up
to the boundary.

= 3, means integration continued up to the boundary
for ith iteration; but after the increment the
integration breaks down at intermediate point.
The subroutine, if this number is specified,
automatically takes care of the situation.

= 4, the attempt by the subroutine to extend the
integration to the boundary has not succeeded; the
subroutine again attempts to resolve this within
reasonable number of iterations (about seven
iterations in the subroutine).

JJ, = 1, error is not satisfied; continue the iteration
cycle.

= 2, error is satisfied; write down the results.

= 3, error is not satisfied within specified
number of iterations.

= 4, attempt by the subroutine to extend the

integration to the boundary has failed; but see the listing given by the subroutine.

E.4. Derivation of General Correlation for Peak Burning Temperatures

Integrating equation (68) after concentrating all reaction at the surface, $(n_0 = 0, n_{CO} = 1.0)$

$$\varepsilon_{CO,w} - \varepsilon_{CO,\infty} = \frac{\Gamma_g}{\xi_w} Y_{CO,w} \qquad (E.37a)$$

where

$$\Gamma_g = D_{III,g} \; e^{-1/\theta_w}/\theta_w \qquad (E.37b)$$

From the conservation equation for the gas phase, $(Y_{CO,\infty} = 0)$

$$\frac{Y_{CO}}{Y_{CO,w}} = \frac{1-e^{-\xi}}{1-e^{-\xi_w}} \qquad (E.38a)$$

one obtains

$$\varepsilon_{CO,\infty} = \frac{Y_{CO,w}}{1-e^{-\xi_w}} \qquad (E.38b)$$

Substituting equation (E.38) in equation (E.37), and using equation (68) after letting $\Gamma_b \to 0$,

$$\frac{Y_{CO,w}}{1-e^{-\xi_w}} + \frac{\Gamma_g}{\xi_w} Y_{CO,w} = (1+\nu_a) \qquad (E.39)$$

Letting ξ_w be small, and then expanding $1-e^{-\xi_w} \simeq \xi_w$,

$$\frac{Y_{CO,w}}{\xi_w} = (\frac{1+\nu_a}{1+\Gamma_g}) \qquad (E.40)$$

Similarly obtaining $Y_{CO,w}$ from equation (67) after letting $\Gamma_b \to 0$ and ξ_w be small

$$\frac{Y_{CO,w}}{\xi_w} = \{ (1+\nu_b) + \frac{Y_{0,\infty}}{\nu_g} + \frac{1}{\nu_a \Gamma_g} - \frac{Y_{0,\infty}}{\nu_g} \frac{1}{\xi_w} \} \qquad (E.41)$$

Comparing equations (E.40) and (E.41), then solving for ξ_w,

$$\xi_w = \frac{Y_{0,\infty}/\nu_g}{[\frac{Y_{0,\infty}}{\nu_g} + \frac{1}{\Gamma_a} \frac{1}{\nu_g} + (1+\nu_b) - \frac{(1+\nu_a)}{(1+\Gamma_g)}]} \qquad (E.42)$$

In order that ξ_w to be a maximum, then $[\frac{1}{\Gamma_a \nu_g} - \frac{(1+\nu_a)}{(1+\Gamma_g)}]$ must be a minimum. Thus using calculus and considering only exponential terms, we obtain the following equation at the peak burning point:

$$\frac{\Gamma_g \Gamma_a}{(1+\Gamma_g)^2} = \frac{E_{w,a}^+}{(1+\nu_a)} \qquad (E.43)$$

Note that this temperature is independent of the ambient oxygen mass fraction. Many times $1 + \Gamma_g \simeq 1$, at the peak burning temperature. Hence,

$$\Gamma_g \Gamma_a \simeq \frac{E_{w,a}^{+}}{(1+\nu_a)} \qquad (E.44)$$

APPENDIX F

DISCUSSION ON DIRAC-DELTA APPROXIMATION
FOR CHEMICAL REACTIONS

The formulation of the Dirac-delta approximation for chemical reaction was introduced by Peskin [48] without any emphasis on the coordinate-independent physical quantity. Later Marathe and Jain [68] applied the same technique to the problem of flame characteristics of an opposed jet diffusion flame. The present dissertation followed a similar mathematical procedure. It is found that Dirac-delta function is dimensional (in a mathematical sense) and as such, the magnitude of the integral varies by a constant factor depending on the selection of the coordinate system; however, the physical quantity must remain invariant to obtain meaningful results at least in a qualitative sense. A physical understanding of the flame surface approximation will lead to the proper approximation for the chemical reactions.

If Dirac-delta function is introduced in the same coordinate used by Peskin [48] (ξ_w/ξ), the flux fraction of oxygen at the reaction surface will be equal to

$$- (\varepsilon_0)_0 = D_{III,g} \frac{\xi_w}{\xi^{*2}} \frac{e^{-1/\theta^*}}{\theta^{*n}} Y_0^{*n_0} Y_V^{*n_V} \qquad (F.1)$$

Comparing equation (F.1) with (A.4), one finds that the results differ by a factor (ξ_w/ξ^{*2}). The discrepancy can be explained as follows.

Consider equation (37) <u>without</u> the Dirac-delta approximation. Integrating

$$-(\epsilon_0)_o = D_{III,g} \; \xi_w^2 \int_0^{\xi_w} Y_0^{n_0} Y_V^{n_V} \frac{e^{-1/\theta}}{\theta^n} \, d\xi \qquad (F.2)$$

Since most of the reaction takes place in the neighborhood of the stoichiometric surface

$$-(\epsilon_0)_o \simeq D_{III,g} \; \frac{\xi_w^2}{\xi^{*4}} \; Y_0^* \; Y_V^* \int_0^{\xi_w} \frac{e^{-1/\theta}}{\theta^n (d\theta/d\xi)} \, d\theta \qquad (F.3)$$

where the transformation from ξ coordinate to θ coordinate has been carried out.

For a steeply varying exponential function, and when $\theta_w \ll \theta^*$

$$-(\epsilon_0)_o \simeq -D_{III,g} \; \frac{\xi_w^2}{\xi^{*4}} \; Y_0^* \; \frac{Y_V^*}{\theta^{*n}} \; \frac{\theta^{*2}}{(d\theta/d\xi)_{\xi^*}} \; e^{-1/\theta^*} \qquad (F.4)$$

For an ignition problem with adiabatic ignition criterion

$$\left(\frac{d\theta}{d\xi}\right)_{\xi^*} \simeq \{- Q_w^+ - (\theta^* - \theta_w)\}/2 \qquad (F.5)$$

Using equation (F.5) in (F.4)

$$-(\varepsilon_0)_o \simeq + D_{III,g} \frac{\xi_w^2}{\xi^{*4}} Y_0^{*n_0} Y_V^{*n_V} \frac{e^{-\frac{1}{\theta^*}}}{\theta^{*n}} [\frac{2\theta^{*2}}{Q_w^+}] \qquad (F.6)$$

The terms in square brackets in equation (F.6) are weak functions of ξ^* and particle size. When $\theta^* \simeq .065$, $Q_w^+ \simeq .0585$,

$$\frac{2\theta^{*2}}{Q_w^+} \simeq .1 \qquad (F.7)$$

Thus,

$$-(\varepsilon_0)_o \simeq .1 \, D_{III,g} \frac{\xi_w^2}{\xi^{*4}} \frac{Y_0^{*n_0}}{\theta^{*n}} e^{-1/\theta^*} Y_V^{n_V} \qquad (F.8)$$

Comparing equation (F.8) with (A.4) one notices that the Dirac-delta approximation, introduced in the present dissertation is physically and qualitatively meaningful both with respect to variation in particle size and oxygen concentration.

REFERENCES

1. Essenhigh, R. H. and Howard, J. B., "Toward a Unified Combustion Theory," Ind. Engg. Chem., 58, pp. 14-23 (1966).

2. Essenhigh, R. H., "On the Inter-Influence of Classical Combustion Research and Related Aerospace Problems," Eleventh Symposium (International) on Combustion, The Combustion Institute, Pittsburgh, pp. 292-308 (1967).

3. Hamor, R. J., Smith, I. W. and Taylor, R. J., "Kinetics of Combustion of Pulverized Brown Coal Char Between 630 and 2200°K," Combustion and Flame, 21, pp. 153-162 (1973).

4. Howard, J. B. and Essenhigh, R. H., "Pyrolysis of Coal Particles in Pulverized Fuel Flames," Ind. Eng. Chem. Process Design Develop., 6, pp. 74-84 (1967).

5. Strickland-Constable, "Theory of the Reaction of Graphite with Oxygen in the Temperature Range of 1000-2400°C," Second Conference on Industrial Carbon and Graphite, Society of Chemical Industry, London, 7-9th April, pp. 235-242 (1965).

6. Kimber, G. M. and Gray, M. D., "Reaction Rates of Charcoal and Coal Char Particles (100 μm) with Oxidizing Gases in the Range 1800-2800°K," Third Conference on Industrial Carbon and Graphite, Imperial College of Science and Technology, London SW 7, pp. 278-281 (1971).

7. Russell, D. A. and Christiansen, W. H., "Shock Tube Lasers," Eighth International Shock Tube Symposium, London, England, July (1971).

8. Christiansen, W. H. and Tsongas, G. A., "Gain Kinetics of CO_2 Gasdynamic Laser Mixtures at High Pressures," The Physics of Fluids, 14, pp. 2611-2619 (1971).

9. Lovis, Bement, et al., "Open Cycle Coal Burning MHD Power Generation: An Assessment and a Plan for Action," R and D No. 71, Office of Coal Research, Department of Interior, Washington, D. C. 20240 (1971).

10. Dicks, L. M., Crawford, L. W. and Kornstell, K. W., "Direct Coal Fired MHD Power Generation," Journal of Engineering for Power, Transactions of ASME, 96, Series A, pp. 153-157 (1974).

11. Wen, C. Y., "Production of Electricity Via Coal and Coal-Char Gasification," R and D Report No. 66, Office of Coal Research, Department of Interior, Washington, D. C. 20240 (1973).

12. Anthony, D. B., Howard, J. B., Meissner, H. P. and Hottel, H. C., "Apparatus for Determining High Pressure Coal-Hydrogen Reaction Kinetics Under Rapid Heating Conditions," Rev. Sci. Instrum., 45, pp. 992-995 (1974).

13. Skinner, D. G., "The Fluidized Combustion of Coal," Chemical Engineering, M&B Monographs, Mills and Boon Ltd., London (1971).

14. Nettleton, M. A. and Stirling, R., "The Ignition of Clouds of Particles in Shock Heated Oxygen," Proc. Roy. Soc. London. A., 300, pp. 62-77 (1967).

15. Nettleton, M. A. and Stirling, R., "The Combustion of Clouds of Coal Particles in Shock Heated Mixtures of Oxygen and Nitrogen," Proc. Roy. Soc. London. A., 322, pp. 207-221 (1971).

16. Frank-Kamenetskii, D. A., Diffusion and Heat Transfer in Chemical Kinetics, 2nd Edition, Plenum Press, New York (1969).

17. Supriya Bandyopadhyay and Debdas Bhaduri, "Prediction of Ignition Temperature of a Single Coal Particle," Combustion and Flame, 18, pp. 411-415 (1972).

18. Thomas, G. R., Stewansen, A. J. and Evans, D. G., "Ignition of Coal Particles Without Temperature Jump," Combustion and Flame, 21, pp. 133-136 (1973).

19. Nelson, E. T., Jean Worrel, and Walker, P. L., "Kinetics of Volatile Matter Release from Pennsylvania Anthracites," American Coal Conference on Coal Science, The Pennsylvania State University (1964).

20. Howard, J. B. and Essenhigh, R. H., "Mechanism of Solid Particle Combustion with Simultaneous Gas Phase Volatiles Combustion," Eleventh Symposium (International) on Combustion, The Combustion Institute, Pittsburgh, pp. 399-408 (1967).

21. Griffiths, D. M. I. and Standing, H. A., "Thermodynamic Aspects of the Reaction of Carbon and Coal at High Temperatures," _American Chemical Society_, _Advances in Chemical Series_, 55, pp. 666-676 (1966).

22. Stickler, D. B., Gannon, R. E. and Kobayashi, H., "Rapid Devolatization Modeling of Coal," Eastern Section of the Combustion Institute, Applied Physics Laboratories, John Hopkins University, Maryland, Nov. 12-13 (1974).

23. Essenhigh, R. H., "Dominant Mechanisms in the Combustion of Coal," Fuels Division, ASME Paper No. 70 WA/Fu-2 (1970).

24. Essenhigh, R. H., "The Influence of Coal Rank on the Burning Times of Single Captive Particles," _Journal of Engineering for Power_, 85, pp. 183-190 (1963).

25. Thomas, G. R., Harris, J. J. and Evans, D. G., "The Ignition of Pulverized Brown Coal," _Combustion and Flame_, 12, pp. 391-393 (1968).

26. Nettleton, M. A. and Stirling, R., "The Influence of Additives on the Burning of Clouds of Coal Particles in Shock Heated Gases," _Combustion and Flame_, 22, pp. 407-414 (1974).

27. Wicke, E., "Contribution to the Combustion Mechanism of Carbon," _Fifth Symposium (International) on Combustion_, Reinhold Publishing Corporation, New York, pp. 245-252 (1955).

28. Baum, M. M. and Street, P. J., "Predicting the Combustion Behavior of Coal Particles," _Combustion Science and Technology_, 3, pp. 231-243 (1971).

29. Bryant, J. T., "The Combustion of Premixed Laminar Graphite Dust Flames at Atmospheric Pressures," _Combustion Science and Technology_, 2, pp. 389-399 (1971).

30. Essenhigh, R. H., Froderg, R. and Howard, J. B., "Combustion Behavior of Small Particles," _Ind. Engg. Chem._, 57, pp. 33-43 (1965).

31. Nagle, J. and Strickland-Constable, "Oxidation of Carbon Between 1000-2000°C," _Proc. of 5th Conf. on Carbon_, 1, pp. 154-164 (1962).

32. Blyholder, G., Binford, J. S. and Eyring, H., "A Kinetic Theory for the Oxidation of Carbonized Filaments," J. Phys. Chem., 62, pp. 263-267 (1958).

33. Smith, I. W., "The Kinetics of Pulverized Semi-Anthracite in the Temperature Range 1400-2200°K," Combustion and Flame, 17, pp. 421-428 (1971).

34. Smith, I. W., "Kinetics of Combustion of Size Graded Pulverized Fuels in the Temperature Range 1200-2270°K," Combustion and Flame, 17, pp. 303-314 (1971).

35. Walker, P. L., Frank Rusinko, Jr. and Austin, L. G., "Gas Reactions of Carbon," Advances in Catalysis, 11, pp. 133-221 (1959).

36. Rosner, D. E. and Allendorf, A. D., "High Temperature Oxidation of Carbon by Atomic Oxygen," Carbon, 3, pp. 153-156 (1965).

37. Rosner, D. E. and Allendorf, A. D., "High Temperature Kinetics of Graphite Oxidation by Dissociated Oxygen," AIAA Journal, 3, pp. 1522-1523 (1965).

38. Fendell, F. E., "The Burning of Spheres Gasified by Chemical Attack," Combustion Science and Technology, 1, pp. 13-24 (1969).

39. Williams, F. A., Combustion Theory, Addison Wesley Publishing Company, Inc., Reading, Massachusetts (1965).

40. Spalding, D. B., "Theory of Particle Combustion at High Pressures," ARS Journal, 29, pp. 829-835 (1959).

41. Edelman, R. B., Fortune, O. F., Weilerstein, G. Cochran, T. H., and Haggard, J. B., "An Analytical and Experimental Investigation of Gravity Effects upon Laminar as Jet Diffusion Flames," Fourteenth Symposium (International) on Combustion, Combustion Institute, Pittsburgh, Pennsylvania, pp. 399-412 (1973).

42. Anthony, D. B., Howard, J. B., Hottel, H. C. and Meissner, H. P., "Rapid Devolatization of Pulverized Coal," Fifteenth Symposium (International) on Combustion, Tokyo, Japan, Aug. 25-31 (1974).

43. Grassie, H., Chemistry of High Polymer Degradation Processes, Butterworth Scientific Publications, London (1956).

44. Sirignano, W. A., "A Critical Discussion of Theories of Flame Spread Across Solid and Liquid Fuels," Combustion Science and Technology, 13, pp. 559-562 (1969).

45. Takashi Kashiwagai, "A Radiative Ignition Model of a Solid Fuel," Combustion Science and Technology, 8, pp. 225-236 (1974).

46. Majumdar, B. K. and Chatterjee, N. N., "Mechanism of Coal Pyrolysis in Relation to Industrial Practice," Fuel, 52, pp. 11-19 (1973).

47. Spalding, D. B., "Theory of Mixing and Chemical Reaction in an Opposed Jet Diffusion Flame," ARS Journal, 31, pp. 763-771 (1961).

48. Peskin, R. L. and Wise, H., "A Theory for Ignition and Deflagration of Fuel Drops," AIAA Journal, 4, pp. 1646-1650 (1966).

49. Annamalai, K. and Durbetaki, P., "Extinction of Spherical Diffusion Flames: Spalding's Approach," International Journal of Heat and Mass Transfer, 17, pp. 1416-1418 (1974).

50. Hermance, C. E., Shinnar, R., and Summerfield, M., "Ignition of an Evaporating Fuel in a Hot Stagnant Gas Containing Oxidizer," AIAA Journal, 3, pp. 1584-1592 (1965).

51. Peskin, R. L., Polymeropoulos, C. E. and Yeh, P. S., "Results from Theoretical Study of Fuel Drop Ignition and Extinction," AIAA Journal, 5, pp. 2173-2178 (1967).

52. Alkidas, A., "The Steady State Theory of Ignition of Flowing Gaseous Mixtures by Hot Surfaces," Ph.D. Thesis, School of Mechanical Engineering, Georgia Institute of Technology, Atlanta, March (1972).

53. Alkidas, A. and Durbetaki, P., "Ignition Characteristics of a Stagnant Point Combustible Mixture," Combustion Science and Technology, 3, pp. 187-194 (1971).

54. Alkidas, A. and Durbetaki, P., "Ignition of a Gaseous Mixture by a Heated Surface," Combustion Science and Technology, 7, pp. 135-140 (1973).

55. Brokaw, R. S., "Analytic Solution to the Ignition Kinetics of the Hydrogen-Oxygen Reaction," Tenth Symposium (International) on Combustion, The Combustion Institute, Pittsburgh, pp. 269-278 (1965).

56. Glass, G. P., Kistiakowsky, G. B., Michael, J. V. and Kiki, H., "The Oxidation Reactions of Acetylene and Methane," *Tenth Symposium (International) on Combustion*, The Combustion Institute, Pittsburgh, pp. 513-522 (1965).

57. Badzioch, S. and Hawksley, P. G. W., "Kinetics of Thermal Decomposition of Pulverized Coal Particles," *Ind. Eng. Chem. Process Design Develop.*, 9, pp. 521-530 (1970).

58. Vandenabeele, H., Corbeels, R., and Van Tiggelen, A., "Activation Energy and Reaction Order in Methane-Oxygen Flames," *Combustion and Flame*, 4, pp. 253-260 (1960).

59. Annamalai, K. and Durbetaki, P., "On the Ignition of a Volatile Coal Particle," *Eastern Section, The Combustion Institute*, Fall Technical Meeting, John Hopkins University, Maryland (1974).

60. Khitrin, L. N., *The Physics of Combustion and Explosion*, Office of Technical Services, U. S. Department of Commerce, Washington, D. C. (1962).

61. Khitrin, L. N., "Fundamental Aspects of Carbon Consumption and Factors Intensifying the Burning of Solid Fuels," *Sixth Symposium (International) on Combustion*, Reinhold Publishing Corporation, New York, pp. 565-573 (1956).

62. Golovina, E. S. and Khaustovich, G. P., "The Interaction of Carbon with Carbon Dioxide and Oxygen at Temperatures Up to 3000°K," *Eighth Symposium (International) on Combustion*, Williams and Wilkins Company, Baltimore, pp. 784-792 (1962).

63. von Fredersdorff, C. G., "Reactions of Carbon with Carbon Dioxide and with Steam," Institute of Gas Technology, Chicago, Research Bulletin 19 (1955).

64. Howard, J. B., Williams, G. C. and Fine, D. H., "Kinetics of Carbon Monoxide Oxidation in Preflame Gases," *Fourteenth Symposium (International) on Combustion*, The Combustion Institute, Pittsburgh, pp. 975-986 (1973).

65. Sobolev, G. K., "High Temperature Oxidation and Burning of Carbon Monoxide," *Seventh Symposium (International) on Combustion*, Butterworths Scientific Publications, London, pp. 386-391 (1959).

66. Nachsteim, D. R. and Swigert, P., "Satisfaction of
    Asymptotic Boundary Conditions in Numerical Solutions
    of a System of Non-Linear Equations of Boundary Layer
    Type," NASA TN D-3004, N 65-35951 (1961).

67. Annamalai, K., Alkidas, A. and Durbetaki, P., "On
    Droplets Burning: Concentration Dependent Transport
    Properties," Proceedings of the Eighth Southeastern
    Seminar on Thermal Sciences, Vanderbilt University,
    Tennessee, pp. 101-137 (1972).

68. Marathe, A. G. and Jain, V. K., "Some Studies on Opposed-
    Jet Diffusion Flow Considering General Lewis Numbers,"
    Combustion Science and Technology, 6, 151-157 (1972).

VITA

Kalyanasundaram Annamalai was born July 14, 1943, in Thakkolam, India. He attended the College of Engineering, Guindy of University Madras, India, from which he received a Bachelor's Degree in Mechanical Engineering in 1966. After this he obtained a Master's Degree in Mechanical Engineering (Internal Combustion Engineering) in 1968 from the Indian Institute of Science, Bangalore, India, and worked as Senior Technical Assistant in the same Institute for two years. He entered graduate school at the Georgia Institute of Technology in September, 1970, for a program of study leading to the doctorate. He is a member of the Combustion Institute and Sigma Xi.

Mr. Annamalai is married to the former Miss Vasanthal of Tamil Nadu, India.